CHEMERIN AS A LINK BETWEEN HYPERTENSION AND OBESITY

By

David J. Ferland

A DISSERTATION

Submitted to
Michigan State University
in partial fulfillment of the requirements
for the degree of

Pharmacology and Toxicology – Doctor of Philosophy

2020

ABSTRACT

CHEMERIN AS A LINK BETWEEN HYPERTENSION AND OBESITY

By

David J. Ferland

Chemerin is a novel protein with growing recognition in the clinical sphere but limited basic science advancements. Hypertension and obesity have strong positive correlations with chemerin protein levels in the blood and are two diseases of the past decade that have continued to grow at alarming levels. Equipped with the limited knowledge that chemerin can directly stimulate the blood vessel to contract and that chemerin is secreted by the fat, we developed the hypothesis that adiposity-associated hypertension is promoted by the release of chemerin from the mesenteric perivascular adipose tissue (mPVAT; primarily adipocytes).

We first interrogated the blood vessel and the mPVAT to determine the mechanistic role of chemerin in each of these two tissue types. In the blood vessel, we isolated primary smooth muscle cells and used calcium flux as an indicator of smooth muscle stimulation. Chemerin stimulated calcium flux in a manner dependent on concentration and chemerin$_1$ (the primary receptor for chemerin on the vasculature). We also used various antagonists and inhibitors of the second messenger system to aggregate a basic profile of the actions of chemerin in the blood vessel. Chemerin not only stimulates direct constriction of the blood vessel but mediates this effect through the smooth muscle of the vessel.

Chemerin is a critical protein for the adipogenesis of 3T3-L1 cells. Using a germline knockout of chemerin in the rat, we observed the in vivo role of chemerin in the fat,

specifically the mPVAT. Histochemistry and polymerase chain reaction (PCR) revealed that chemerin is in fact vital to adipo- and lipogenesis (already known) but is crucial in a location-dependent manner (novel). Specifically, chemerin knockout limited the adipo- and lipogenesis of the mPVAT but not of the neighboring retroperitoneal fat.

To determine the effects of chemerin on blood pressure, we used antisense oligonucleotides (ASOs) to knock down chemerin and radiotelemetry to measure blood pressure and other cardiovascular measures. A whole-body knockdown of chemerin reduced the mean arterial pressure by 7 mmHg in a normal Sprague Dawley (SD) rat and by 30 mmHg in a high-fat (hypertensive) Dahl salt-sensitive rat. Surprisingly, an ASO specific to the liver did not change mean arterial pressure but still abolished plasma circulating levels of chemerin. The liver and the fat are the two largest producers of chemerin. While the liver appears to control plasma chemerin levels, the fat is a primary candidate for the contributions of chemerin to blood pressure. A way of targeting drugs (like the ASO) directly to the fat did not exist so we also sought to develop this technology.

Using the adipocyte targeting sequence with 9-arginine tag (ATS-9R) electrostatically bonded to the ASO, we are creating a nanoparticle to deliver the ASO in a fat-specific manner. While the in vivo efficacy of this particle is still to be validated, chemerin remains a protein with considerable potential to effect blood pressure, especially blood pressure precipitated by a high-fat diet.

Taken together, these data demonstrate a substantial ability for chemerin to alter blood pressure, propose mechanisms by which the fat and blood vessel may interact, and set the stage for future translational therapeutics using chemerin as a target.

ACKNOWLEDGEMENTS

I could not have completed this thesis without a village of people to support me. The most influential person in this journey has been my PhD mentor, Stephanie Watts. She taught me the basics of the scientific method as an undergraduate, mentored me through my master's degree at Tufts University (in conjunction with John Castellot) and molded me into the PhD scientist I am today. She has been patient, kind, pushed me beyond my limits, and during the COVID-19 pandemic, gracious and professional.

I need to thank those who believed in me when it seemed like no one else would. Edward Watts picked me out of an undergraduate English class and helped me start my journey in research. Justin McCormick and Bethany Heinlen brought me into the DO-PhD program supporting me personally and financially.

The Department of Pharmacology and Toxicology at Michigan State has been a model for what a collaborative work environment looks like. Thank you to Rick Neubig and Anne Dorrance for your personal contributions to my thesis and for creating a thriving environment. The office and support staff are essential to all the research contained in this document contributing to grant applications, academic support, and making the department a fun place to work. Because of this community atmosphere, I have benefited from thriving collaborations with people like Greg Fink (and his lab), Andres Contreras (and his lab), Xuefei Huang, Mehdi Nasr, Kunli Liu, Jamie Bernard (and her lab), Tom Dexheimer, Bridget Seitz and the rest of the In Vivo Core Facility.

When I stepped into this thesis, I was fortunate that our lab already had a wonderful collaboration with Adam Mullick and Ionis Pharmaceuticals (previously known as ISIS

Pharmaceuticals). Adam provided us with essential materials (antisense oligonucleotides) but also gave us his mind. From thousands of miles and three time zones away, Adam was an active collaborator helping us think through both in vivo and in vitro experiments.

In addition to the generous donations of time by my committee members listed previously, I was fortunate to have the mentorship of Christopher Sinal from Dalhousie University on my committee. Chris is a prominent member of the chemerin community and has been vital to our investigations of this novel protein.

I thank the National Heart Lung and Blood Institute at the National Institutes of Health for the ability to conduct my research under an F31 fellowship. The American Heart Association and Department of Pharmacology and Toxicology have also been important financial contributors to the work of this thesis.

Including my time as an undergraduate, I spent about eight years with many members of the Watts lab. I consider my fellow lab members like Emma Flood and Janice Thompson to be family. I thank the PhD students like Nadia Ayala-Lopez who came before me, Ramya Kalyanakumar who could commiserate in lab with me, Vanessa Benham, Robert Freeborn, Di Zhang, and Kevin Baker who were great friends and collaborators in the classroom, and undergraduates like Maleeha Ahmad, Alex Ismail, and Alexis Orr who helped with this project in addition to their own independent research.

Finally, none of this could be possible without the family and talents provided by God. Thank you to Catherine and Francis for your unending support.

TABLE OF CONTENTS

LIST OF TABLES x

LIST OF FIGURES xi

KEY TO ABBREVIATIONS xiii

INTRODUCTION 1
1. Obesity and hypertension 1
1.1 Contextualizing the problem: two diseases on a crash course 1
1.2 The problem: the need for a mechanism in obesity-associated hypertension 2
1.3 Implications of the visceral fat and adipokines 4
2. History and pharmacology of chemerin 6
2.1 Chemerin: a protein with diverse functions 6
2.2 Receptors and chemerin-binding proteins 9
2.3 Tools and pharmacology of chemerin 12
2.4 Antisense oligonucleotides 13
2.5 Nanoparticles and drugging the fat 16
3. Inflammation paradox: making sense of the epidemiology 17
3.1 Pro-inflammatory attributes 18
3.2 Anti-inflammatory attributes 19
3.3 At a crossroads of mechanistic and clinical data 20

HYPOTHESIS 22

AIM 1.1: Mechanism of chemerin stimulation in vascular smooth muscle cells 23
1. Introduction 24
2. Methods 26
2.1 Animal use 26
2.2 Chemicals 26
2.3 Isometric contraction 27
2.4 Cell culture 28
2.5 Calcium kinetics 29
2.6 Immunocytochemistry 30
2.7 Western blot analyses 31
2.8 Data analysis and statistical procedures 33
3. Results 34
3.1 Chemerin causes a contraction and calcium flux that is G_i-dependent. 34
3.2 Chemerin signaling in smooth muscle most likely acts through the chemerin receptor. 36
3.3 Chemerin-9 activation of smooth muscle cells lacks Erk MAPK signaling 40
3.4 Calcium flux with chemerin-9 exhibits the same dependence on signaling elements as physiologic contraction 43

4. Discussion 43
4.1 Chemerin-induced contraction is dependent on calcium flux 43
4.2 Receptors mediating chemerin's action in smooth muscle cells 46
4.3 Chemerin signaling relies on various second messengers 47
4.3.1 Chemerin and L-type calcium channels 47
4.3.2 Chemerin and Rho Kinase 48
4.3.3 Chemerin and Src 49
4.3.4 Chemerin and PLC 50
4.3.5 *Chemerin and Erk MAPK* 50
4.4 Chemerin-9 as a model for recombinant chemerin? 51
4.5 Limitations 52
4.6 Conclusions 53

AIM 1.2: Beneficial and site-specific effects of chemerin on mPVAT 55
1. Introduction 56
2. Methods 57
2.1 Animal care and handling 57
2.2 Animal model 58
2.3 MicroCT 58
2.4 Tissue collection 59
2.5 Western blot 59
2.6 Histology and adipocyte analysis 60
2.7 PCR 60
2.8 Cytoscape network 61
2.9 Statistics and analysis 61
3. Results 63
3.1 KO rats have reduced visceral adiposity 63
3.2 Chemerin's adipogenic potential is location-specific 63
3.3 Adiponectin is important to the actions of chemerin 66
4. Discussion 66
4.1 Chemerin is a regulator of adipocyte development in mesenteric fat 66
4.2 Interactions of chemerin with other regulators of the adipocyte 69
4.3 Limitations 70
4.4 Conclusions 71

AIM 2.1: In vivo effects of chemerin on blood pressure 72
1. Introduction 73
2. Methods 75
2.1 Animal care 75
2.2 ASO Synthesis 76
2.3 Radiotelemetry and in vivo pharmacology 76
2.4 Gen 2.5 chemerin ASO dosing study 77
2.5 Gen 2.5 chemerin and GalNAc chemerin ASO blood pressure studies 77
2.6 Real-time quantitative PCR 77
2.7 Western analysis 78
2.8 Data analyses and statistics 79

3. Results.....80
3.1 Gen 2.5 Chemerin ASO must be dosed at 25 mg/kg for effective knockdown.....80
3.2 Minimal off-target effects with a 4 week chemerin ASO regimen.....82
3.3 Whole-body removal of chemerin lowers blood pressure.....82
3.4 Removal of liver chemerin alone does not show the same blood-lowering effects..86
4. Discussion.....88
4.1 The liver provides the majority of circulating chemerin.....88
4.2 Blood pressure is locally regulated by chemerin.....89
4.3 Limitations.....91
4.4 Conclusions.....92

AIM 2.2: In vivo effects of chemerin on obesity-associated hypertension.....93
1. Introduction.....94
2. Methods.....96
2.1 Animal handling.....96
2.2 Rat models of disease.....97
2.3 Radiotelemetry and ASO administration.....97
2.4 Western blots.....99
2.5 PCR.....100
2.6 Analyses and statistics.....100
3. Results.....101
3.1 Chemerin ASOs knockdown mRNA expression and translated protein.....101
3.2 Organ analysis of HF vs. HS Dahl S animals.....103
3.3 Chemerin ASOs in HF Dahl S animals cause a fall in blood pressure.....103
3.4 Liver-specific ASOs have a minor effect on fat-associated hypertension.....106
4. Discussion.....108
4.1 Chemerin's influence on high-fat diet hypertension.....108
4.2 Source of the chemerin matters.....111
4.3 Limitations.....114
4.4 Conclusions.....115

AIM 2.3: In vivo targeted destruction of chemerin mRNA in fat.....116
1. Introduction.....117
2. Methods.....119
2.1 Animal handling.....119
2.2 Drug and nanoparticle development.....119
2.3 ICP analysis of iron-oxide nanoparticle.....120
2.4 Primary adipocyte isolation.....120
2.5 Primary hepatocyte isolation.....122
2.6 Ex vivo effects of peptide and IVIS analysis.....122
2.7 In vivo injection.....123
2.8 PCR.....123
2.9 Western blots.....124
2.10 Analysis and statistics.....125
3. Results.....125
3.1 Iron-oxide nanoparticle delivers ASO but does not confer specificity.....125

3.2 Transition to ATS9R-FITC supports specificity for fat 127
3.3 Validation of single-injection ASO administration 132
3.4 ASO-ATS9R-FITC lacks efficacy for chemerin knockdown 134
3.5 ATS9R peptide may stimulate chemerin production 136
4. Discussion 136
4.1 Uncovering the efficacy of ASO after the first injection 136
4.2 Using iron nanoworms for ASO delivery 138
4.3 Moving in vivo with ATS9R 139
4.4 Conclusions 141

CONCLUSIONS 142
1. Reframing the epidemiology 142
1.1 Giving context to new chemerin mechanisms in the cardiovascular system 142
1.2 Does circulating chemerin even matter? 146
1.3 Local vs. systemic roles of chemerin 149
2. How chemerin isoforms could be impacting research 150
2.1 Re-examining chemerin pharmacology in the vasculature 150
2.2 Antisense oligonucleotides and isoforms 151
3. Applications to other pathologies 152
3.1 Obesity alone 152
3.2 Metabolic syndrome 153
3.3 Heart failure 153
4. Next Steps 154
5. Final perspectives 156

REFERENCES 157

LIST OF TABLES

Table 1: *Forward and reverse sequences for Sigma-Aldrich KiCqStart SYBR primers used in this study*.....62

Table 2: *Baseline values of treatment groups are similar*.....105

Table 3: *ASO does not wash off the NP*.....129

LIST OF FIGURES

Figure 1: *Chemerin signal processing* 7

Figure 2: *Expression of chemerin mRNA* 10

Figure 3: *Chemerin stimulates rat aorta and smooth muscle cells* 35

Figure 4: *Chemerin responses are blocked by PTX* 37

Figure 5: *Chemerin acts through the chemerin receptor* 39

Figure 6: *The chemerin receptor predominates at the cell perimeter over GPR1* 41

Figure 7: *Chemerin does not signal through Erk MAPK* 42

Figure 8: *Contraction and calcium are mediated by L-type calcium channels, ROCK, and Src* 44

Figure 9: *Schematic figure* 45

Figure 10: *KO rats have reduced visceral adiposity* 64

Figure 11: *Chemerin's adipogenic potential is location-specific* 65

Figure 12: *Adipocyte development network in chemerin KO rats* 67

Figure 13: *Dosing of chemerin ASO* 81

Figure 14: *Body and organ weights after given ASO* 83

Figure 15: *Chemerin ASO knockdown of mRNA and protein* 84

Figure 16: *Chemerin ASO reduces circulating chemerin protein* 85

Figure 17: *Chemerin ASO reduces blood pressure in SD rats* 87

Figure 18: *ASOs knocked down chemerin expression in HF and HS animals* 102

Figure 19: *High-fat animals have increased proportional fat mass* 104

Figure 20: *HF animals experience a profound drop in blood pressure with whole-body chemerin ASO* 107

Figure 21: *Liver-specific ASOs knock down chemerin in liver but not completely in plasma* 109

Figure 22: *Liver-specific ASOs in HF animals result in a modest fall in blood pressure* 110

Figure 23: *Chemical reactions for drug development* 121

Figure 24: *NP-ASO is efficacious and NP-ATS appears selective* 126

Figure 25: *NP-ATS-ASO knocks down chemerin but not better than ASO alone* 128

Figure 26: *Validation of the ATS9R* 130

Figure 27: *Ex vivo testing of the ATS9R-FITC* 131

Figure 28: *One injection of chemerin ASO is sufficient to induce chemerin knockdown* 133

Figure 29: *ATS9R appears to have in vivo specificity but not efficacy* 135

Figure 30: *ATS9R increases chemerin expression* 137

Figure 31: *Chemerin in the vasculature* 144

Figure 32: *Relationship between blood pressure and plasma chemerin* 148

KEY TO ABBREVIATIONS

ACE	Angiotensin Converting Enzyme
Adipoq	Adiponectin
ANG II	Angiotensin II
ASGPR	Asialoglycoprotein
ASO	Antisense Oligonucleotide
ATS9R	Adipocyte targeting Sequence with 9-Arginine
BMI	Body Mass Index
CT	Computed Tomography
Dahl S	Dahl Salt-Sensitive
Dahl R	Dahl Salt-Resistant
Fasn	Fatty Acid Synthase
GalNAc	N-Acetylgalactosamine
GLP-1	Glucagon-like Peptide 1
HF	High Fat
HR	Heart Rate
HS	High Salt
KO	Knock Out
Lep	Leptin
mPVAT	Mesenteric Perivascular Adipose Tissue
miRNA	Micro Ribonucleic Acid
mRNA	Messenger Ribonucleic Acid

NP	Iron nanoworm
PCR	Polymerase Chain Reaction
Plin1	Perilipin
PP	Pulse Pressure
PPAR	Peroxisome Proliferator-Activated Receptor
PTX	Pertussis Toxin
PVAT	Perivascular Adipose Tissue
RP	Retroperitoneal
Scr9R	Scrambled Adipocyte Targeting Sequence with 9-Arginine
SD	Sprague Dawley
WT	Wild Type

INTRODUCTION

1. Obesity and hypertension

1.1 Contextualizing the problem: two diseases on a crash course

Obesity prevalence has risen worldwide at rates triggering some researchers to label it as a “pandemic” [1]. As of 2016, the United States was ranked highest in its rate of obesity coming in over 38% [2]. Even more alarming is the steep rise in childhood obesity rates. Worldwide between 1975 and 2016, childhood obesity has risen from 0.7% to 5.6% in girls and 0.9% to 7.8% in boys [3]. Obesity is defined as a body-mass index (BMI) of 30 or above. This clinical measurement is associated with a number of other pathologies but carries with it a decreased life expectancy of 5-20 years [1].

One pathology that has followed a similar clinical track to obesity is high blood pressure, also known clinically as hypertension [4]. Guidelines for the diagnosis of hypertension in the United States were adjusted in 2017. A systolic blood pressure above 130 mmHg or diastolic blood pressure above 80 mmHg is considered stage 1 hypertension and above 140 mmHg systolic or 90 mmHg diastolic is considered stage 2 hypertension. It is projected that 46% of American adults will qualify for the diagnosis of hypertension [5].

The upward trends of obesity and hypertension appear to be related. People with obesity are 3.5-times more likely to develop hypertension [6] and weight loss to ideal body weight is expected to lead to a 5 mmHg fall in systolic blood pressure [5]. Blood pressure and waist circumference are key factors in the diagnosis of metabolic syndrome which also encompasses the dysregulation of triglycerides, HDL, and glucose handling [7]. Both

obesity and hypertension are clearly multifaceted disorders that have complex interactions with other systems in the body. The exact underpinnings of this relationship are still unclear but there appear to be a wide variety of valid explanations from the gut microbiome [8] to alterations in the adipokinome [9].

1.2 The problem: the need for a mechanism in obesity-associated hypertension

Drug developers have struggled to develop novel treatments for hypertension and obesity independently, much less obesity-associated hypertension or metabolic syndrome. Aliskiren (renin inhibitor) was the most recent drug introduced for hypertension with a novel mechanism and was approved in 2007 [10]. In 2014, about 20% of adults in the United States exhibited resistant hypertension (taking 4 classes of medication or taking 3 classes with uncontrolled blood pressure) [11]. The drought of new anti-hypertensive medication and levels of resistant hypertension present an urgent need for new therapies in hypertension alone.

Current pharmacological treatment of obesity is limited to drugs that act as an adjunct to lifestyle modification. The main goal of these drugs is to enhance weight loss which, among other things, reduces the risk of diabetes. A 7% decrease in weight can result in long-term protection from developing type 2 diabetes and a 15% decrease in weight is associated with remission from type 2 diabetes. Phentermine (amphetamine analog) is the most commonly prescribed adjunct and has a 41% success rate getting people to 5% weight loss and Liraglutide (glucagon-like peptide-1 agonist; GLP-1) is the most recent (2015) with a 28% chance of getting people past 5% weight loss. However, all of these drugs come with significant side effects so if 5% weight loss is not achieved

in 3 months, medication usually stops and physicians have to consider if bariatric surgery is appropriate [12].

There are some promising advances in obesity pharmacotherapy that involve GLP-1 (Liraglutide target) and other gut hormone targets like SGLT1/2. However, most of these are stuck in long clinical trials and are demonstrating severe side effect cases of diarrhea and vomiting [13].

Given the limitations of pharmacology to treat both obesity and hypertension together, those looking to treat metabolic syndrome have turned to lifestyle modification in children. Obesity, poor nutrition, and BMI are strong predictors of cardiovascular risk in adults [14]. But even when lifestyle modification in children fails, the pharmacotherapy is limited in its efficacy and children have to undergo therapy of each of the individual components of metabolic syndrome they qualify for. Apart from lifestyle modification (in both children and adults) there is no therapy that touches multiple aspects of metabolic syndrome [15].

The absence and limited efficacy of such treatments has led researchers to take a creative and detailed look at the possible causes of these two diseases. There is a growing recognition for the role of the gut microbiome in both hypertension and obesity. In hypertension, the microbiome may have negative modification on vitamins, may secrete compounds like trimethylamine N-oxide, or stimulate oxidative stress in the gut that leads to cardiovascular disease [8]. In obesity, many of the interactions between microbiome and pathology have been linked to polyphenols and LPS crossing the gut barrier [16]. To this end, the immune system has grown in relevance to obesity-associated hypertension. Eosinophils, Th2 T cells (promoting M2 macrophages), and innate

lymphoid cells type 2 are all thought to maintain the anti-inflammatory environment in the adipose tissue while M1 macrophages and Th1 T cells promote inflammation that leads to obesity [17].

These investigations of the immune cell in adipose tissue highlight two recent changes in dogma: 1) the immune cells have roles outside of fighting pathogens; and more importantly to this discussion, 2) adipose tissue plays a greater role in physiologic homeostasis than simply being a storage reservoir for carbohydrates. Adiponectin was one of the first and most prominent adipokines to be recognized for its positive role in metabolic homeostasis and its ability to protect the vasculature [18]. Especially given the close geographical relationship between adipose tissue and mesenteric resistance vessel [19], adipokines and communication between the fat and blood vessel provide a promising avenue to discover new mechanisms in the association of obesity and hypertension.

1.3 Implications of the visceral fat and adipokines

Increased visceral fat is associated with the negative outcomes of both obesity and hypertension [4, 20]. In humans, the visceral fat is made up of the omental and mesenteric fat. On Computed Tomography (CT) in clinical literature, the definition of visceral will also include retroperitoneal fat because the retroperitoneal and mesenteric fats are indistinguishable in the abdominal cavity [21]. However, functionally, these two fat depots are very different.

Mesenteric fat is a white perivascular adipose tissue (PVAT) and though retroperitoneal fat is also a white fat, it is not perivascular [21, 22]. The mesenteric fat

surrounds mesenteric resistance vessels. These vessels are responsible for a large amount of total peripheral resistance and are heavily involved in regulating blood pressure [19]. The superior mesenteric artery, just upstream of the mesenteric resistance vessels, also contains PVAT though this is more of an equal mix of brown and white adipose tissue. Moving further upstream to the aorta, this vessel contains PVAT that is mostly brown.

PVAT is dynamic and can change both its quality (white/brown) and adipokine profile throughout life and progression of pathology [23]. These genes and adipokines will influence the local adipogenesis and maintenance of the fat but also have targets outside the fat. Adiponectin promotes healthy lipid accumulation but also may stimulate nitric oxide production in the endothelium of the vasculature. Leptin is secreted by adipocytes primarily as a line of communication with the peripheral nervous system to increase lipolysis [18].

Chemerin is one of these adipokines whose plasma levels have been positively associated with blood pressure [24-30], BMI [24, 26, 31-34], and is being clinically considered as a marker for metabolic syndrome [35-37]. It is proposed to play a role in the autocrine/paracrine development of adipocytes [38] but also has the potential to be directly contractile to smooth muscle of the vasculature [39]. Chemerin is a relatively new adipokine but its strong epidemiological and clinical support offers promise towards chemerin playing a key role in the intersection of these disorders.

2. History and pharmacology of chemerin

2.1 Chemerin: a protein with diverse functions

The first mention of chemerin's gene (then referred to as tazarotene induced gene-2 or *TIG2*, now known as retinoic acid responder 2 or *RARRES2*) was in conjunction with psoriasis in 1997 [40]. For the next decade, chemerin would be known as a chemokine that interacts with the immune system. The first mechanistic study to analyze chemerin looked at the synovial fluid and provided us with much of the molecular knowledge on chemerin that we still rely on today. As a transcribed protein, chemerin exists as 163 amino acids (preprochemerin) but the first 20 amino acids reflect a membrane-bound signaling peptide. As a secreted protein, prochemerin is 143 amino acids (mouse variants are one amino acid shorter [41]) but lacks any ability to stimulate chemotaxis or calcium flux [42] (Figure 1). Rather, chemerin's activity is regulated by small changes, in some cases single amino acids, to the carboxy-terminus. These chemerin isoforms are often labeled for the last remaining amino acid including both the letter of the amino acid and its number out of the original 163 amino acids (in human and rat; 162 in mouse).

Proteolytic cleavage to the S^{157} isoform resulted in the most calcium mobilization at the $chemerin_1$ receptor [43] and using the last 9 amino acids of the recombinant S^{157} isoform recapitulates these findings [44]. The resulting 9 amino acid peptide was termed "chemerin-9" and has been an integral tool in analysis and study of chemerin. The fragments cleaved from the end of the C-terminal end of chemerin are believed to be inactive [45] but this has yet to be fully investigated.

As a chemokine, chemerin is shown to have influence over a number of adaptive and innate immune cells. Chemerin can stimulate the chemotaxis of macrophages and

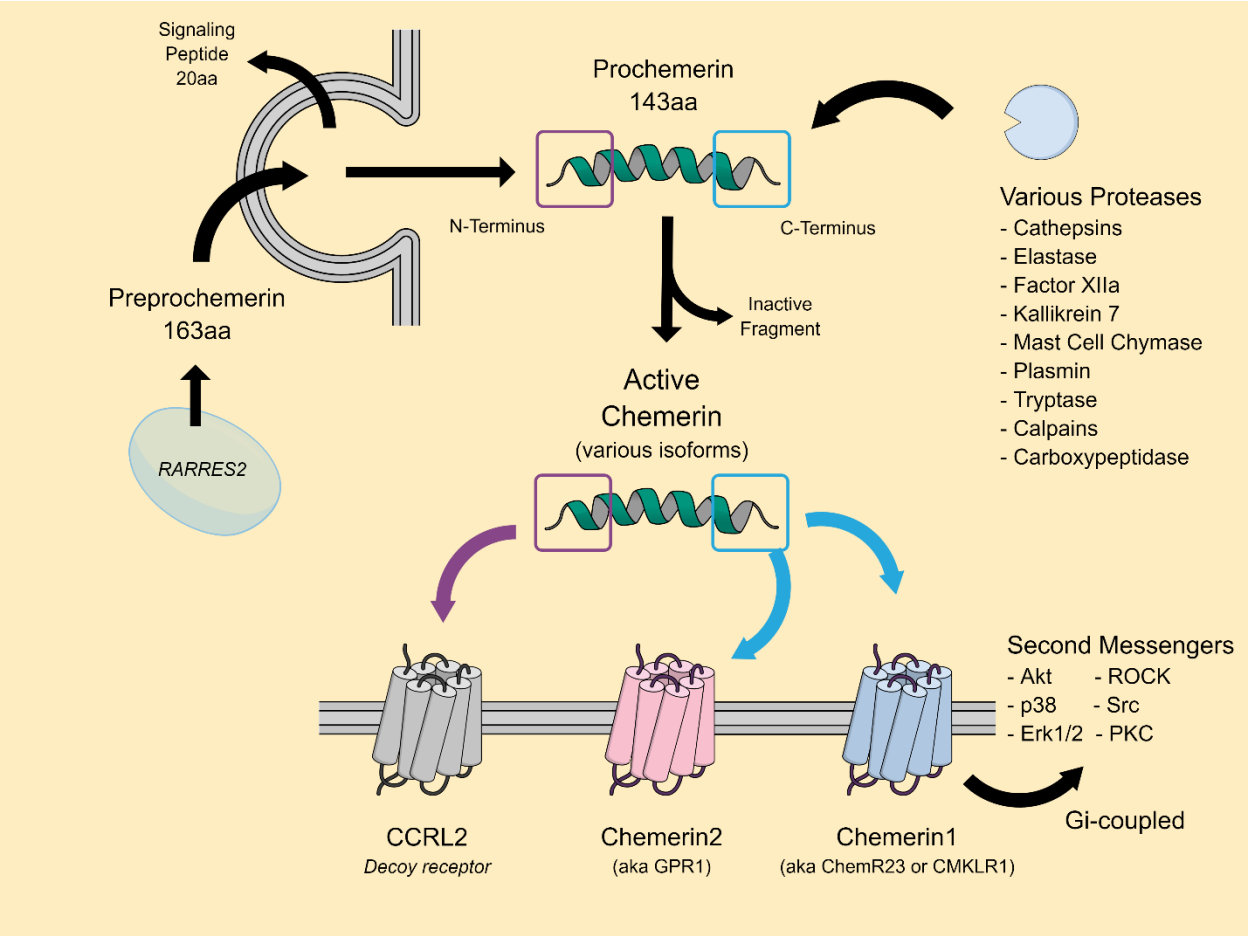

Figure 1: *Chemerin signal processing*
Amino acid (aa) length is listed under the associated protein.

immature dendritic cells [42]. Dendritic cells can be divided into two types: myeloid (most common and associated with inflammation) and plasmacytoid (produce interferons and activate adaptive immunity). Chemerin stimulates the chemotaxis of plasmacytoid dendritic cells but its receptor, chemerin$_1$, is down regulated upon maturation [46]. Natural killer cells, specifically CD56^{low} cells (the migratory population) also express chemerin$_1$ and can be found colocalized with dendritic cells in the presence of active chemerin [47].

In contrast to the chemokine roles being described at the time, in 2007 chemerin was labeled by two separate groups as an adipokine [35, 38]. Both groups observed that chemerin was necessary for the differentiation of a fibroblastic-adipocyte precursor to a mature adipocyte. If chemerin was knocked down before differentiation, cells did not accumulate lipid and failed to expression differentiation markers. Additionally, in normally differentiating cells, chemerin expression increased throughout the process. The authors concluded that chemerin was an autocrine and paracrine stimulator of adipo- and lipogenesis. The two groups differed in their analysis of how the receptors for chemerin were changing throughout the differentiation process. However, both groups performed expansive surveys of tissue to determine the distribution of chemerin expression in the body (Figure 2).

The vast majority of chemerin is expressed by the liver and adipose tissue. While multiple reports emphasize chemerin's expression is higher in white (especially visceral) adipose tissue than brown adipose tissue [24, 35, 38], chemerin expression and secretion is still present in the subcutaneous brown adipose tissue [48].

On one hand, it can seem like chemerin is a protein in search of a primary role. Some people claim it is a chemokine, others an adipokine, and even others make claims about

its role in angiogenesis [25, 49-52]. While there is plenty more for us to learn about chemerin itself, studying the receptors for chemerin can also help us make sense why chemerin appears to play numerous roles in the body.

2.2 Receptors and chemerin-binding proteins

Chemerin$_1$ was first discovered in 1996 under the name CMKLR1 as an orphan G protein-coupled receptor [53] then again in 1998 under the name chemerin receptor 23 (ChemR23) [54]. A mouse ortholog was discovered in 1997 named DEZ [55] and a rat ortholog was named CMKRL3 also in 1997 [56]. In accordance with the International Union of Basic and Clinical Pharmacology Committee on Receptor Nomenclature and Drug Classification (NC-IUPHAR), the receptor was renamed "chemerin$_1$" however, ChemR23 and CMKLR1 are still popular indicators in the literature.

At the initial discovery of the chemotactic properties of chemerin, chemerin$_1$ transfected into CHO-K1 cells and stimulated with recombinant chemerin S^{157} displayed inhibition of cAMP sensitive to pertussis toxin (indicative of coupling to a G_i alpha subunit), flux of intracellular calcium, and phosphorylation of ERK1/2 [42]. The role of ERK1/2 has been confirmed by multiple groups in different systems like chemotaxis, angiogenesis, and adipogenesis [38, 50, 57]. However, this receptor has also been shown to activate p38 and Akt in angiogenesis and granulosa cells [58, 59]. The receptor is internalized through clathrin-independent PKC signaling [60]. It is clear that chemerin$_1$ has the ability to work through different signaling mechanisms depending on the cell type and/or environment.

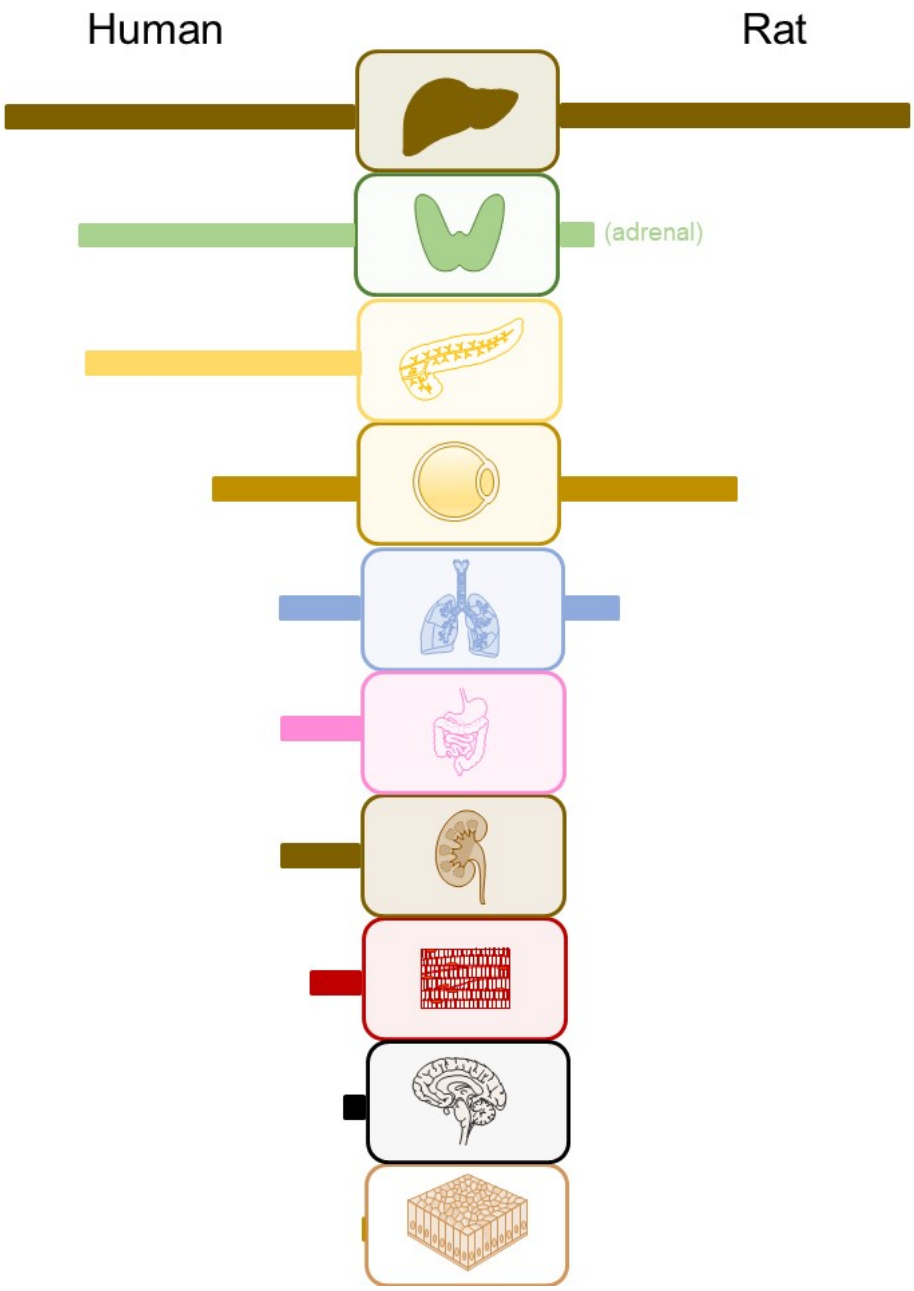

Figure 2: *Expression of chemerin mRNA*
Human (adapted from https://www.proteinatlas.org/ENSG00000106538-RARRES2/tissue) and rat organs chemerin expression where liver expression is set as the maximum and results are reported comparatively. Rat data were derived from studies done by Adam Mullick, Ionis Pharmaceuticals.

Chemerin$_2$ was the first of the chemerin receptors to be discovered (1994) and as such, was also labeled as an orphan G protein-coupled receptor. This discovery focused on the hippocampus of the brain where this receptor tends to be concentrated [61]. When chemerin$_2$ was first associated with chemerin in 2008, it stimulated calcium flux in an artificial HEK293T cell system designed to measure specific receptor activity [62]. This assay, the "Tango Assay," will prove to be an important tool when coupled to chemerin$_1$ [63] but some researchers have called into question whether chemerin$_2$ has functional relevance to the vasculature and hypertension [64]. Chemerin$_2$ is present in the stromal vascular fraction of the adipose tissue but not the adipocyte. Knockout of this receptor lead to glucose intolerance but did not affect adiposity or body weight [65]. Given its sensitivity to pertussis toxin, it is also proposed to be G_i coupled [66]. However, chemerin$_2$ is quickly internalized and produces a far shorter calcium mobilization response when compared to chemerin$_1$ [67]. As such, evidence is mounting that chemerin$_2$ may not play a functional role in intracellular signaling.

CCRL2 is able to bind chemerin but is not internalized and does not transduce a signal across the membrane. However, this binding protein is unique in that it binds the N-terminus of the chemerin protein (Figure 1) leaving the active C-terminus available. One example of the potential for CCRL2 to play a unique role is its high expression on mast cells during tissue swelling. The researchers proposed that CCRL2 may be used to concentrate active isoforms of chemerin in an immune response [68]. While this binding protein has a unique and interesting function, for the purposes of analyzing adipose tissue and chemerin's influence on blood pressure, it will largely be ignored.

2.3 Tools and pharmacology of chemerin

Recombinant prochemerin is 143 amino acids long and recombinant chemerin S^{157} is 138 amino acids. Some have used this recombinant protein in their in vivo [69] and in vitro [46] assays but most of these labs have internal methods of producing the protein. For some, the production or purchase of this recombinant chemerin is not feasible, especially at the concentrations necessary for in vivo and ex vivo experiments. For this reason, chemerin-9 is an important tool to assess chemerin's activity at $chemerin_1$.

Both chemerin-9 and recombinant chemerin have a single nM EC_{50} in calcium flux functional assays and single nM IC_{50} in competition binding assays. Recombinant prochemerin and a similar prochemerin peptide (139-163) did not have any calcium flux activity until the uM range and binding was not able to be determined in the competition assay [44]. However, in vivo use of both recombinant chemerin and chemerin-9 can be complicated by the plethora of enzymes that exist to degrade the protein or cleave the C-terminal end [70-73]. Other groups have refined the chemerin-9 peptide by making d-Tyr^{147}, d- Ser^{151}, d-Ala^{154}, Tic^{155} substitutions. In their assays, this modified peptide maintained similar calcium mobilization EC_{50} levels compared to chemerin-9 but the modified peptide persisted at 100% original peptide concentrations over 4 hours in isolated mouse plasma compared to chemerin-9 which was almost instantly degraded. In vivo, the modified peptide had a half-life in the tens-of-minutes (not explicitly reported by the authors) compared to chemerin-9 which again, was almost immediately degraded.

Another tool used both in vivo and in vitro has been a receptor antagonist for $chemerin_1$, CCX832. Developed by ChemoCentryx as a possible treatment for psoriasis (a call back to the first description of chemerin), the antagonist was discontinued in 2012

during phase I trials. However, this antagonist has single nM IC_{50}s for chemerin at human, rat, and mouse chemerin$_1$. Additionally, binding affinity for chemerin$_2$, CCRL2, and a panel of 19 other chemokine receptors is over 10 uM. While groups have had success using CCX832 in vivo [74, 75], the use of a chemerin$_1$ antagonist is complicated by the discovery that the mouse does not have a functional chemerin$_1$ receptor in the vasculature.

Chemerin systems have been assayed using siRNA since the beginning [38]. Chemerin knockout (KO) [76] and chemerin$_1$ KO [77] mice have also been used to study the function of chemerin in energy metabolism and adipocyte function. It wasn't until recently that the chemerin was knocked out in the Sprague Dawley rat (the primary model for cardiovascular measurements) [78]. These rats did not display any initial differences in blood pressure between wild-type (WT) and KO. When challenged with a DOCA-salt model of hypertension, female KO blood pressure fell below WT blood pressure but male KO blood pressure was above their WT counterparts [78].

2.4 Antisense oligonucleotides

RNA was first isolated in the 1960s but the late 1990s into the early 2000s saw an explosion of reports describing its regulation. Discovery of microRNA (miRNA), a small non-coding RNA that can bind and silence messenger RNA (mRNA), prompted researchers to develop drugs that would function in the same way. These drugs, antisense oligonucleotides (ASOs), are single stranded DNA-like molecules that bind different types of RNA through Watson and Crick base pairing to facilitate RNA destruction. If bound to mRNA, ASOs can temporarily block translation of protein but if

bound to endogenous miRNA, ASOs can enhance the translation of mRNA (that would normally be degraded by miRNA) into protein [79].

The most common and best understood mechanism of action for ASOs is destruction of RNA through the enzyme RNase H. This enzyme is naturally occurring in the nucleus and cleaves RNA in RNA-DNA duplexes in an effort to maintain proper DNA replication. Both DNA and RNA backbones are inherently unstable so progressive modifications have been made to these synthetic DNA backbones to improve drug parameters [79].

The first major discovery was substitution of a non-bridging phosphate oxygen atom with a sulfur. This simple substitution, called a phosphorothioate (PS)-containing oligonucleotide, improves pharmacokinetic stability allowing it to reach its site of action and more efficiently elicits an RNase H response (compared to normal DNA). An ASO with this PS modification is considered a first generation ASO [80].

While there are many other methods of modifying the phosphodiester linkage, second generation ASOs would be defined by modification to the 2' sugar of the backbone. Introduction of a 2'-alkyl, 2'-fluoro, or 2'-O-methyl all increase affinity for target RNA and resist drug degradation by RNase H, but they also reduce RNase H cleavage of the target RNA strand. Using a gapmer strategy, where internal nucleotides have normal backbones and external nucleotides contain the sugar modification, drug developers were able to protect the drug against degradation while still allowing target RNA degradation. Today, the 2'-O-methoxyethyl modification is the most popular second-generation modification because it also seems to reduce non-specific protein binding [80].

To further enhance ASO binding affinity, a method to increase selectivity, researchers bridged the 2'-hydroxyl with the 4'-carbon, essentially creating a bicyclic constrained ligand. There have been several different iterations of creating this constrained drug, but the most recent and most promising uses a (S)-constrained ethyl in a gapmer formulation to maintain efficacy at RNase H [80]. These drugs are referred to as Gen 2.5 ASOs.

ASOs have a broad distribution throughout the body with highest levels in the liver and kidney. Because of their size and charge, they do not cross the blood brain barrier but can be given intrathecally. ASOs have the most success given subcutaneously or intravenously but efforts are underway to co-administer ASO with drugs increasing gut permeability and allow for a possible oral route of administration. To be eliminated, ASOs must be degraded by nucleases into fragments, reducing their binding to plasma proteins, and allowing them to be cleared in the urine by the kidney. Due to nuclease resistance conferred by Gen 2.0 and Gen 2.5 modifications, ASOs typically have half-lives on the order of weeks to months [80].

Toxicology of ASOs are generally divided into two camps: off-target RNA interactions and protein interactions. Off-target RNA interactions have been mitigated through the advancement of preclinical models and bioinformatics. Protein interaction toxicities include activation of Toll-like receptors. The first bicyclic ASOs were hepatotoxic in rodents due to this type of hybridization but the current (S)-constrained ethyl ASOs have largely reduced this effect [80].

The use of conjugated tags can allow researchers to enhance the pharmacokinetic profile of the ASO especially through uptake by a specific organ or tissue. Many lipid and

cholesterol tags, like palmitate and tocopherol, have been used to increase uptake of the drug by the liver. But the most popular liver-specific tag is the trivalent N-acetylgalactosamine (GalNAc). This tag can increase potency of an ASO at a liver target by 30-fold [80].

2.5 Nanoparticles and drugging the fat

While ASOs have been very successful at targeting drugs to the liver, the fat has been a very elusive target. Many of the drugs that are currently used for obesity and diabetes target the central nervous system (phentermine), pancreas (orlistat), or gastrointestinal tract (liraglutide) but very few directly target the adipocyte [81]. Agonists of peroxisome proliferator-activated receptor γ (PPARγ) are used in diabetes increase adipocyte progenitor differentiation and divert free fatty acids away from skeletal muscle and the norepinephrine released by phentermine increases lipolysis but these treatments affect broad systems and have undesirable side effects (weight gain in the former and cardiovascular side effects in the latter) [82]. Recently, one group attempted to deliver a transgene to visceral adipose tissue using a dual-cassette adeno-associated virus where the first cassette contained the targeted transgene and the second contained an albumin promoter which if bound, activated a microRNA that would inhibit expression of the first cassette [83]. Here the authors recognize that one of the difficulties in targeting fat, especially visceral fat, is having a high enough selectivity between the fat and liver.

Nanoparticles have emerged as a drug option that allows for customization of both the targeting ligand and payload. Recently, researchers have attempted to target an shRNA to the visceral adipose tissue (with high selectivity over the liver) using a

nanoparticle coated with a peptide that binds to the prohibitin receptor. Prohibitin is expressed constitutively, especially in the mitochondria, but they found it was also expressed on the surface of adipocytes. Using a nonapeptide called the adipocyte targeting sequence (ATS; CKGGRAKDC) followed by a 9-arginine (9R) to the abdominal and gonadal fat with selectivity over the liver and kidney [84]. These reports have yet to be substantiated by other labs, but they demonstrate the creativity needed to successfully drug this difficult target.

These nanoparticles could also be useful simply as tools used to assay the physiology of chemerin. Here at Michigan State, iron-based nanoworms have been conjugated to a variety of ligands from targeting saccharides to FITC labels. Depending on the ligand conjugated to the nanoparticle and the bodily target, a variety of imaging techniques can be used to visualize the distribution and function of the nanoparticle and ligand. Iron-based nanoparticles can be traced ex vivo with Prussian blue staining or in vivo with magnetic resonance. Fluorescence from FITC tags can also be visualized both ex vivo or in vivo [85]. Nanoparticles provide an opportunity to assay the fat with a wide variety of ligands as well as translate this physiology into a potential therapeutic.

3. Inflammation paradox: making sense of the epidemiology

One issue that has plagued the advancement of chemerin both in the clinic and at the lab bench is the discussion of whether chemerin is inflammatory or anti-inflammatory. On the whole, human epidemiological literature has labeled plasma chemerin as inflammatory derived from positive associations with various inflammatory diseases. But what is to be made of the obvious healthy effects of chemerin in the fat. There is a

paradoxical dichotomy of chemerin that must be considered during any investigation of chemerin's potential mechanisms.

3.1 Pro-inflammatory attributes

The first and best characterization of chemerin came from synovial fluid [42]. Synovial fluid is present in and around the major joints in the body. With early reports that chemerin might be involved as a chemoattractant in psoriasis [40], synovial fluid would be a natural place to look for a chemokine that might influence arthritis [42]. This manuscript on synovial fluid, along with a series of reports to follow, provided mechanistic support for chemerin's positive role in chemotaxis of immune cells and inflammation [44, 46, 72, 73].

The epidemiological literature followed suit with reports of chemerin being positively associated with a number of inflammatory pathologies. Clinicians found positive associations with plasma chemerin levels and non-alcoholic fatty liver disease [86-88], atherosclerosis [26, 89, 90], dyslipidemia [37, 91], preeclampsia [92], c-reactive protein [93] type II diabetes [27, 35], certain types of cancer [51], both systolic and diastolic blood pressure [24-30], and BMI/obesity [24, 26, 29, 31-34]. Complimentary to chemerin's positive association with blood pressure, there is preliminary mechanistic data proposing that chemerin is contractile to the vasculature [39].

Both the mechanistic and epidemiological data are overwhelming but in considering current and future chemerin advances, it will be important to qualify these data in a few ways. First, *where was chemerin measured?* These data only describe chemerin as it pertains to the plasma or plasma filtrate (e.g. synovial fluid). Second, *where*

is the chemerin$_1$ receptor? The chemerin$_1$ receptors in most of these cases are present on immune cells and smooth muscle cells. Third, *what isoform of chemerin is being measured?* The tools to measure isoforms, especially in clinical data, is still in its infancy but many of these reports are assumed to be referring to the S^{157} isoform. Interestingly, there is a large amount of mechanistic data for chemerin that indicates a potential anti-inflammatory role.

3.2 Anti-inflammatory attributes

While the first report of chemerin in psoriasis proposed an anti-inflammatory effect of chemerin [40], the first mechanistic report of the anti-inflammatory role of chemerin in the immune system was published by Cash *et. al.* in 2008. They found that a specific isoform of chemerin, C15 (a 15 amino acid peptide analogous to recombinant chemerin A^{154}), inhibited macrophage and neutrophil recruitment in peritonitis in a manner dependent on chemerin$_1$ expression [94]. The initial studies that sorted out the activation properties of chemerin on chemerin$_1$ showed that in an artificial cell culture system, C15 did not have any affinity for chemerin$_1$ [44] but the Cash *et. al.* studies were all performed in vivo. A similar study in lipopolysaccharide-induced lung disease by a different group also saw chemerin$_1$-dependent anti-inflammatory effects of C15 on dendritic cells and macrophages [95].

Resolvin E1 (a lipid ligand) has been proposed to interact with chemerin$_1$ in an anti-inflammatory manner [96]. This lipid bound to the receptor on dendritic cells attenuated nuclear factor-κB signaling, inhibited IL-12 production, and reduced chemotaxis. In endothelial cells, chemerin binding with chemerin$_1$ also attenuated nuclear

factor-κB signaling which resulted in increased nitric oxide signaling. Vascular adhesion factor-1 and p38 were also inhibited further supporting an anti-inflammatory niche for chemerin in the vasculature [97]. Coincidentally, chemerin-9 does not exhibit a contractile effect on the vasculature unless the endothelium is removed or damaged [39].

In addition to the antagonist or biased agonist (possible mechanism of Resolvin E1) actions of chemerin, we must consider that the basis for chemerin's classification as an adipokine lies in a healthy support of adipocyte maturation [35, 38]. Without chemerin or its receptor in the fat, it fails to differentiate or accumulate the appropriate amount of lipid. With the majority of clinical data touting the pathological associations of plasma chemerin with blood pressure and obesity and mechanistic data proposing the beneficial effects of local chemerin in the fat, chemerin is in need of research that will elucidate connections between the fat an vasculature.

3.3 At a crossroads of mechanistic and clinical data

In the mechanisms of obesity, adipose tissue dysfunction is often thought of as a slow transition of healthy fat to "sick" fat [98]. As fat goes through this transition, its secretory profile changes as levels of adipokines and inflammogens like adiponectin, TNF-alpha, leptin, and chemerin go up and down. Given the dual roles of chemerin in inflammation already discussed, it is likely that the expression and localization of chemerin are determining characteristics in the role of chemerin in the body.

One of the places in the body we can look for such a change is the fat surrounding the mesenteric resistance vessels. This perivascular adipose tissue (PVAT) is a white fat uniquely situated around a vessel responsible for a large amount of vascular resistance

[19]. This fat is also well-documented to express both chemerin and chemerin$_1$ [35, 38, 39]. By studying both the mechanistic and in vivo importance of chemerin in the mesenteric PVAT, we can clarify the method by which chemerin leads to obesity-associated hypertension and possibly identify chemerin-related targets for treatment of this disease.

HYPOTHESIS

Overall Hypothesis: Adiposity-associated hypertension is promoted by the release of chemerin from mPVAT (primarily adipocytes).

Aims Overview

1. Chemerin influences the adipogenesis of the mPVAT and has the ability to directly act at on the blood vessel.
2. Knockdown of chemerin reduces blood pressure in adiposity-associated hypertensive rats vs. control rat models.

AIM 1.1: Mechanism of chemerin stimulation in vascular smooth muscle cells

This chapter was adapted from:

Ferland DJ, Darios ES, Neubig RR, Sjögren B, Truong N, Torres R, Dexheimer TS, Thompson JM, Watts SW. Chemerin-induced arterial contraction is Gi- and calcium-dependent. Vascul Pharmacol. 2017 Jan;88:30-41. doi: 10.1016/j.vph.2016.11.009.

1. Introduction

Obesity and hypertension are pathologies that continue to become more prevalent around the world, particularly in adolescent populations [99]. Chemerin is a relatively novel protein with the potential to connect these two diseases. Identified as an adipokine [35], serum chemerin concentrations have been positively correlated with increased levels of human white adipose tissue [24], increased body mass index [32, 88], obesity [88], and even childhood obesity [31]. Loss of white adipose tissue through exercise or bariatric surgery reverses the levels of circulating chemerin [33]. Additionally, the active form of chemerin (chemerin S^{157}) is positively associated with blood pressure in both humans [26] and mice [25].

Chemerin is produced by hepatocytes and adipocytes [35] and may be converted to an active isoform before it leaves the cell [38]. There are currently three receptors known to bind chemerin: CCRL2 [68], GPR1 [62] and the chemerin receptor [53]. CCRL2 binds chemerin without transducing a signal [68]. GPR1 is able to actively transduce a signal through G_i proteins, RhoA, and MAPK pathways [66]. Our laboratory was the first to demonstrate that chemerin-9 (a nonapeptide derived from the C-terminus of the S^{157} isoform [44]) directly caused isometric contraction of aorta through the chemerin receptor [39, 100]. Although the chemerin receptor has been known by several names in the literature (CMKLR1, ChemR23 or DEZ), the currently accepted name for the receptor, as given by *IUPHAR/BPS*, is the “chemerin receptor” [101]. Although GPR1 and CCRL2 can bind chemerin, the term “chemerin receptor” describes a specific protein that is separate from GPR1 or CCRL2.

When chemerin signals through the chemerin receptor, it recruits a wide range of second messengers in a cell-specific manner: ERK stimulates chemotaxis in immune cells [57], p38 and Akt stimulate angiogenesis in endothelial cells [58], and PKC can trigger internalization of the receptor [60]. Our lab has shown that chemerin-9-induced isometric contraction is potentiated by phenylephrine and prostaglandins *via* a calcium-dependent mechanism. Additionally, chemerin-9 also directly simulated chemerin receptor-dependent contraction of the rat aorta when the endothelium was removed [39]. This broad heterogeneity of potential signaling mechanisms led us to ask the mechanistic question of how chemerin brings about smooth muscle contraction in a calcium-dependent manner that could contribute to the elevated total peripheral resistance commonly found in hypertension.

Calcium signaling is an essential part of smooth muscle contraction. After a flux of calcium into the cytoplasm, it binds and activates calmodulin which activates myosin light chain kinase (MLCK) to phosphorylate myosin heads, promote cross-bridging with actin, and allow contraction [102]. Although calcium is not the direct activator of myosin-actin cross-bridging, it is still a necessary and easily quantifiable step.

With the hypothesis that chemerin causes constriction of vascular smooth muscle through the chemerin receptor in a calcium-dependent manner, we first set out to characterize the pathways that are essential to support contraction of isolated aorta. We started with pharmacological inhibitors that target processes known to be important to smooth muscle signaling: verapamil for the L-type calcium channel [103], PP1 for Src [104], Y27632 for Rho kinase [105], PD098059 for Erk MAPK [100], and U73122 for PLC [106]. Because of the previous G_i protein link to the chemerin receptor [42], PTX was also

tested. In whole tissue, there are different cell types that can communicate to influence the concerted action that results in contraction. Because endothelium-denuded aorta showed the greatest response to chemerin [39, 100], we designed parallel studies to investigate how the smooth muscle cells in the tissue are responsible for the physiological effects of chemerin on aortic constriction. The same inhibitors that produced significant reductions of contraction in aortic rings were tested in rat aortic smooth muscle cultures using a calcium fluorophore in a real-time calcium flux detection assay. By comparing the results from these two approaches, we identified which pathways in the smooth muscle are responsible for a chemerin-induced contraction of the vasculature.

2. Methods

2.1 Animal use

All procedures that involved animals were performed in accordance with the institutional guidelines and animal use committee of *Michigan State University* and the *NIH Guidelines on Use of Lab Animals*. Animals were maintained on a 12/12 light/dark cycle at a temperature of 22-25^{o}C. Normal male Sprague-Dawley rats (225–300 g; Charles River Laboratories, Inc., Portage, MI, USA) were used. Prior to all dissection, rats were anesthetized with Fatal Plus® (60-80 mg/kg, i.p.).

2.2 Chemicals

Chemerin-9 was purchased from GenScript (#RP20248, Piscataway, NJ, USA), recombinant chemerin from BioVision (#4002, San Francisco, CA, USA), and both solubilized in deionized water. Pertussis toxin (#P7208), angiotensin II (#A9525),

acetylcholine (#A6625), clonidine (#C7897) and phenylephrine (#P6126) were obtained from Sigma Chemical Company (St. Louis, MO, USA). Verapamil (#0654), Y27632 (#1254), PD098059 (#1213), and PP1 (#1397) were purchased from Tocris Bioscience (R & D, Minneapolis, MN, USA). U73122 (#70740) was purchased from Cayman Chemical (Ann Arbor, MI, USA). CCX832 was a gift from Chemocentryx (Mountain View, CA, USA).

2.3 Isometric contraction

Aortic rings [cleaned of perivascular adipose tissue (as an endogenous chemerin source), and endothelium-denuded] were mounted in tissue baths for isometric tension recordings using Grass transducers (FT03) and PowerLab data acquisitions running Chart 7.0 (ADInstruments, Colorado Springs, CO, USA). The endothelium was removed so as to focus on a vascular smooth muscle response. Baths contained standard physiological salt solution (PSS) [mM: NaCl (130.00); KCl (4.70); KH_2PO_4 (1.18); $MgSO_4$-$7H_2O$ (1.17); $CaCl_2$-$2H_2O$ (1.60); $NaHCO_3$ (14.90); dextrose (5.50); and $CaNa_2EDTA$ (0.03), pH 7.2], warmed to 37ºC and aerated (95% O_2/CO_2). Rings were placed under optimum resting tension (4 grams) and equilibrated for one hour, with washing, before exposure to compounds. Administration of an initial concentration of 10 μM phenylephrine (PE) was used to test arterial viability and the absence of the endothelium was verified by a lack of acetylcholine (1 μM)-induced relaxation of a half-maximal PE-induced contraction; this was <10% in all tissues included for analysis.

Tissues were then washed out and incubated with either vehicle (water, 0.1% ethanol, 0.1% DMSO, or 0.01% DMSO) or one of the following inhibitors for one hour: L-

type calcium channel inhibitor verapamil, Rho kinase inhibitor Y27632, PLC inhibitor U73122, Erk MAPK inhibitor PD098059, Src inhibitor PP1 or CCX832. Following this incubation, cumulative response curves were generated to the agonist chemerin-9 (10^{-10} – $3x10^{-6}$ M). Three different isolated tissue bath systems with four individual organ baths were used to generate these curves (no system or bath dependence of results), vehicle or inhibitors were randomized but incubated with tissues from the same animal when possible, and tissues were exposed to only one vehicle or inhibitor. In other experiments, chemerin-9 (1 μM) was incubated with tissues for zero or five minutes in the isolated tissue bath, and tissues were frozen in liquid nitrogen at this point in contraction for western blot analyses.

For the study of pertussis toxin (PTX) in isometric contraction, perivascular adipose tissue and endothelium were removed from paired aortic rings before incubating them on a rotator overnight at 37ºC in Complete Medium (described in *cell culture* below) with either PTX (1000 ng/mL) or vehicle (water). Tissues were washed in PSS, placed in a tissue bath (conditions described above), and pulled to a resting tension of 4 grams. After the 10 μM PE challenge and 1 μM acetylcholine test to confirm endothelial removal, tissues were challenged with a cumulative response curve to chemerin-9 and clonidine (α_2 adrenergic agonist). The order of agonists, baths, and force transducers was randomized.

2.4 Cell culture

Aorta was removed and cleaned of fat and endothelium in a sterile environment with phosphate buffered saline (PBS) containing 2% penicillin-streptomycin (P/S)

(#15140122, Gibco/Thermo Fisher, Waltham, MA, USA). Sections were placed lumen side-down on a p60 dish and allowed to grow in Dulbecco's Modified Eagle's Medium (DMEM, Gibco/Thermo Fisher) with 45% Fetal Bovine Serum (FBS; #16000044, Gibco/Thermo Fisher), 1% P/S, and 1% glutamine (#25030081, Gibco/Thermo Fisher). Once confluent, cells were passed and allowed to grow in Complete Medium (DMEM, 10% FBS, 1% P/S, and 1% glutamate). Smooth muscle was confirmed by an immunocytochemistry stain with FITC-conjugated smooth muscle alpha-actin (#F3777, Sigma Chemical; method described below in *immunocytochemistry*). Cells were harvested for use in all experiments between passage 2 and passage 5.

2.5 Calcium kinetics

Initial studies titrated the concentration of smooth muscle cells between 5,000 and 20,000 cells/well to determine the lowest seed density with discernable signal in a 384-well plate. We recognize that *in vivo* smooth muscle cells are tightly packed and denser than what we have titrated, but this titration was necessary to maintain the high sensitivity of the instrument and is standard practice in the field. Once optimized, smooth muscle cells were suspended in Complete Medium and allowed to incubate (37°C and 5% CO_2) in a 384-well plate overnight at a density of 10,000 cells/well. If applicable, PTX (500 ng/mL) was added to the media for an overnight incubation. At the t-60 minutes time point before agonist injection, excess media was washed off and replaced by calcium dye (Fluo-4 NW, #F36206, Thermo Fisher). Calcium dye buffer contains 98% HBSS [#14025092, Thermo Fisher; mM: $CaCl_2$ (1.26), $MgCl_2$-$6H_2O$ (0.49), $MgSO_4$-$7H_2O$ (0.41), KCl (5.33), KH_2PO_4 (0.44), $NaHCO_3$ (4.17), NaCl (137.93), Na_2HPO_4 (0.34), dextrose

(5.56)] and 2% HEPES (#15630106, Thermo Fisher). The plate was incubated at 37°C for 30 minutes, followed by 30 minutes at room temperature. Inhibitors were manually added along with the calcium dye at the t-60 minutes time point. Calcium dye (and inhibitor, if applicable) was not washed off. The assay plate was loaded directly into the FDSS/μcell (Hamamatsu Photonics, Japan) along with separate compound plates (one containing chemerin receptor antagonist for a t-170 seconds injection and one for an agonist t=0 injection). Recording began at the t-3 minutes time point and both the t-170 seconds and t=0 injections were made directly by the FDSS/μcell. For wells that received a manual t-60 minutes injection, there was no volume added at the t-170 seconds injection. Recording occurred every second starting at t-3 minutes continuing through t+5 minutes. A sub-baseline value was taken at t+2 seconds (after injection of the agonist). Reported values are in the format of “max-min” where “max” equals the maximum value occurring after t+2 seconds and “min” equals the t+2 seconds sub-baseline. Each biological replicate was analyzed in triplicate and the N values represent the total number of calcium curves analyzed.

2.6 Immunocytochemistry

Cells were suspended in Complete Medium and allowed to adhere to a coverslip overnight, washed with PBS, then fixed with chilled 1:1 acetone-methanol. If applicable, cells were washed with PBS and incubated for 10 minutes with wheat-germ agglutinin tagged with an Alexa Fluor 555 (W32464, Thermo Fisher). Cells were washed with PBS and blocked for one hour (horse serum, #S-2000, Vector Laboratories, Burlingame, CA, USA) at room temperature followed by an incubation with a FITC-conjugated alpha

smooth muscle actin (anti-mouse, 1:500 concentration), GPR1 antibody (anti-mouse, clone 43.28.4, gift from Dr. Brian Zabel, 1:100 concentration), or chemerin receptor antibody (anti-mouse, #398769, Santa Cruz Biotechnology, Dallas, TX, USA, 1:50 concentration) for one hour at 37°C. After a wash with PBS, a FITC secondary (Alexa Fluor 488, #A11029, Thermo Fisher, 1:1000 concentration) was applied for 30 minutes at room temperature (not needed for FITC-conjugated alpha smooth muscle actin) followed by a final wash with PBS. Prolong Gold with DAPI (#P36935, Gibco/Thermo Fisher) was added before sealing the coverslip to a slide with nail polish. Imaging and normalization for autofluorescence was done using the Olympus FluoView 1000 Confocal Laser Scanning Microscope at Michigan State University Center for Advanced Microscopy. Minimum detection thresholds were set using the no-primary control. Images were taken every 0.2 μm for the entire depth of the cell (about 4-5 μm). Using DAPI to match depth, images were taken from the same level and paired with the no-primary control. To help visualize the signal, all channels were enhanced equally on both primary and no-primary controls using Adobe Photoshop CS6.

2.7 Western blot analyses

For Erk MAPK westerns, protein was isolated from previously frozen vessels (see *Isometric contraction*) homogenized in the presence of tyrosine, threonine and serine phosphatase inhibitors (10 mg/mL leupeptin, 10 mg/mL aprotinin, and 10 mM PMSF) and western blotting procedures were performed on equivalent amounts of total protein per lane, as measured by a bicinchoninic acid kit (Sigma Chemical Co, St. Louis, MO USA). The positive control was calyculin treated Jurkat cells (Cell Signaling, MA, USA).

Nitrocellulose membranes were blocked for three hours in 5% bovine serum albumin [4°C, TBS-0.1% Tween + 0.025% NaN_3]. Primary antibody for Erk (Cell Signaling #4696S, 1:1000 in 5% milk; Boston, MA, USA) or phosphoErk (Millipore #05-797R, 1:1000 in 5% milk; Billerica, MA, USA) was incubated with blots overnight at 4°C with rocking. Blots were washed (3 times, 10 minutes each) in TBS-0.1% Tween, then incubated with IRDye 680LT goat anti-mouse (Li-Cor #926-68020, 1:1000 in Li-Cor Blocking Buffer; Lincoln, Nebraska, USA) for testing Erk or IRDye 800CW goat anti-rabbit (Li-Cor #926-32211, 1:1000 in Li-Cor Blocking Buffer) for testing phosphoErk. The blots were visualized using the Odyssey Infrared Imaging System and the Odyssey FC Infrared Imaging System (Li-Cor Biosciences, Lincoln, NE, USA). Blots were reprobed for alpha-actin (#113200, EMD Millipore, Billerica, MA, USA) as a loading control.

For the chemerin receptor, GPR1 and calponin-1, protein was isolated from smooth muscle cells isolated as described in section 2.4. Cells were placed in RIPA buffer (R3792, Teknova, Hollister, CA USA; with added 10 mg/mL leupeptin, 10 mg/mL aprotinin, and 10 mM PMSF) and rocked at 4°C for one hour. The positive control for GPR1 was rat adrenal gland and for the chemerin receptor was rat aorta. Both were isolated in-lab and homogenized by liquid nitrogen and mortar/pestle. Protein was measured by a bicinchoninic acid kit (Sigma Chemical Co). Standard western blotting procedures were performed on positive controls loaded at 75 µg of protein/lane and rat aortic smooth muscle cell lysates at 25 µg of protein/lane. This difference was necessary because of the concentrated nature of the smooth muscle cell lysate. For this reason, the quantity of signal from smooth muscle cell lysates were not compared to their positive controls. Nitrocellulose membranes were blocked with 4% chick egg ovalbumin (A5378,

Sigma Chemical). Primary antibody for the chemerin receptor (1:100, anti-mouse, #398769, Santa Cruz Biotechnology), GPR1 (1:250, anti-mouse, clone 43.28.4, gift from Dr. Brian Zabel), calponin-1 (anti-mouse, 1:2000, #MA5-11620, Thermo Fisher), and beta actin (anti-goat, 1:500, #ab8229, Abcam, Cambridge, MA USA) were added one at a time with individual overnight incubations at 4^{o}C. While GPR1 and the chemerin receptor were not visualized on the same blot, the remainder of the bands were separated by molecular weight and wavelength of the secondary antibodies. Blots were washed (3 times, 10 minutes each) in TBS-0.1% Tween, then incubated with IRDye 680LT donkey anti-goat (Li-Cor #926-68024, 1:1000 in Li-Cor Blocking Buffer) for testing beta actin or IRDye 800CW goat anti-mouse (Li-Cor #926-32210, 1:1000 in Li-Cor Blocking Buffer) for testing the chemerin receptor, GPR1, or calponin-1. The blots were visualized using the Odyssey FC Infrared Imaging System. Calponin-1 was used as a loading control for quantification of the smooth muscle cell lysates. Beta actin was used to visualize the presence of protein from the rat adrenal gland (does not contain a substantial amount calponin-1).

2.8 Data analysis and statistical procedures

Contractility results are reported as means ± SEM. Contraction from baseline tone is reported as a percentage of the initial contraction to PE. All EC_{50}, E_{max}, pA_2, curve fitting, t-test and analysis of variance (ANOVA) tests were performed using GraphPad Prism 6.0 (La Jolla, CA, USA). For western analyses of Erk MAPK, each lane shown represents a separate animal, and densitometry was performed using NIH Image J (v 1.45) for the number of animals indicated in parentheses. Changes in ERK or pERK are represented as fold-change from vehicle by dividing chemerin-9-incubated densitometry

by vehicle-incubated densitometry. pERK values were not divided by ERK values in an effort to reduce bias in their interpretation. For western analyses of GPR1, the chemerin receptor, and calponin-1, Li-Cor Image Studio (v 5.2.5) was used. For two group statistical comparisons, the appropriate Students t-test was used. For one-way ANOVA, a Tukey's post hoc test was used and for two-way ANOVA, a Bonferroni correction was made. A p value ≤ 0.05 was considered statistically significant.

3. Results

3.1 Chemerin causes a contraction and calcium flux that is G_i-dependent

Chemerin-9 (highlighted from the full S^{163} isoform, Figure 3A), a nonapeptide derived from the C-terminus of the recombinant chemerin S^{157} isoform (all experiments referencing recombinant chemerin were performed with the S^{157} isoform) [44], contracted the isolated rat aorta (Figure 3B). Smooth muscle cells explanted from aorta were processed for a molecular interrogation of muscle activation. Presence of aortic smooth muscle cells in culture was confirmed by alpha actin staining (Figure 3C).

These cells were used in calcium kinetics experiments where the procedure for the addition of inhibitor/antagonist and agonist to the cells is graphically outlined in Figure 3D. In these cells, chemerin-9 and recombinant chemerin S^{157} increased cytosolic calcium in a concentration-dependent manner (Figure 3E). Calcium response with recombinant chemerin was not assessed at same concentration range used for chemerin-9 because we were limited in our supply of recombinant chemerin, and a maximal response was already observed at 100 nM. These basic measures of chemerin-9 and recombinant chemerin-induced calcium flux in the smooth muscle cells are also used in later figures

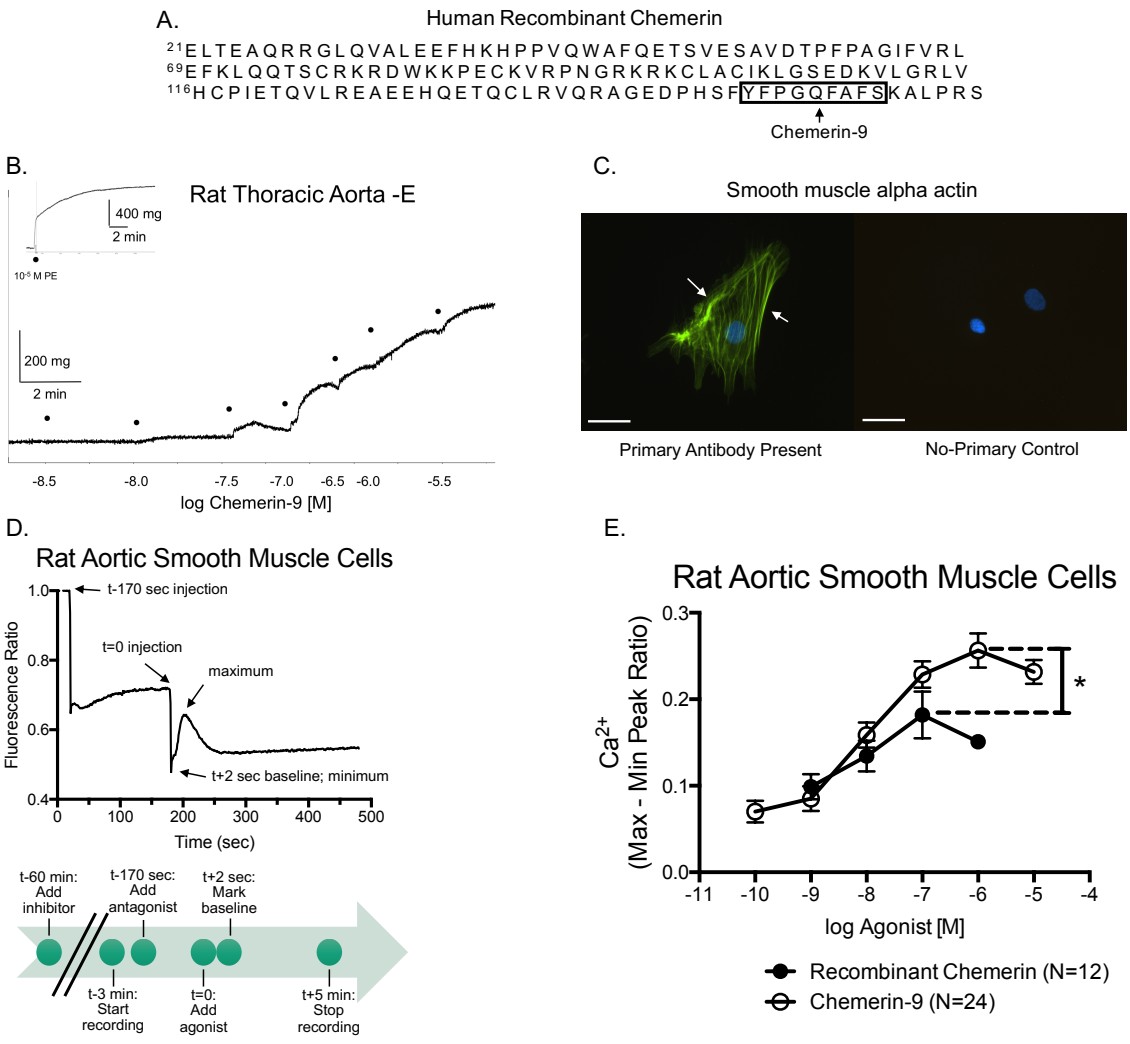

Figure 3: *Chemerin stimulates rat aorta and smooth muscle cells*

A) The amino acid sequence for human chemerin S^{163} after cleavage of the preprochemerin fragment (aa 1-20). The sequence for the chemerin-9 peptide is surrounded by a black box. B) A representative tracing of a chemerin-9 concentration-response curve in rat thoracic aorta without endothelium measuring isometric contraction. A phenylephrine (PE) contraction used to normalize results is shown in the upper-left corner. C) The presence of isolated smooth muscle cells was confirmed by immunofluorescence with smooth muscle alpha-actin. This image is representative of four independent isolations. White bars represent 50 μm and arrows point to areas of interest. D) A representative tracing of a calcium mobilization response. The process by which these cells were assayed is graphically derived from the *Methods*. E) Smooth muscle cells display a concentration-dependent calcium response to chemerin. Magnitude of the calcium peak is measured by taking a "max – min" value of the originally normalized "ratio" tracing. Points/bars represent mean ± SEM for the number of replicates performed. * represents a $p < 0.05$.

to make comparisons with different conditions. The E_{max} (top value of the curve) of recombinant chemerin (0.17 ± 0.02 arbitrary units) was smaller than chemerin-9 (0.25 ± 0.01 arbitrary units) by 40% (significant with a $p<0.05$) but their potencies were not significantly different (-log EC_{50}[M]: 8.1 ± 0.7 and 8.0 ± 0.2 respectively; Figure 3E). The calcium response stimulated by both agonists was abolished by pertussis toxin (PTX) (Figure 4A and B). The viability of cells after incubation with PTX was confirmed by observing a normal positive calcium elevation to angiotensin II in cells with and without PTX (Figure 4C). PTX, importantly, also reduced chemerin-9-dependent contraction of an aorta in an isolated tissue bath (Figure 4D). Tissue viability after overnight PTX incubations was confirmed by a phenylephrine contraction (used to normalize the data; 1920 ± 240 mg force and 1330 ± 230 mg force for vehicle and PTX treatment, respectively; mean ± SEM, not statistically significant $p = 0.114$). Clonidine (α_2 adrenergic agonist and G_i-coupled) was used as a positive control for PTX (Figure 4E). This indicates that the receptor type(s) that chemerin binds to in the rat aorta are G_i-coupled.

3.2 Chemerin signaling in smooth muscle most likely acts through the chemerin receptor

CCX832 is a selective antagonist for the chemerin receptor that does not show affinity for GPR1 or CCRL2 [16]. As replicated from previous studies [16], 100 nM CCX832 reduced chemerin-9-dependent contraction of the aorta (Figure 5A). Compared to Figure 4D, the E_{max} of chemerin-9 and vehicle was higher but not to a statistically significant degree. This difference can be explained by the incubation time needed to create a proper control for the PTX experiments (24 hours) versus the fresh tissue shown here. Calcium flux in smooth muscle cells also exhibited a concentration-dependent

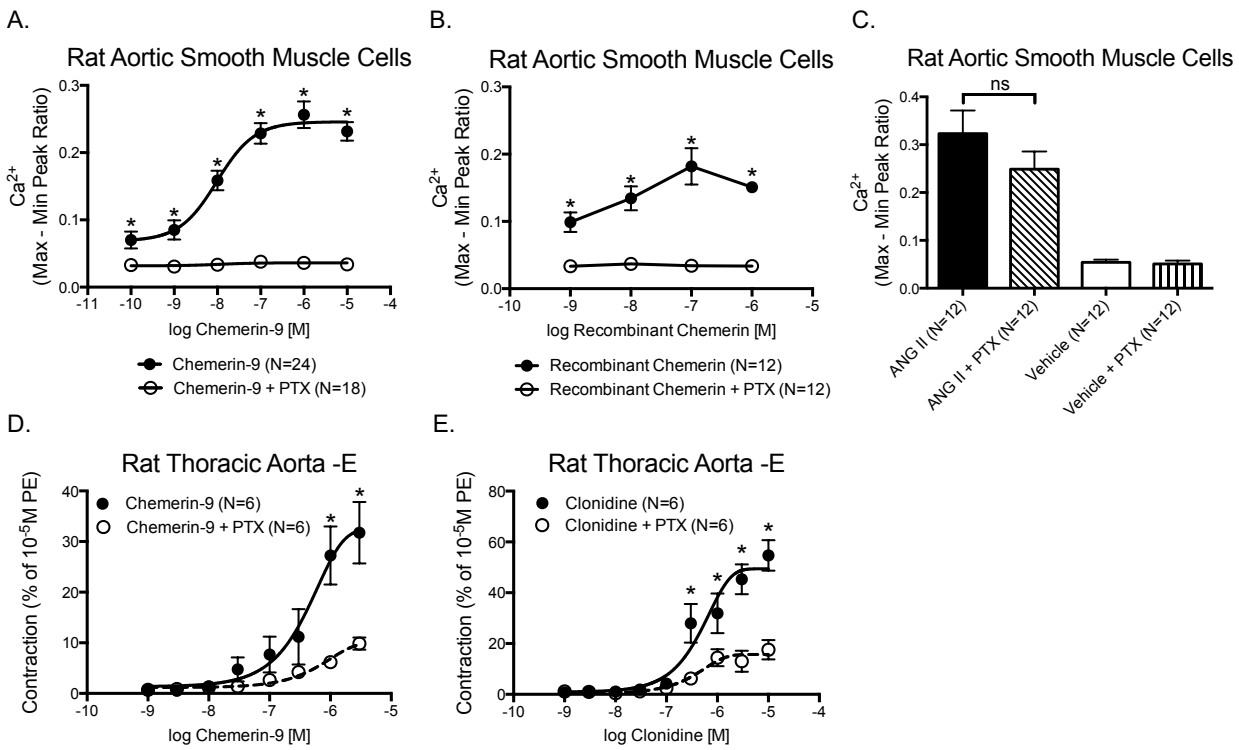

Figure 4: *Chemerin responses are blocked by PTX*

Concentration-response curves measuring calcium peaks of chemerin-9 (A, best fit line shown; portions reproduced from figure 1E) and recombinant chemerin (B; portions reproduced from figure 1E) when treated with and without pertussis toxin (PTX, 500 ng/mL). Magnitude of the calcium peak is measured by taking a "max – min" value of the originally normalized "ratio" tracing. C) Separate wells in the same plate were treated with angiotensin II (ANG II, 1 μM) with and without PTX (500 ng/mL). This was used to confirm cell viability after treatment with PTX. D) Chemerin-9-dependent isometric contraction was inhibited by PTX (1000 ng/mL). E) Inhibition of a clonidine-dependent contraction (α_2-adrenergic agonist) by PTX confirms that the PTX reached the desired target (G_i protein). Points/bars represent mean $\pm$ SEM for the number of replicates performed. * represents a $p < 0.05$ when compared to the vehicle/agonist of the same concentration.

reduction by CCX832. A Schild analysis of chemerin-9 with CCX832 gave a pA_2 of 8.2 and a clear concentration-dependent, competitive relationship with chemerin-9 (Figure 5B; significance was specifically calculated between chemerin-9 + vehicle and chemerin-9 + 1 μM CCX832 to make comparisons with recombinant chemerin). However, while 1 μM CCX832 produced a 30-fold shift of EC_{50} with chemerin-9 and significantly inhibited 1, 10, and 100 nM chemerin-9-dependent calcium flux, it did not shift recombinant chemerin-dependent calcium flux (Figure 5C).

Immunocytochemistry with confocal microscopy examined smooth muscle cells for GPR1 and chemerin receptor, the two possible receptors that could be responsible for chemerin-9 signal transduction. The rat adrenal and rat brain were used as positive controls for GPR1 and chemerin receptor, respectively. These slides were co-stained with wheat-germ agglutinin to provide context to the cell (Figure 6A; because cells were permeabilized, most glycoproteins including those in the endoplasmic reticulum and Golgi were also stained). Use of the antibodies and positive controls for the chemerin receptor and GPR1 in immunohistochemistry has been validated by previously published reports [16,28]. GPR1 was not present in smooth muscle cells while the chemerin receptor was present and localized to the perimeter of the cell.

To support the relative amount of signal from GPR1 and the chemerin receptor seen in figure 4A, western blots were performed probing for the chemerin receptor, GPR1, and calponin-1 (Figure 6B). The presence of calponin-1 confirmed our isolation of smooth muscle cells from the rat aorta. In our western blots, we see expression of the chemerin receptor and no expression of GPR1 which supports the conclusions drawn by the

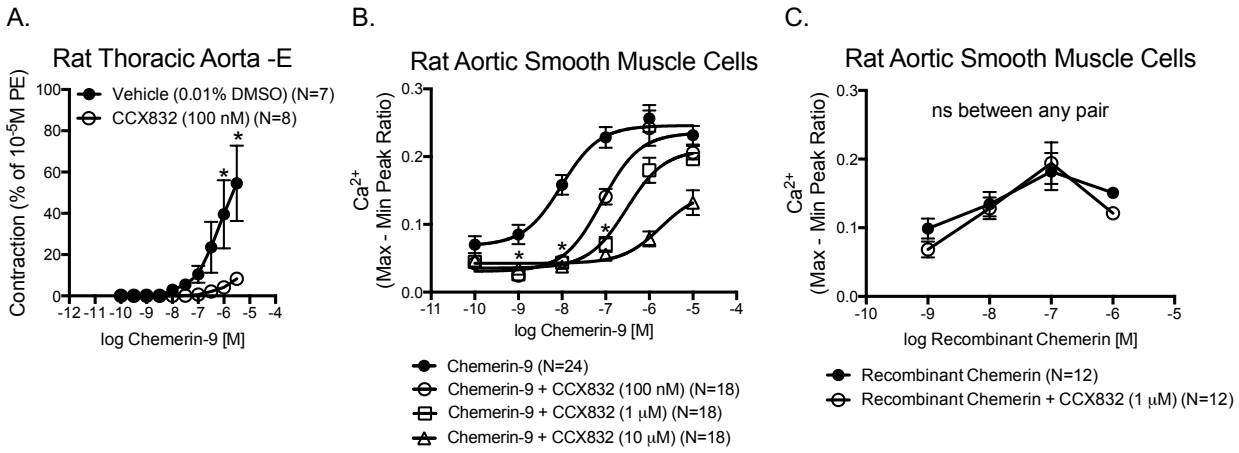

Figure 5: *Chemerin acts through the chemerin receptor*

A) A cumulative response curve measuring isometric contraction with and without CCX832 (100 nM). This molecule antagonized the receptor for chemerin-9 and inhibited chemerin-9-dependent contraction. B) A CCX832 concentration-dependent shift of chemerin-9 calcium flux shows a concentration-dependent and competitive relationship between chemerin-9 and CCX832 (portions reproduced from figure 1E). * represents a $p < 0.05$ for chemerin-9 versus chemerin-9 + CCX832 1 μM only (for comparisons to figure 3C). C) Recombinant chemerin with CCX832 (1 μM) did not change calcium flux (portions reproduced from figure 1E). Points represent mean ± SEM for the number of replicates performed. Magnitude of the calcium peak is measured by taking a "max – min" value of the originally normalized "ratio" tracing.

immunocytochemistry – the chemerin receptor predominates while GPR1 is virtually absent.

3.3 Chemerin-9 activation of smooth muscle cells lacks Erk MAPK signaling

Because of a previous report citing a Erk MAPK mechanism in chemerin-dependent vascular contraction [17], we assessed PD098059 as an inhibitor of this contraction. In the hands of multiple researchers, 1 μM PD098059 did not inhibit chemerin-9 contraction in rat aorta (Figure 7A). Levels of phosphorylated Erk were measured both with and without incubation with 1 μM chemerin in the tissue bath (Figure 7B and C). In tissues receiving a bolus of chemerin-9, the contraction achieved was plateaued at a 5-minute time point and was 40.0±5.22% PE (10 μM) initial contraction. These tissues were frozen and homogenized for analysis in western blots. Each lane represents tissue from one rat, with the blot showing two independent experiments for 0 min and 5 min chemerin exposure where both 0 and 5 minute samples were taken from the same rat (internal control). Consistent with the lack of effect of PD098059 on chemerin-9-induced contraction, western analyses supported no statistically significant increase in Erk MAPK phosphorylation in tissues contracted with chemerin-9 [pErk MAPK = 1.12±30.14 (44 kDa) and 1.11±0.29 (42 kDa) fold-increase with chemerin-9 contraction compared to vehicle, $p>0.05$].

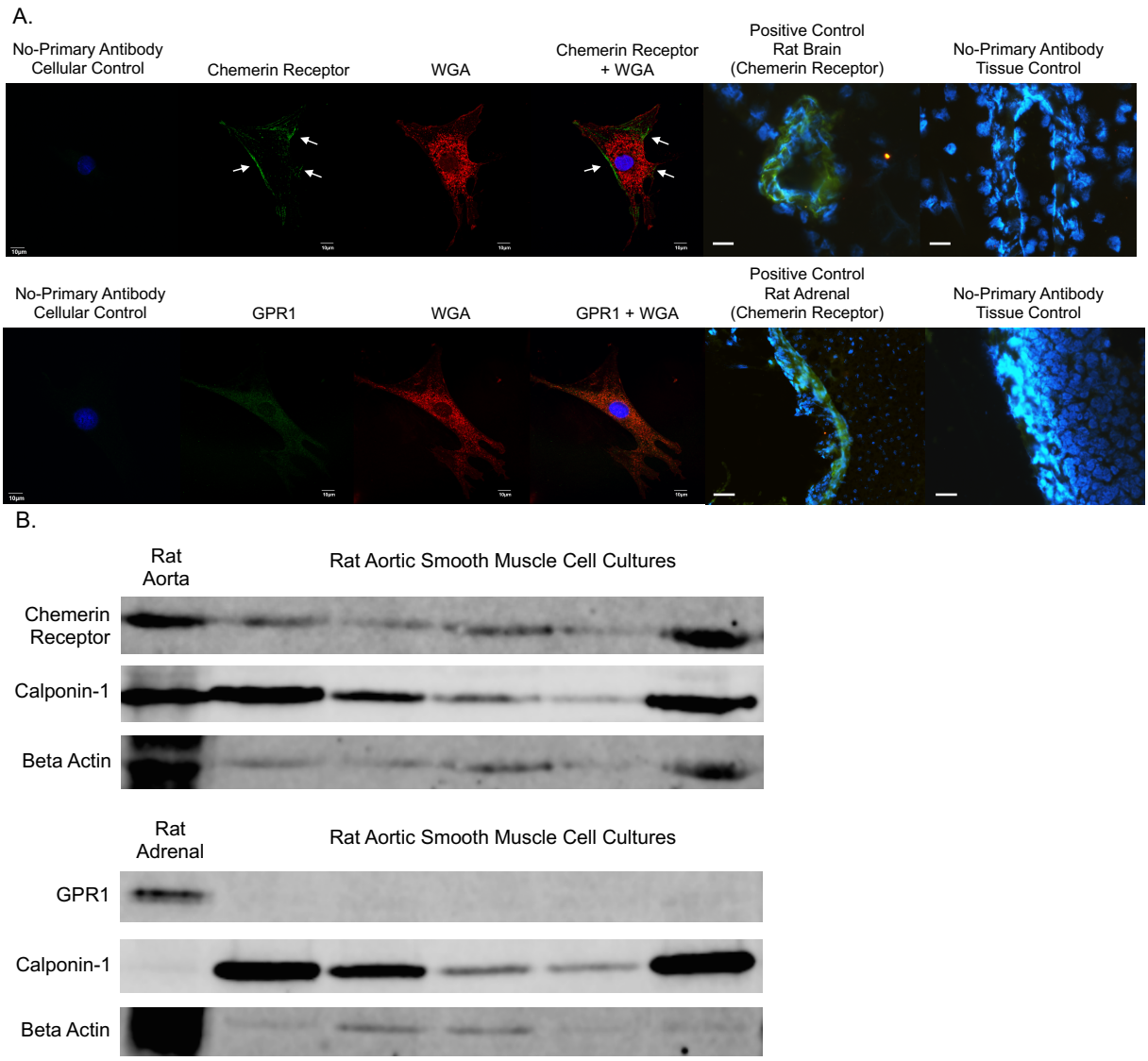

Figure 6: *The chemerin receptor predominates at the cell perimeter over GPR1*

A) Immunocytochemistry imaged using confocal microscopy. The chemerin receptor and GPR1 are imaged in green (FITC), wheat-germ agglutinin (WGA) is in red (TRITC), and the nucleus is stained blue (DAPI). Only one slice is shown but from the same depth in each cell. These images are representative of four independent isolations. No-primary cells/tissue controls received secondary antibody but no primary antibody. Positive controls for both GPR1 (rat adrenal) and chemerin receptor (blood vessel in rat brain) are also shown. Arrows represent points of interest. White bars represent 10 μm in the samples and 50 μm in the positive controls (images were taken at different magnifications). B) Representative images of the chemerin receptor, GPR1, calponin-1, and beta actin expressed in rat aortic smooth muscle cells. Each lane of the rat aortic smooth muscle cell cultures represents an isolation from a different animal (N=5). Positive controls (rat aorta for the chemerin receptor and rat adrenal for GPR1) are also shown.

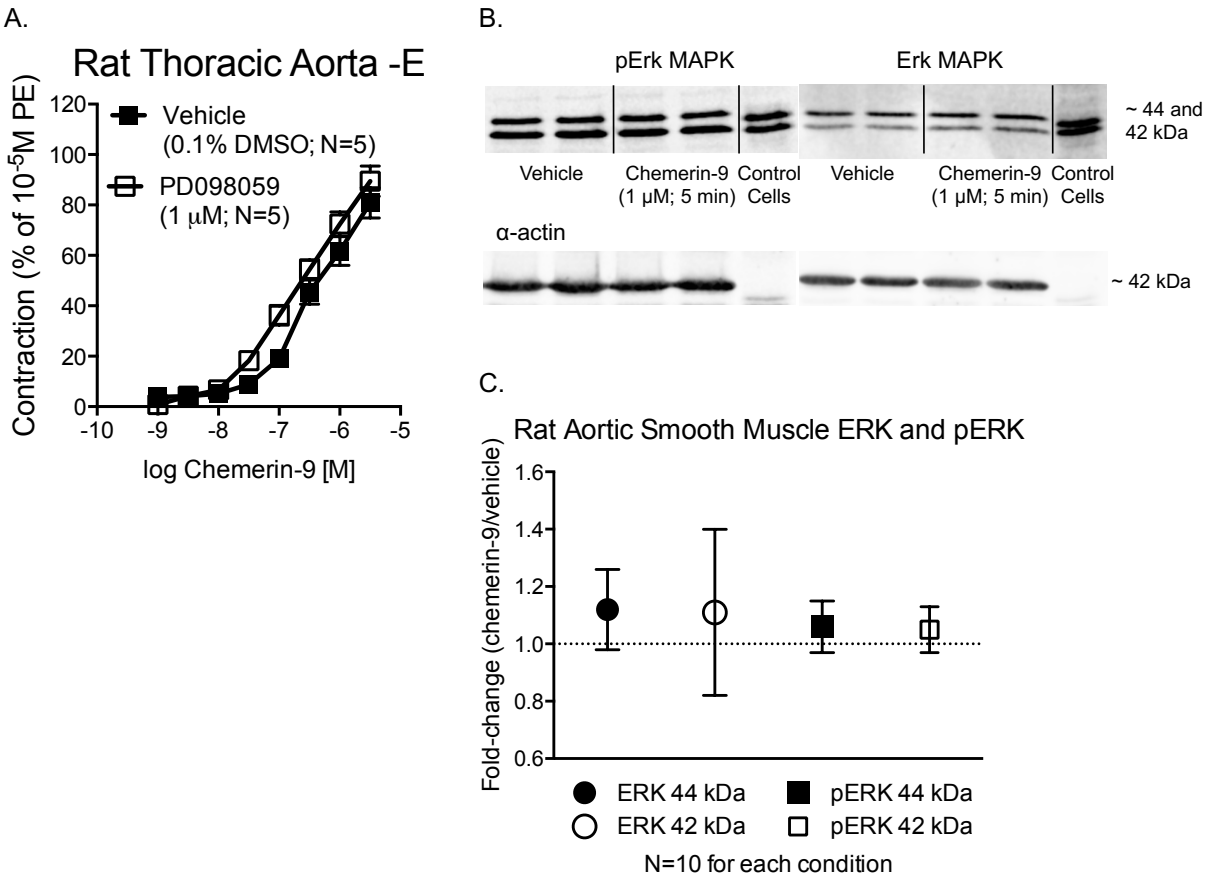

Figure 7: *Chemerin does not signal through Erk MAPK*

A) Isometric contractility measurements with PD098059 (Erk MAPK inhibitor) and chemerin-9. B) Biochemical analysis of chemerin-9 induced activation of Erk MAPK in the isolated male thoracic aorta. Representative blot of pErk MAPK and Erk MAPK in aorta contracted at time 0 (vehicle) or 5 minutes after exposure to chemerin-9 (1 μM). Each lane represents a separate rat aorta; two 0 and two 5 minute samples are shown on this blot. The positive control is calyculin treated Jurkat cells. C) After densitometric analyses where signals were normalized to α-actin as a loading control, chemerin-9 incubated values were divided by vehicle treated values to give a fold-change from vehicle. Points/bars represent means ± SEM. N=10 for each experimental condition (Erk vehicle, Erk chemerin-9, pErk vehicle, pErk chemerin-9). Points that remain above the dotted line (representing the signal given by vehicle treatment) are considered to have produced a statistically significant change in signal wither chemerin-9 compared to vehicle ($p < 0.05$), however, no significance was observed.

3.4 Calcium flux with chemerin-9 exhibits the same dependence on signaling elements as physiologic contraction

The pathway of chemerin signaling was further investigated by measuring cumulative response curves in isometric contractility and calcium flux. For both, the near-maximal chemerin-induced response with inhibitor was normalized to the near-maximal chemerin-induced response with the vehicle of the inhibitor and is represented as a percent of vehicle response (Figure 8A and B). Values of isometric contraction were measured at a chemerin concentration of 1 μM (arrows in 8A) while calcium flux was measured at 100 nM (arrows in 8B) due to a 10-fold shift in the EC_{50} values of the different methods (100 nM and 10 nM, respectively). Isometric contraction was significantly inhibited by verapamil (L-type calcium channel), Y27632 (Rho kinase), and PP1 (Src) (Figure 8C). U73122 also had significant inhibition of contraction but not to the magnitude of the other inhibitors. The calcium profile with a 1 hour incubation models the inhibitor incubation in the isometric experiments. At this 1-hour incubation, verapamil, Y27632, and PP1 all caused significant inhibition of calcium flux stimulated by chemerin-9 while U73122 did not (Figure 8D). A graphical representation of the predicted signaling pathway is represented in Figure 9.

4. Discussion

4.1 Chemerin-induced contraction is dependent on calcium flux

Establishing a clear path by which chemerin-9 causes smooth muscle contraction is essential to define the action of this isoform as opposed to other potentially anti-inflammatory isoforms [94], but also to define chemerin's role in smooth muscle (and

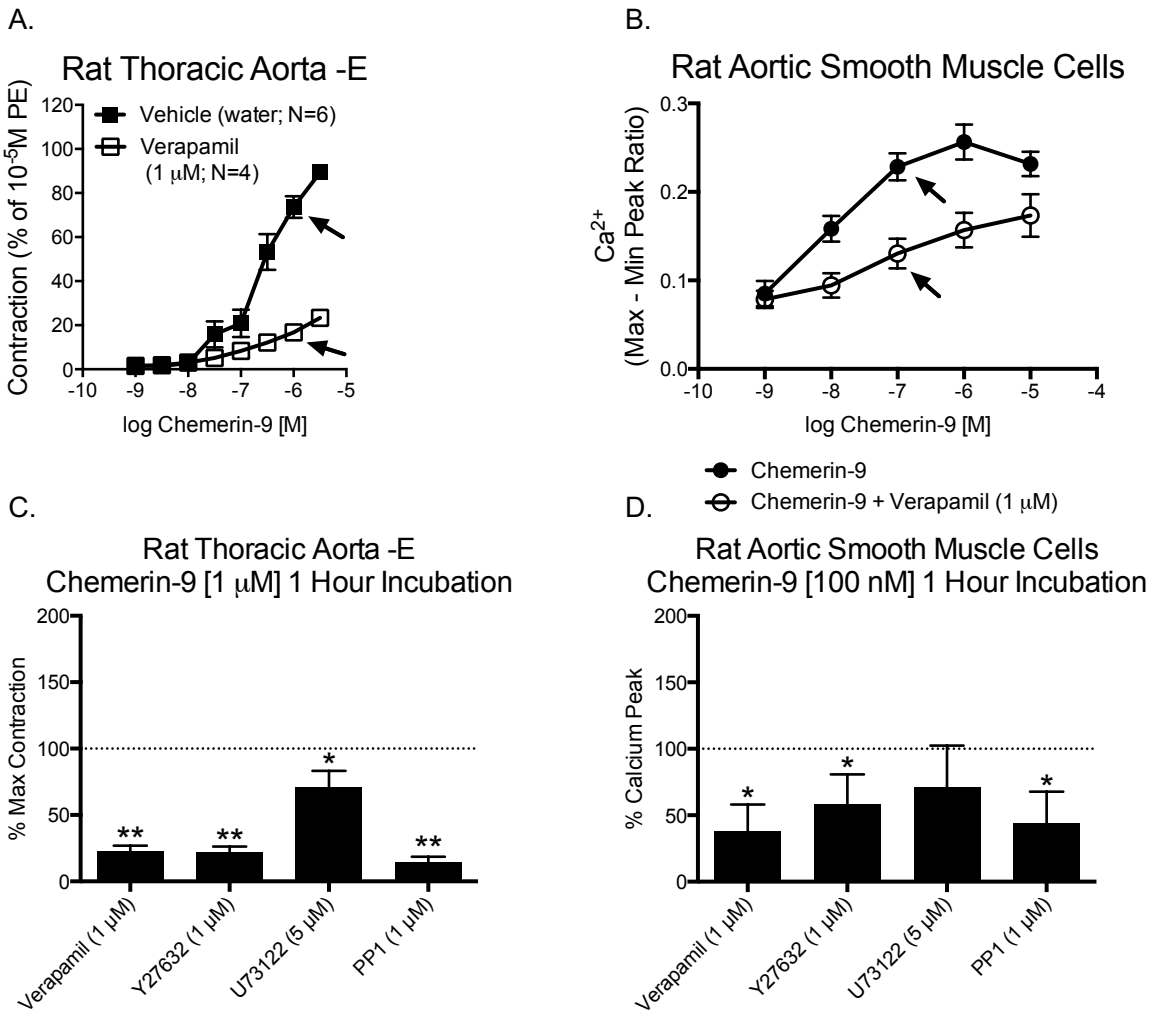

Figure 8: *Contraction and calcium are mediated by L-type calcium channels, ROCK, and Src*

Representative concentration response curves are shown for verapamil in isometric contraction (A) and calcium flux (B). Arrows represent the values used to make the bars in the subsequent graphs. Although full concentration-response curves to chemerin-9 were performed for each inhibitor, concentrations shown in subsequent graphs are near maximal concentrations for chemerin in their respective approaches (the EC_{50} for isometric contraction is 100 nM while EC_{50} for calcium flux is 10 nM). Values indicate the percent of total contraction (1 μM chemerin-9; C) or calcium peak (100 nM chemerin; D) when inhibitor is present. All values are represented as mean ± SEM. If the error bar does not cross the dotted line (representing 100% agonist response), the inhibitor produced a significant reduction of the agonist-induced contraction or calcium flux. * represents $p < 0.05$ and ** represents $p < 0.01$. N values are as follows: B) chemerin-9 + vehicle = 24, chemerin-9 + inhibitor = 12; C) verapamil (vehicle = 6, treatment = 4), Y27632 (vehicle = 4, treatment = 6), U73122 (vehicle = 5, treatment = 7), PP1 (vehicle = 4, treatment = 4); D) chemerin-9 + vehicle = 24, chemerin-9 + inhibitor = 24.

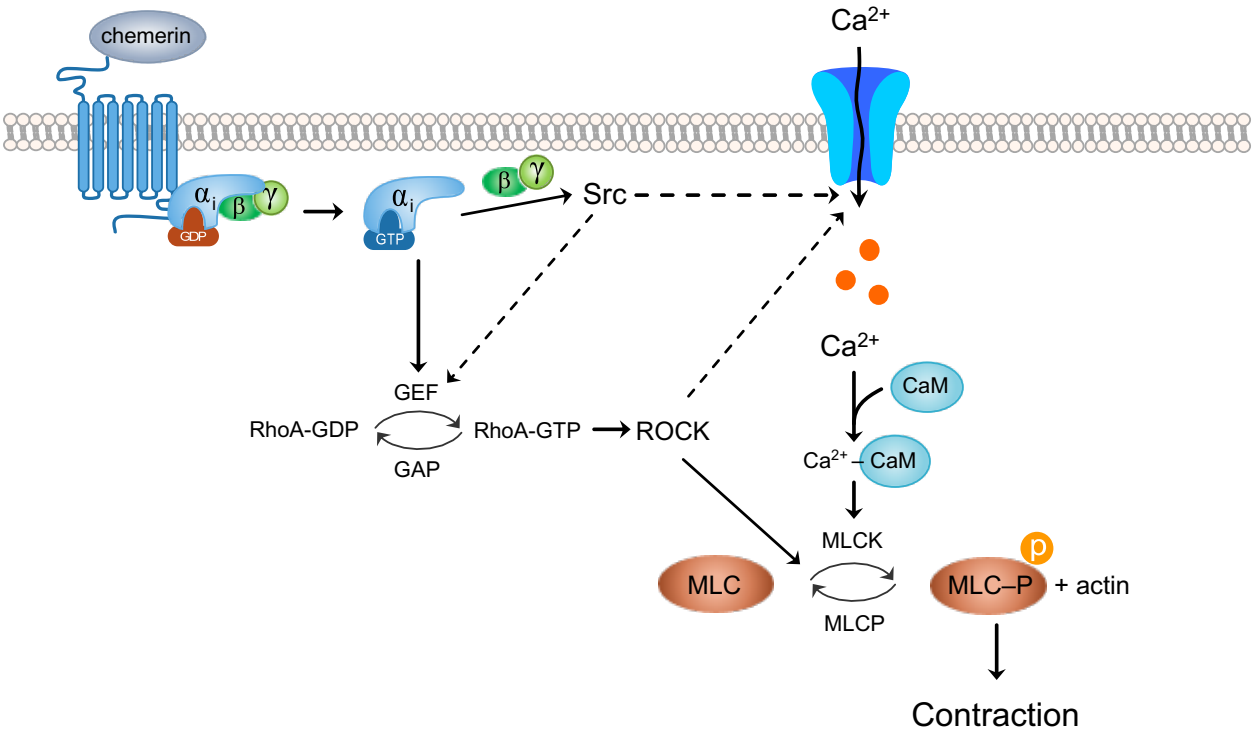

Figure 9: *Schematic figure*

Depiction of the potential interaction of chemerin-9 with the chemerin receptor and signaling pathways identified within the work of this manuscript. Dashed lines represent predictions.

hypertension) as opposed to its role elsewhere in the body (e.g. tumor angiogenesis, immune cell migration, and adipogenesis). We confirmed the contraction of aorta to chemerin-9 (Figure 3B), discovered that the smooth muscle cells initiated a calcium flux in response to chemerin-9/recombinant chemerin (Figure 3E) and localized the chemerin receptor to the perimeter of the cell (Figure 6A). All together, these data build on previous work [39] to support the connection between the physiological contraction and the smooth muscle cell through the chemerin receptor.

4.2 Receptors mediating chemerin's action in smooth muscle cells

Macrophages, dendritic cells [42], and artificial systems like the HEK293A cell line [66] show chemerin-related G_i mechanisms involved in cell migration and transcription (respectively). However, ours is the first report to show this mechanism in smooth muscle cells. Of all the inhibitors tested, PTX was the only one to abolish calcium flux at all concentrations of agonist (Figure 4A and B). Importantly, chemerin-9-induced contraction of the aorta was affected by PTX, but the effects were not as pronounced as those in the isolated cells (Figure 4D and E) and required a higher concentration (1000 ng/mL versus 500 ng/mL in the cellular assay). This difference can be explained by needing higher concentration of PTX to penetrate the tissue. These results suggest that all other tested elements of the signaling cascade leading to calcium mobilization must funnel through this heterotrimeric G protein. The lack of compete inhibition of aortic contraction by PTX (Figure 4D) indicates there may still be other G_i-independent mechanisms involved in chemerin-dependent contraction, but they are likely calcium-independent. The data from PTX combined with immunocytochemistry (Figure 6A) and CCX832 (Figure 5A and B)

point to the chemerin receptor being G_i-coupled and the primary functional receptor in these cells. Additionally, there is recent data suggesting that the receptor GPR1 does not significantly activate G-proteins and may act like a decoy receptor [67]. This is consistent with our data and further solidifies the chemerin receptor's role as the principle receptor for chemerin in vascular smooth muscle cells.

4.3 Chemerin signaling relies on various second messengers

Because of the direct importance calcium has on the activation of myosin light chain, the study of real-time calcium mobilization in cells can give us insight into the mechanisms necessary for smooth muscle contraction. The similarities between the qualitative outcome of isometric contraction and calcium flux implies that all three inhibitors block contraction by modulating calcium levels.

4.3.1 Chemerin and L-type calcium channels

L-type calcium channels are voltage gated and regulate extracellular calcium entry. As mentioned previously, this calcium flux is essential to smooth muscle contraction so it is logical that these channels would be involved. It has been implied before (by use of nifedipine and KCl-potentiated chemerin-9 isometric contraction) that the chemerin receptor and chemerin signaling is linked to L-type voltage gated calcium channels [39], but this is the first study to show that direct stimulation by chemerin-9 is dependent on these channels. Although others suggest that calcium is vital to the chemerin signaling of immune cells [42, 107], hematopoietic [108] and mesenchymal stem cells [109], we are the first to link chemerin to the smooth muscle cell and to the L-type voltage gated calcium channel in any system. In both rat myocytes and vascular smooth muscle cells, L-type

calcium channels have been linked to G_i-protein mechanisms [110, 111], lending support to the finding that extracellular calcium is essential to chemerin-induced vasoconstriction.

4.3.2 Chemerin and Rho Kinase

Rho kinase (ROCK) inhibits myosin light chain phosphatase (MLCP) and promotes vascular contraction [112]. Because this effect is downstream of calcium flux but upstream of smooth muscle contraction, inhibition of isometric contraction by ROCK inhibitor Y27632 can be explained by conventional mechanisms. However, the inhibition of calcium flux by Y27632 cannot be explained in the same way. Others have demonstrated that chemerin can signal through ROCK but these studies were performed in HEK293A and lymphocytes [66]. There is a preponderance of evidence to support that Y27632 inhibits KCl-induced contraction (voltage activated) of smooth muscle while leaving KCl-induced calcium flux unchanged [113-117]. This supports the previous mechanism that Y27632 does not block voltage-gated calcium channels but can block contraction by inhibiting phosphorylation of MCLP. In human purified protein activity assays with 10 μM Y27632, there were negligible off-target effects on other kinases [118]. We are confident that Y27632 is selective for ROCK but we are not the only ones to report that it has the ability to reduce intracellular calcium levels [119, 120]. Most interestingly, a recent paper assessed the ability for Y27632 to inhibit the contractility and calcium mobilization in rat aortic and mesenteric arteries stimulated by norepinephrine, AlF_4^- (G protein activator), and KCl (voltage activator) [121]. In this study, Y27632 inhibited both contractility and calcium release stimulated by norepinephrine and AlF_4^- but only inhibited contractility and not calcium flux in rat aorta stimulated by KCl. After additional testing, they concluded that ROCK was stimulated by G proteins to directly interact with

extracellular cationic channels not stimulated by voltage, not involved in regulating membrane potential, and not associated with potassium. Their hypothesis led them to suspect TRPC6 channels as the target of ROCK. Independent from these studies, TRPC6 channels are associated with G protein agonists, smooth muscle contraction, and positively correlated with hypertension [122]. Although ROCK is commonly associated with $G_{12/13}$ [123, 124], there is evidence in vascular endothelial cells that supports a link between G_i and ROCK [125]. Taken together, it is possible that chemerin-induced contraction could be mediated through ROCK activation of non-voltage dependent ion channels, like TRPC6. Future studies will need to directly assess the involvement of TRPC6 in a chemerin-induced response.

4.3.3 Chemerin and Src

GPCRs can influence Src to alter respiratory smooth muscle in a calcium-dependent manner [126, 127]. In both myometrial and vascular smooth muscle, Src has been linked specifically to the G_i protein [128, 129]. One study showed that in vascular smooth muscle, PP1 did not change calcium flux induced by sphingosylphosphorylcholine or KCl. However, PP1 still reduced smooth muscle contraction by indirect inhibition of ROCK [130]. To our knowledge, there are no previous reports that link chemerin signaling to Src. If Src is an upstream modulator of Rho, the previous evidence on ROCK and its actions on TRPC6 could explain our observed results. A recent report on Src stated that its influence is not on ROCK but rather on the guanine nucleotide exchange factor (RhoGEF) [131]. Independently from ROCK, Src is required for the activity of TRP channels [132] and can phosphorylate L-type calcium channels to enhance their activity [133]. The results in this report agree with the notion that Src could have influence over

ROCK's new mechanism proposed above (through a RhoGEF) but does not rule out Src's direct action at a calcium channel.

4.3.4 Chemerin and PLC

The evidence in our study as a whole does not support the role of PLC in chemerin-dependent vascular contraction. Although PLC has been associated with smooth muscle signaling pathways [106], it has not yet been directly linked to chemerin signaling. There was a minor inhibition of isometric contraction but the lack of significant inhibition of calcium flux suggests that this is not a major pathway activated by chemerin in a rat aorta. The primary mechanism for PLC is to activate IP_3-mediated intracellular calcium channels so if calcium flux is not changing, altogether it is not a major participant.

4.3.5 *Chemerin and Erk MAPK*

A previous report suggested that chemerin potentiates phenylephrine and endothelin-1-induced contraction through an Erk MAPK pathway [100]. A recent report also noted that the binding of chemerin-9 to the chemerin receptor activated Erk MAPK [67]. Beyond this, Erk MAPK is extensively associated with the actions of chemerin in chemotaxis [57], angiogenesis [50], and adipogenesis [38]. We tested the Erk MAPK pathway in smooth muscle with PD098059 against direct chemerin-induced contraction. When we failed to observe a reduction in isometric contraction with PD098059, we tested the phosphorylation of Erk MAPK. A five minute treatment of 1 μM chemerin-9 (the same concentration that produced a near-maximal chemerin-9-dependent contraction of rat aorta) did not change the level of phosphorylation of Erk MAPK. It is possible that Erk MAPK could be involved in the signaling pathways of phenylephrine or endothelin-1, but

it is clear in this report that Erk MAPK does not have any role in the contraction of the aorta by direct stimulation of chemerin-9.

4.4 Chemerin-9 as a model for recombinant chemerin?

From a practical standpoint, the existence of short peptides (like chemerin-9) is crucial to the feasibility of *in vitro* studies involving expensive recombinant proteins. Chemerin-9 was confirmed to bind the chemerin receptor with the same affinity as recombinant chemerin [44]. However, the effects of chemerin-9 differ from the recombinant version in a number of ways. Chemerin-9 activated smooth muscle calcium flux with a higher E_{max} than recombinant chemerin but both had similar EC_{50}. Both peptides appear to act on the same receptor, as shown by PTX inhibition, but the lack of inhibition of recombinant chemerin by CCX832 reveals that these analogs are not binding the chemerin receptor in the same manner. It is possible that the two agonists could be binding different sites on the receptor. The chemerin receptor can bind a number of different ligands to initiate different outcomes: the active chemerin S^{157} typically triggers inflammatory responses [42, 72] while other ligands like chemerin-15 (analogous to mouse chemerin A^{154}) [94] or lipid resolvin E1 [96] are anti-inflammatory. These outcomes, presumably mediated by the same receptor, suggest that the chemerin receptor may act in a biased fashion. This is the first report the authors are aware of that implicates biased agonism as accounting for the disparity between the actions of chemerin-9 and recombinant chemerin.

4.5 Limitations

We recognize limitations of the present study. Although recombinant chemerin was used in these calcium flux studies, it was not feasible to use in an isolated tissue bath. Additionally, as mentioned previously in section 3.1, this limited use of recombinant chemerin restricted the breadth of the concentration-dependent response curves.

Calcium is not the final step in smooth muscle contraction and cannot inform us about any effects intracellular signals may have on the myosin light chain itself. In this way, ROCK or Src may have actions outside of what was investigated here. Future studies may examine myosin activation as the ultimate step in muscle contraction to uncover calcium-independent mechanisms.

One inherent limitation of analyzing these cells for calcium flux is that the instrument used requires we titrate the cell count to be as low as possible. This maintains the sensitivity of the instrument and also allows us to run a host of experiments on cells at the same passage. The downfall is its ability to replicate the *in vivo* environment of a multilayered, tightly packed structure as in the aorta. Since the results in the isometric contractility reflect the results in the calcium flux, it is unlikely the difference in cell density played a significantly limiting role in our research. It should be taken into account for future experiments.

The contraction of vessels to chemerin-9 was also variable. In figure 5A, the contraction of the aorta to 3 μM chemerin-9 was about 60% while in figure 7A the contraction to the same concentration of chemerin-9 was about 80%. These measures were taken at different times, with different sets of animals (although all from the same source) and is consistent with the variability of this adipokine. The possible correlation

between an increase in maximal isometric contraction and an increase in DMSO concentration is not consistent with the current biological mechanism of DMSO and is not a factor contributing to the variability.

While the focus of this research is the smooth muscle of the vasculature, we recognize that the endothelium is also an important component to the vascular system. Because the vasculature did not contract to chemerin in the presence of endothelium [39], we did not initially consider the endothelium to play an important role in chemerin signal transduction thus, it was not the focus of this current study. However, determining the role of the endothelium and a comparison to the now-defined role of smooth muscle would be an important next step.

The animal model was a major consideration when formulating the experiments in this paper. We have previously reported that the mouse as a model for vascular actions of chemerin should be avoided because this aorta lacks a functional response to chemerin-9. By contrast, arteries from the rat as a model for chemerin in the human do contract to chemerin-9 [39]. This limits the technologies available to us that may otherwise be used if we were using the mouse. For example, Cre-Lox and other transgenic techniques are more difficult to perform in the rat.

4.6 Conclusions

Contraction of vascular smooth muscle by chemerin is dependent on G_i proteins, L-type Ca^{2+} channels, Src, and Rho kinase that all work by altering calcium flux. Erk MAPK and PLC are not involved in chemerin-dependent calcium flux and contraction. With a host of literature describing the possibility of chemerin's involvement in

hypertension [24-26, 31-33, 88], further research is needed to connect this knowledge with an actual treatment. This specific pathway helps to characterize a once unknown mechanism by which chemerin may contribute to obesity-related hypertension. Understanding these mechanisms is necessary to develop treatments against novel targets like chemerin. It also highlights a new role for Src and Rho kinase as well as possible benefits and pitfalls for future use of the nonapeptide, chemerin-9.

AIM 1.2: Beneficial and site-specific effects of chemerin on mPVAT

This chapter was adapted from:

Ferland DJ, Garver H, Contreras GA, Fink GD, Watts SW. Chemerin contributes to *in vivo* adipogenesis in a location-specific manner. PLOS One.

1. Introduction

With the rising obesity crisis around the world, obesity-related diseases such as diabetes [134], non-alcoholic fatty liver disease [135], high blood pressure [136], and even a compound pathology like metabolic syndrome [137] are now more frequent. Metabolic syndrome is defined as having three of the following five characteristics: high blood pressure, high BMI, dyslipidemia, impaired insulin sensitivity, and a large waist circumference [7]. To better treat patients and predict their prognosis, physicians have looked for blood markers of each of these diseases. Circulating concentrations of adiponectin (low) and leptin (high) are often thought of as classic markers of obesity-related diseases. However, a new class of adipokines, including vaspin and chemerin, also have strong positive correlations to these same diseases [138, 139].

Chemerin plasma levels increase in diabetes [140, 141], increased visceral adiposity [24, 88], dyslipidemia [37, 91], and high blood pressure [26, 30] independently but these positive correlations often become even more powerful in people diagnosed with metabolic syndrome [28, 35, 36]. Chemerin is made in various tissues of the body but is most prominently produced by the liver and white adipose tissue [35]. Clinicians and basic scientists have implicated the abdominal visceral white adipose tissue as the major contributor of chemerin from fat [24, 35] and that chemerin production is substantially lower in the brown adipose tissue compared to the white adipose tissue. After secretion, the binding of chemerin with chemerin receptor 1 initiates a number of different actions depending on the cell type it is affecting: chemotaxis on immune cells [42], calcium flux in smooth muscle cells [142], or matrix metalloproteinase activity for vascular growth [58].

Basic science research on chemerin suggests a link to inflammation: specifically how various forms of chemerin may [42] or may not [94] induce migration of immune cells. In 2007, several papers using shRNA knockdown of chemerin in the 3T3-L1 mouse fibroblast cell line – a classic adipogenesis model that can differentiated into adipocytes – demonstrated that chemerin and its receptor were necessary for lipogenesis or accumulation of lipid [35, 38]. Adipogenesis as a whole is likely regulated through chemerin's influence over cyclins A2 and B2 [143].

This current study focuses on the impact of a germline chemerin knockout on adipogenesis and lipogenesis. We hypothesized that the chemerin knockout rat, when compared to its WT counterpart, would have impaired white adipose tissue lipid accumulation and reduced expression of genetic markers of adipogenesis and lipogenesis related to lipid accumulation like PPAR gamma, adiponectin, perilipin, fatty acid synthase, and leptin (reflecting what was previously seen with 3T3-L1 cells [38]).

2. Methods

2.1 Animal care and handling

All procedures that involved animals were performed in accordance with the Institutional Animal Care and use Committee (AMEND201900134 / PROTO201900089) of Michigan State University that approved this study. Animals were maintained on a 12/12 hour light/dark cycle at a temperature of 22-25°C.

2.2 Animal model

The knockout of the chemerin gene in the Sprague Dawley rat has been previously validated [78] and all animals were genotyped by ear punch at weaning. Female KO and WT rats were fed a normal chow (Envigo Teklad 22/5 #8640; 17% kcal from fat) from weaning until 8 weeks of age then switched to a low-fat normal diet (Research Diets D12450J; 10% kcal from fat) from 8 weeks till 25 weeks of age. Total body weight and food consumption were measured weekly.

2.3 MicroCT

MicroCT scans of rats were performed by a core facility at Michigan State University using the Perkin Elmer Quantum GX microCT Imaging System (Waltham, MA, USA). The following image acquisition scan parameters were standardized and used at each scan interval time point: scan mode, Standard; gantry rotation time, 2-minutes; power, 90kVp/88uA; Field of View (FOV), 72mm; number of slices, 512; slice thickness, 144um; voxel resolution, $144um^3$. Animals were maintained on isoflurane (1-3%) and given supplemental heat while monitoring respiratory rate and heart rate. Image rendering, tissue segmentation, and analysis were performed using Caliper AnalyzeDirect© (v12.0, Biomedical Imaging Resource, Mayo Clinic, Rochester, MN). Transverse images were taken at the same abdominal point on each animal. Instances where the field of view was too small to adequately measure subcutaneous fat, resulting in a Hounsfield unit standard deviation above 70, were excluded from the study due to an unreliable threshold analysis.

2.4 Tissue collection

Animals were euthanized at 25 weeks of age with 2% isoflurane followed by pneumothorax. Liver, heart, kidney, ovarian/uterine fat, and retroperitoneal fat were removed in their entirety and weighed. Samples of retroperitoneal fat and mesenteric fat were fixed with 4% paraformaldehyde for histology or flash frozen in liquid nitrogen for mRNA analysis. Samples placed in paraformaldehyde were transferred to 30% ethanol after 24 hours before sending to the MSU Histopathology lab for sectioning and staining.

2.5 Western blot

Blood was centrifuged at 500 *xg* for 20 minutes at 4°C. Plasma was diluted 1:25 and a bicinchoninic acid assay was used to determine protein content (#BCA1, Sigma Chemical Co, St. Louis, MO, USA). Fifty micrograms of protein was loaded into a 15% polyacrylamide gel run at 120 V. Protein was transferred for 1 hour at 100 V to a PVDF-FL membrane (#IPFL00010, EMD Millipore, Billerica, MA, USA). After drying, Total protein stain was added, imaged, and reverted (#926-11011, Li-Cor). Samples were blocked with chick egg ovalbumin for 3 hours. Chemerin primary antibody (1:1000; Abcam Cat# ab112520, Cambridge, MA, USA; ab registry: AB_10864055) was incubated with the membrane for 48 hours at 4°C, washed three times, and secondary antibody (1:1000; IRDye 800 anti-Mouse, LI-COR Biosciences Cat# 926-32210, Lincoln, NE, USA; ab registry: AB_621842) was incubated for one hour at 4°C. With total protein as a loading control, blots were visualized with the Odyssey CLx Infrared Imaging system (Li-Cor) and quantified with Image Studio (5.2.5, LI-COR Image Studio Software). When using Image

Studio to perform the analysis, modification of LUTs does not affect the signal quantification.

2.6 Histology and adipocyte analysis

Retroperitoneal and mesenteric fat samples were stained with H&E and imaged with a Nikon (Tokyo, Japan) Eclipse Ti microscope using a Nikon DS-Fi3 camera. Five fields of each biological replicate were collected at 4x magnification for quantification. Uncompressed tif files were analyzed for adipocyte area by the Adiposoft plugin (v. 1.15) for ImageJ Fiji (v 2.0.0). The Adiposoft plugin gated for adipocytes with an equalized diameter between 25 and 200 microns used a “micron per pixel” ratio of 0.86 according to the calibration of the microscope. Images were spot checked for appropriate quantification. Data represent a biological replicate n = 5 for each condition. All image capture and analysis were carried out with random identifiers to blind the operator to the genotype of the animal.

2.7 PCR

Flash frozen tissue was processed by the Zymo Research (Irvine, CA, USA) QuickRNA kit for RNA isolation. Reverse transcription was performed by the Applied Biosystems (Foster City, CA, USA) High Capacity cDNA Reverse Transcription kit and the Applied Biosystems SimpliAmp Thermal Cycler at the following conditions: 10 minutes 25°C, 2 hours at 37°C, 5 minutes at 85°C, then hold at 4°C. PCR was performed with Applied Biosystems Quant Studio 7 Flex and Applied Biosystems Fast SYBR Green Master Mix under the following conditions: 95°C 20 sec, 40x 95°C 1 sec then 60°C 20

sec, then melt using 95°C 15 sec and 60°C 1 min. Sigma Aldrich (St Louis, MO, USA) KiCqStart SYBR Green primer sequences can be found in Table 1. Beta-2-microglublin was used as a reference gene.

2.8 Cytoscape network

PCR ΔC_T values from KO mesenteric adipocytes were divided by WT counterparts for a fold change. Genes that did not have statistically significant differences when comparing the ΔC_T means of KO and WT adipocytes were assigned a fold change of one. Protein interactions from the tested genes were imported to a Cytoscape (3.7.1) network using the STRING app (1.4.2) and STRING database (string-db.org) which compiles known protein-protein interactions from the literature in specific species of animal. All analyses were performed using the rat database. These interactions were mapped to edge width. Fold changes from experimental data were mapped to node color.

2.9 Statistics and analysis

All samples, images, and data were coded so that all handling and initial analyses were blinded before the final statistical analysis. Statistics and graphing were performed with Prism (v.8, Graphpad). Time course data was analyzed with a 2-way ANOVA. Analyses comparing the WT and KO animals were performed with a two-tailed students t-test. PCR data comparing the gene expression of four groups utilized a one-way ANOVA with Sidak correction. Significance was considered $p < 0.05$. Histograms were analyzed for significant shifts with the Kolmogorov-Smirnov test for distributions. PCR data is represented as $2^{-\Delta C_T}$ where ΔC_T is the difference between the target gene and the beta-2

Gene Abbreviation	Gene Name	Forward Primer Sequence	Reverse Primer Sequence
Pparg	Peroxisome Proliferator Activated Receptor Gamma (rat)	AAGACAACAGACAAATCACC	CAGGGATATTTTTGGCATACTC
Adipoq	Adiponectin (rat)	TGGCGATTTTCTCTTCATTC	AGGATTAAGAGGAACAGGAG
Fasn	Fatty Acid Synthase (rat)	AAAAGGAAAGTAGAGTGTGC	GACACATTCTGTTCACTACAG
Plin1	Perilipin (rat)	TTACGGATAACGTGGTAGAC	GAGGATTATCGATGTCTTGG
Lep	Leptin (rat)	CTCATCAAGACCATTGTCAC	TGAGGATCTGTTGATAGACTG

Table 1: *Forward and reverse sequences for Sigma-Aldrich KiCqStart SYBR primers used in this study*

microglobulin reference gene. All genes were run with a technical duplicate which was averaged for subsequent analysis. All data in figures represent mean ± SEM based on the biological replicates (n).

3. Results

3.1 KO rats have reduced visceral adiposity

Rats were genotyped at weaning but chemerin knockout was confirmed by testing for chemerin protein in the plasma of WT and KO rats (figure 10A-B). Over the course of 17 weeks, female WT and KO rats did not have different total body weights or kcal consumption (figure 10C-D). MicroCT performed at 8 and 25 weeks of age suggests that while the adiposity of both the visceral and subcutaneous fat beds increased in all animals over time, accumulation of visceral but not subcutaneous fat in the KO rat was blunted (figure 10E-F).

3.2 Chemerin's adipogenic potential is location-specific

The two major components of visceral fat measured by CT were mesenteric and retroperitoneal fat. When adipose tissue was fixed, imaged, and analyzed for adipocyte area, the mesenteric adipocytes of the KO animals were significantly smaller than the WT animals (leftward shift in the histogram statistically confirmed by the Kolmogorov-Smirnov test for distributions; figure 11A). By contrast, the adipocyte sizes from the retroperitoneal fat were not different between WT and KO animals (figure 11B).

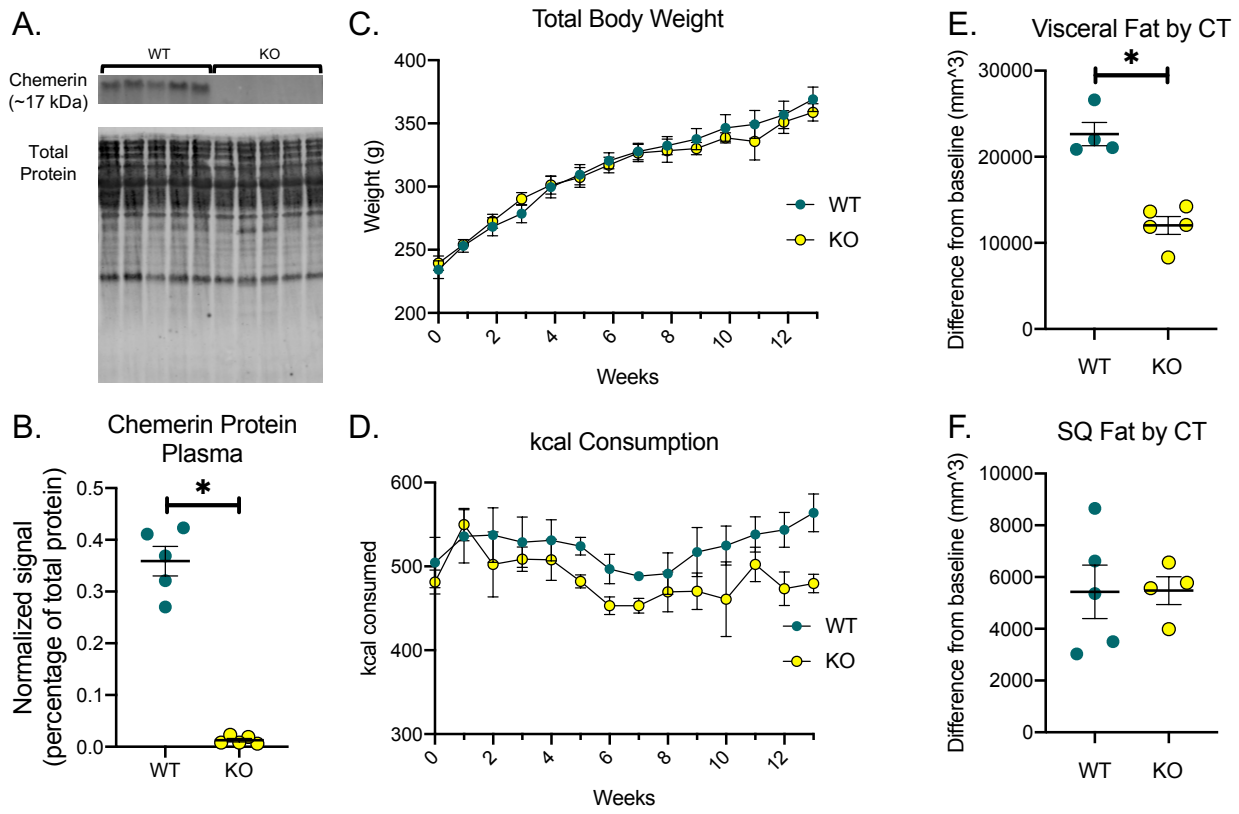

Figure 10: *KO rats have reduced visceral adiposity*

In addition to genotyping done at weaning, chemerin knockout was confirmed by loss of chemerin protein in plasma as measured by Western blot (A-B). Body weight of the rats were measured weekly (C) and kcal consumption was calculated based on food weight consumed multiplied by kcal density (D). Visceral fat (E) and subcutaneous (SQ) fat (F) was calculated by taking the difference between the 8 week and 25 week measurements. Only visceral fat was changed by genotype. All points and bars represent mean ± SEM for a biological replicate N = 5. * represents $p < 0.05$ for the respective statistical test. In the WT group of panel E and KO group of panel F, one animal was excluded due to Hounsfield unit variability discussed in the methods section. Time course data was analyzed by 2-way ANOVA and comparison of two groups was analyzed by two-tailed students t-test.

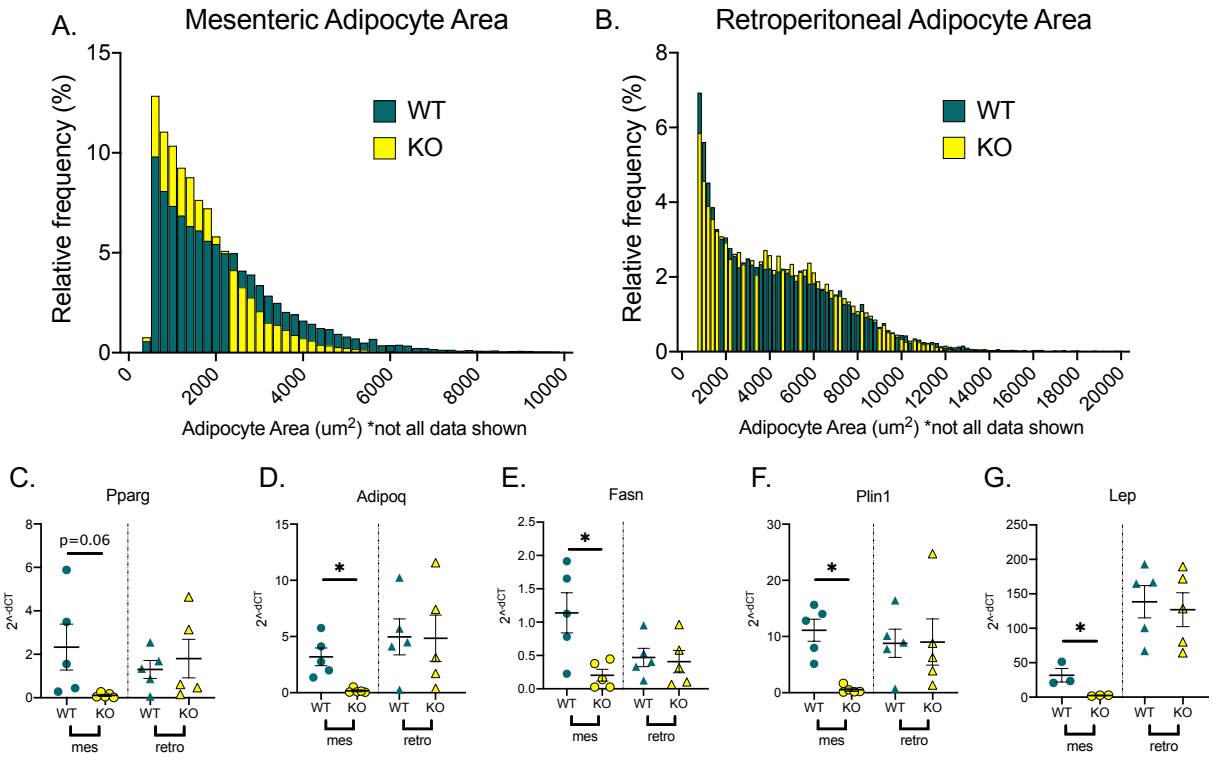

Figure 11: *Chemerin's adipogenic potential is location-specific*

Histograms of adipocyte area show that mesenteric adipocytes with chemerin knocked-out have reduced area (A) whereas in retroperitoneal fat, there is no difference between WT and KO (B). Statistical significance of shifts in the histogram were performed by Kolmogorov-Smirnov test of frequency distribution with a $p < 0.05$. Five images of each biological replicate were analyzed and combined to create the histogram. Each bin was normalized to a percent of the total count for that individual tissue. To see distribution changes early on the x-axis, the x-axis was shortened and does not include some data at higher adipocyte sizes. PCR analysis showed that in these KO mesenteric adipocytes, adiponectin (*adipoq*), fatty acid synthase (*fasn*), perilipin (*plin1*), and leptin (*lep*) were significantly reduced. PPAR gamma (*pparg*) did not show any statistical significance (C-G). All points and bars represent mean ± SEM for a biological replicate N = 5. * represents $p < 0.05$ for the respective statistical test.

The mesenteric and retroperitoneal fats from WT and KO animals were tested for mRNA expression of genes related to adipocyte development. There was no statistical significance ($p = 0.6$) in the expression of *PPAR gamma* but we did observe reduced levels of adiponectin (*adipoq*), fatty acid synthase (*fasn*), perilipin (*plin1*) and leptin (*lep*; figure 11C-G) in the mesenteric but not retroperitoneal fat of the KO rat. This trend did not exist in the WT animals.

3.3 Adiponectin is important to the actions of chemerin

When gene expression data gathered from this study was overlaid on a directional protein-protein network of the genes tested in the mesenteric adipocytes of WT and KO, adiponectin was determined to be an important upstream gene affected by the removal of chemerin (figure 12). The color of the nodes in the network represent the gene expression changes (figure 11) while the width of the edges (with arrows) represent literature data curated by the STRING app within Cytoscape [144].

4. Discussion

4.1 Chemerin is a regulator of adipocyte development in mesenteric fat

Given the rapid expansion of epidemiological references to chemerin in the human literature, there is a dire need for basic science to substantiate the foundations of chemerin's associations with different pathologies like obesity, blood pressure, and inflammation. Through a novel chemerin KO rat, this study provides important in vivo proof that chemerin is a contributor to the adipogenesis in a site-specific way.

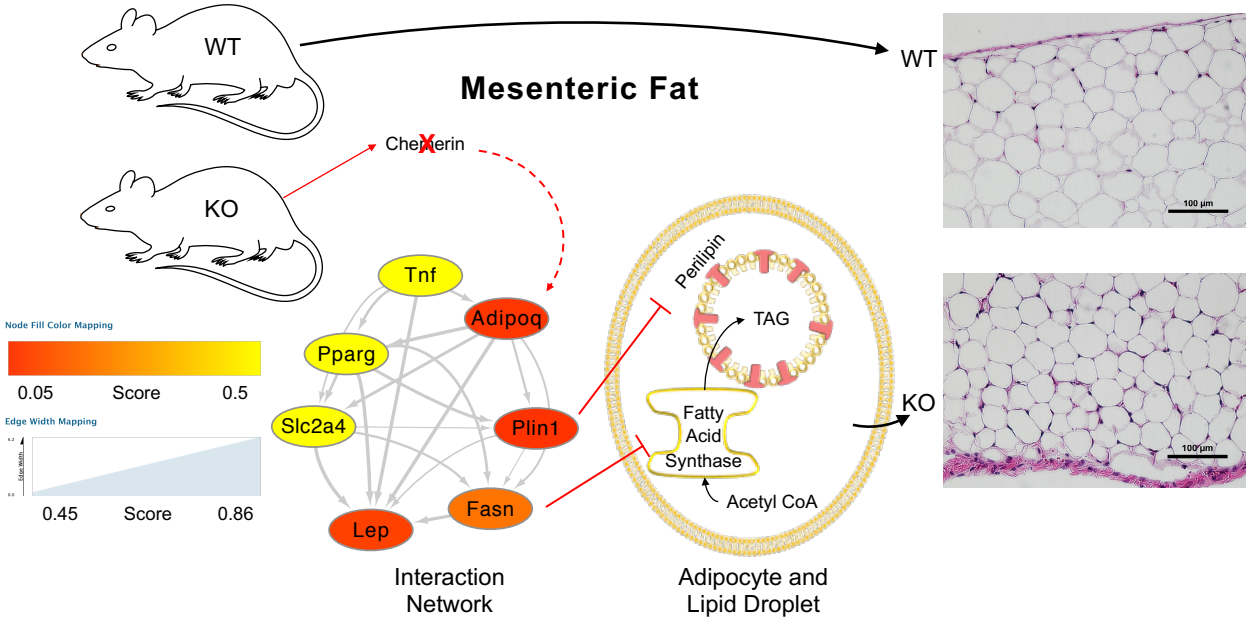

Figure 12: *Adipocyte development network in chemerin KO rats*

This network represents protein-protein interactions curated by the STRING database (edges with arrows) and gene expression data from this study (nodes). Edges are mapped according to the score given by the STRING app (v1.4.2) database correlating to the strength of data supporting their directional interaction. Scores for node mapping were determined by taking the $2^{-\Delta C_T}$ from chemerin KO mesenteric adipocytes and dividing them by the $2^{-\Delta C_T}$ from their WT counterparts. Comparisons of gene expression from KO and WT fats in figure 11 that were not statistically significant were given a score of 1. Genes that were not incorporated into the STRING network (ccng2, ccna2, and tcf21) were not included in this figure. When expression is decreased with chemerin KO versus WT, the node will appear more red. When expression is unchanged, the node will appear yellow. These data were incorporated into the known physiology of the adipocyte and representative images of the WT and KO mesenteric adipose tissue to provide a hypothesis of the system discussed in this manuscript. Scale bars represent 100 um.

From a basic science perspective, the mechanisms by which distinct chemerin isoforms contribute to adipocyte pathophysiology are still a mystery. Cleavage of a single amino acid from the C-terminus of the chemerin protein can dramatically alter affinity and efficacy for the chemerin receptor 1 and thereby alter the chemotactic rates of immune cells [42, 44, 46]. It is probable that the chemerin isoform milieu of the adipose tissue determines how chemerin supports a healthy or pathogenic environment. This study confirmed that chemerin production in the whole, healthy animal does influence the adipocyte development and supports the need for future research investigating how the actions of chemerin on the adipocyte change in metabolic syndrome.

An unexpected finding with important pathophysiological relevance is the location-specific changes in adipocyte-development with chemerin KO. Visceral adiposity has long been associated with negative outcomes in obesity and high blood pressure [4, 20]. Researchers have slightly different definitions of visceral fat in rodents versus humans, which makes the integration of clinical and basic science data somewhat difficult. In rodents, visceral fat is defined based on vascular drainage (fat whose blood drains to the hepatic portal vein; mesenteric and omental fat but not retroperitoneal fat) while clinically it is based on what can be differentiated from subcutaneous adipose on a CT scan (mesenteric, omental, and retroperitoneal fat) [21].

Omental fat does not exist in the rat so it can be excluded from the discussion [21]. But it is also important to note that mesenteric fat is mostly perivascular to the mesenteric resistance vessels, which have substantial exposure to nutrients coming from the intestine which could exert significant control over total peripheral resistance [19, 145]. With mesenteric adipose tissue better poised to influence the development of metabolic

syndrome, it is not surprising that of the two adipose depots, chemerin would play a larger role in the adipocyte development of the mesenteric, rather than the retroperitoneal, fat.

4.2 Interactions of chemerin with other regulators of the adipocyte

The genes that showed reduced expression in the mesenteric KO fat (adiponectin, perilipin, fatty acid synthase, and leptin) may adequately explain the reduction in size of the adipocytes. While the direct actions of adiponectin are catabolic, adiponectin is widely recognized as an adipokine that promotes healthy function. It ensures that adequate lipid is available for adipocyte storage and limits ectopic lipid accumulation [18]. Perilipin surrounds the lipid droplet and is responsible for maintaining the droplet in the adipocyte [146]. Fatty acid synthase is a key enzyme in the packing of lipid into the lipid droplet of the adipocyte [147]. Leptin is considered an endocrine signal of the amount of adipose tissue [18]. The reduced adipose tissue levels in the mesenteric fat have likely led to the reduced leptin expression in our PCR measurements. We tested other genes that might be critical to the preadipocyte development like tcf21 or cell cycle regulators like ccna2 or ccng2, but none of these were significantly changed in the mesenteric fat of the KO rat. From these data, it is possible that the adipogenesis rate was not affected and chemerin only influenced the adipocyte size. We expected PPAR gamma to also be reduced based on previous studies with chemerin in 3T3 cells [38]. While our data on PPAR gamma were inconclusive, it is likely that PPAR gamma activation is upstream of chemerin activation. One report proposed that the chemerin promoter contains a PPAR gamma binding motif [143]. If PPAR gamma expression is upstream of the chemerin gene we knocked out, that could possibly account for the lack of change in PPAR gamma expression.

The network of protein interactions combined with gene expression data outlines one possible way chemerin could influence the actual accumulation of lipid in these mesenteric adipocytes. Even without the involvement of PPAR gamma, chemerin can act at the level of adiponectin to influence the lipid in the cells. One paper describing the effects of chemerin, the chemerin receptor 1, and adiponectin in bovine adipocytes found that both adiponectin and chemerin itself cause expression of the chemerin gene [148]. These data combined with our protein network analysis imply a positive feedback loop where chemerin and adiponectin are able to promote adipocyte growth and lipid expansion. This is congruent with other reports where chemerin expression increases throughout differentiation [35, 38, 148-150].

4.3 Limitations

Though the scope of this current study was on the interactions between chemerin and fat metabolism, it is important to remember that fat is not the only source of chemerin in the body. We did not study chemerin expression in the liver or adrenal – two other major sources of chemerin. While it is possible that chemerin from other sources could influence adipocyte development, the changes in lipid size were location dependent. This indicated a local effect of chemerin on metabolism of the adipocyte rather than a systemic one.

This study utilized female rats and while our previous validation of this transgenic model identified some minor difference in blood pressure regulation between males and females, most other parameters, including clinical blood chemistries, indicated a similar

metabolic function [78]. As such, we would expect experiments in male rats to exhibit similar proportional changes between KO and WT animals.

4.4 Conclusions

Chemerin may not play a global role in adipogenesis, as evidenced by the lack of changes in the total body weight and retroperitoneal adipocyte size in our chemerin KO rats. Yet, through these data, we show that chemerin plays an important in vivo role in the mesenteric fat, a fat depot that plays an important role in the pathogenesis of metabolic syndrome. This study provides a foundational understanding for current and future epidemiological research but also serves as a first step for future in vivo basic science chemerin research. We have demonstrated for the first time that chemerin plays a supportive role in adipocyte development of the rat but this effect is specific to the mesenteric adipose depot.

AIM 2.1: In vivo effects of chemerin on blood pressure

This chapter was adapted from:

Ferland DJ, Seitz B, Darios ES, Thompson JM, Yeh ST, Mullick AE, Watts SW. Whole-Body but Not Hepatic Knockdown of Chemerin by Antisense Oligonucleotide Decreases Blood Pressure in Rats. J Pharmacol Exp Ther. 2018 May;365(2):212-218. doi: 10.1124/jpet.117.245456.

1. Introduction

Chemerin is an adipokine often positively associated with inflammatory conditions like psoriasis [57], metabolic syndrome [34], dyslipidemia, and hypertension [30]. Being an adipokine, chemerin is also positively associated with obesity [33] and visceral adipose tissue in both rat and human models [35].

The Framingham Heart Study established the positive association between hypertension and adiposity [151], but further analysis points towards visceral and retroperitoneal fat as being the specific culprits in the pathological source of obesity [152]. This places chemerin production, with the propensity for inflammatory activity, in the very same place as the source of obesity-associated hypertension, the visceral adipose tissue. One component of this visceral fat depot is the mesenteric perivascular adipose tissue (mPVAT). These white adipocytes directly surround the mesenteric resistance vessels which are thought to play a major role in the regulation of blood pressure [19]. The proximity and possible paracrine release of chemerin from the mPVAT could explain some of the blood pressure effects of chemerin. While there is a possible connection between PVAT and the etiology of hypertension, the role of the liver in this paradigm remains more of a mystery. It is well established that the primary producer of chemerin mRNA is the liver with the second highest being the visceral adipocytes [35]. This begs the question – *which source of chemerin is more important to the association of chemerin with hypertension, liver or fat?*

To begin this investigation into the association of chemerin with hypertension, it was worthwhile to first ask the question of how the physiology of chemerin operates in the healthy normal rat. When isolated aorta, superior mesenteric artery (SMA), and

mesenteric resistance vessels with a normal endothelium are exposed to chemerin, the contraction of the vessel is slight. However, when the vessel is contracted with phenylephrine, the vessel further contracts in response to chemerin to the same degree as when the endothelium is damaged or removed [39]. These conclusions have been supported by other labs noting the importance of the endothelium to protect against chemerin-induced contraction [153]. The normal SMA also has the ability to contract in a chemerin receptor-dependent manner when stimulated with an electrical field, a contraction that was dependent on PVAT and the sympathetic nervous system [154]. We have identified that the mechanism of vascular contraction in normal animals is indeed through the smooth muscle cells themselves, in a calcium-dependent manner [142].

Antisense oligonucleotides (ASOs) represent a class of recent therapeutics that bind RNA through Watson-Crick pairing which promotes RNA degradation or can have other modulatory effects such as redirecting splicing [80]. There are a variety of ASO modifications that enhance *in vivo* stability, distribution and RNA binding affinity. For example, the (S)-constrained ethyl (cET; Gen 2.5) sugar modification improves RNA binding affinity leading to improved *in vivo* activity in hepatic and extrahepatic tissue [155]. Additionally, recent advancements of targeted delivery using the trivalent N-acetylgalactosamine (GalNAc) conjugation have demonstrated improved targeting of the liver [156]. GalNAc conjugation on ASOs containing 2'-O-methoxyethyl (MOE) sugar modification (Gen 2.0) have demonstrated robust liver activity, with little to no activity in adipose tissue [157]. Thus, to dissect the role of liver-derived vs. extrahepatic chemerin, a GalNAc conjugated Gen 2.0 ASO with high specificity for reducing liver chemerin

expression was compared to the Gen 2.5 ASO which potently reduced liver and adipose chemerin expression.

Because chemerin influences contraction of normal rat aorta, SMA, and mesenteric resistance vessels (both with and without prior contraction with phenylephrine) and electrical field-stimulated contraction, we chose to begin our *in* vivo studies with normal SD rats. We hypothesized that 1) a removal of chemerin protein, by decreased mRNA translation, from the body would reduce mean arterial pressure (MAP); 2) the degree of MAP reduction would be correlated to the amount of circulating chemerin; and 3) the liver would be the major contributor to the circulating chemerin stores. Using *in vivo* pharmacology and constant cardiovascular monitoring, we were able to test if knockdown of chemerin by the liver-specific ASO (GalNAc Gen 2.0) or whole-body ASO (Gen 2.5) could reduce MAP. Western blotting and PCR allowed us to determine the relative associations between the terminal tissue or circulating chemerin and the short-term effect on MAP.

2. Methods

2.1 Animal care

All procedures that involved animals were performed in accordance with the institutional guidelines and animal use committee of *Michigan State University* and the *NIH Guidelines on Use of Lab Animals*. Animals were single-housed and maintained on a 12/12 light/dark cycle at a temperature of 22-25ºC. Normal male Sprague-Dawley rats (225–300 g; Charles River Laboratories, Inc., Portage, MI, USA) were used.

2.2 ASO synthesis

Synthesis of the Gen 2.0 and 2.5 antisense oligonucleotides (ASO) described previously (Seth *et al.*, 2008) and GalNAc ASO were described previously (Prakash *et al.*, 2016). *In vitro* activity screens followed by *in vivo* activity and tolerability screens were used to identify leads. The following are lists of the scrambled, GalNAc Gen 2.0 and Gen 2.5 ASOs used in this study:

Scrambled (5'-3'): GGCCAATACGCCGTCA

GalNAc Gen 2.0 (5'-3'): GalNAc-ACAGTTTTATTAGCCTGGAG

Gen 2.5 (5'-3'): GTTTTATTAGCCTGGA

ASOs were diluted in sterile PBS to their final concentration (described below).

2.3 Radiotelemetry and in vivo pharmacology

Rats were implanted with a femoral catheter connected to a subcutaneously implanted radiotelemeter. Early studies used C-40s (DSI, MN, USA) but were replaced with HD-S10s (DSI, MN, USA) for the added capability of measuring core body temperature. After five days of recovery, baseline cardiovascular measures were recorded every ten minutes for ten seconds over one week. Weekly subcutaneous injections were performed under anesthesia (1-2% isoflurane) for four weeks. Physiologic measures were sampled every ten minutes for ten seconds for the duration of the experiment and averaged daily for statistical analysis and graphical representation.

2.4 Gen 2.5 chemerin ASO dosing study

After implantation of radiotelemetry, rats were administered a scrambled control ASO or Gen 2.5 chemerin ASO. Both control ASO and Gen 2.5 chemerin ASO were administered at 25 mg/kg, 12.5 mg/kg, or 6.25 mg/kg. Doses were given subcutaneously on days 0, 7, 14, and 19 with tissue and blood collection on day 21.

2.5 Gen 2.5 chemerin and GalNAc chemerin ASO blood pressure studies

After implantation of radiotelemetry, rats received subcutaneous injection of PBS (average volume of ASO injections), control ASO (25 mg/kg), Gen 2.5 Chemerin ASO (25 mg/kg), or GalNAc Chemerin ASO (10 mg/kg) on days 0, 7, 14, and 19. Animals were sacrificed under anesthesia (1-2% isoflurane) by pneumothorax. The entire retroperitoneal fat pad was dissected away from the posterior abdominal wall and the mPVAT was removed in bulk from the base of the SMA without collecting any of the mesenteric resistance vessels. Tissues were weighed and collected for mRNA and protein analysis. Blood was also collected for plasma. All samples were stored either at -80ºC or under dry-ice until isolation of mRNA or protein. Researchers performing the mRNA and protein analysis were initially blinded as to the treatment conditions of the tissue.

2.6 Real-time quantitative PCR

Quantitative qRT-PCR (qPCR) mRNA analysis was performed with TaqMan primer probes (Thermo Fisher-Applied Biosystems, Foster City, CA, USA). Total RNA was extracted from whole tissue with the RNeasy RNA isolation kit (Qiagen, Valencia,

CA, USA). Samples (50 ng total RNA) were subjected to qPCR analysis with commercial reagents (Thermo Fisher-Invitrogen, Carlsbad, CA, USA) and analyzed with the ABI StepOne Plus Sequence Detector (Thermo Fisher-Applied Biosystems). TaqMan primers and probe for chemerin are as follows: Forward Sequence, CAGGAGATCGGTGTGGACAGT; Reverse Sequence, GAGCTTAAATTCC-AGCCTCACAA; Probe Sequence, TGATGACCTGTTCTTCTCAGCTGGCACCX. The PCR probes were labeled with 5′-FAM (a 6- carboxyfluorescein reporter) and 3′-TAMRA [a 5(6)-carboxytetramethyl rhodamine quencher]. After 40 amplification cycles, absolute values were obtained with SDS analysis software (Thermo Fisher-Applied Biosystems). Values were normalized to total RNA via Ribogreen measurement (Thermo Fisher-Invitrogen). The use of total RNA as a calibration control is validated [158].

2.7 Western analysis

Blood was centrifuged for 20 minutes at 4ºC and 2000 rpm. Plasma was collected and diluted 1:25 before performing a bicinchoninic acid assay for total protein (#BCA1, Sigma Chemical Co, St. Louis, MO, USA). Fat pads were homogenized in an Omni Bead Ruptor 24 (5.65 m/s, 2 cycles, 30 second cycles, 30 seconds between cycles, 6ºC; Omni International, Kennesaw, GA, USA). One-hundred µg of protein was added to a 15% polyacrylamide gel and run at 120 V. Protein was transferred to a PVDF-FL membrane (#IPFL00010, EMD Millipore, Billerica, MA, USA) for 1 hour at 100 V. Blots were dried, Total Protein Stain (#926-11011, Li-Cor) was added (if applicable) and reverted, then blocked with CEO for 3 hours. Chemerin antibody (1:1000; #112520, Abcam, Cambridge, MA, USA) was incubated for 48 hours at 4ºC and the secondary antibody (1:1000; IRDye

800 anti-Mouse, #926-32210, Li-Cor, Lincoln, NE, USA) was incubated for one hour at 4ºC. Transferrin was used as a loading control (1:1000; #82411, Abcam) with an IRDye 680LT secondary (1:1000; anti-rabbit, #926-68021, Li-Cor) for plasma and Total Protein Stain was the loading control for tissues. Total protein quantification is becoming the more preferred method of performing a loading control because it does not rely on the expression of one protein and can more ubiquitously control for leading over a large range of tissue types [159]. Blots were visualized using the Odyssey FC and CLx Infrared Imaging and quantified using Image Studio (5.2.5, Li-Cor).

2.8 Data analyses and statistics

All mRNA data were compiled, normalized to total RNA, then normalized to an average of all controls (PBS and scrambled control ASO). All percentages of mRNA expression were compared to this averaged control. Protein was quantified then normalized to loading controls (total protein or transferrin). If there were comparisons made between different blots, samples were further normalized to their respective PBS control. All percentages of chemerin protein expression were compared to an average of the control ASO measurement. While Western images may have brightness or contrast enhanced as a whole to visualize bands, it does not change the quantification by the Li-Cor Image Studio. All comparisons of significance were performed in Prism 7 (7.0c, Graph Pad, CA) using one-way ANOVA with a Sidak correction for multiple comparisons. Data are reported as mean ± SEM. *In vivo* data was analyzed by 2-way ANOVA (treatment and time) comparing the mean of each treatment with the others using a Sidak correction for multiple comparisons.

3. Results

3.1 Gen 2.5 Chemerin ASO must be dosed at 25 mg/kg for effective knockdown

A small experiment assessed the ability of the Gen 2.5 Chemerin ASO to knockdown chemerin mRNA concentrations at weakly consistent doses of 25 mg/kg, 12.5 mg/kg, and 6.25 mg/kg, comparing them all to the scrambled control ASO at the same dose. Chemerin mRNA expression in the liver (Fig 13A) was completely reduced with the 25 mg/kg dose compared with the control ASO. Expression with 12.5 mg/kg and 6.25 mg/kg dosing of Gen 2.5 chemerin ASO rose to 3.3 ± 0.3% and 9.0 ± 2.3%, respectively. Similarly, retroperitoneal (RP) fat (Fig 13B) exhibited a complete reduction in chemerin expression at 25 mg/kg with expression increasing to 16.0 ± 3.5% and 57.3 ± 2.7% with 12.5 mg/kg and 6.25 mg/kg, respectively. Chemerin expression from the mPVAT (Fig 13C) was variable but the protein and mRNA results from later studies (Fig 15 E-F) indicate that the ASO is working and effective in the mPVAT at 25 mg/kg. Circulating chemerin protein (Fig 13D) was also measured in this dosing study with complete knockdown of chemerin at the 25 mg/kg dose and levels rising to 6.0 ± 1.5% and 10.3 ± 2.7% in the 12.5 mg/kg and 6.25 mg/kg doses, respectively. Thus, 25 mg/kg was used as the dose of the chemerin ASO *in vivo*.

The goal of dosing the GalNAc Chemerin ASO is to confer the complete knockdown of the liver as seen in the Gen 2.5 Chemerin ASO, while maintaining chemerin expression in the fat pads. GalNAc-tagged ASOs have an increased liver potency of 10-30 fold [156]. Based on this information, preliminary activity studies, and the studies we will share in Figure 3, a dose of 10 mg/kg was used and proven effective.

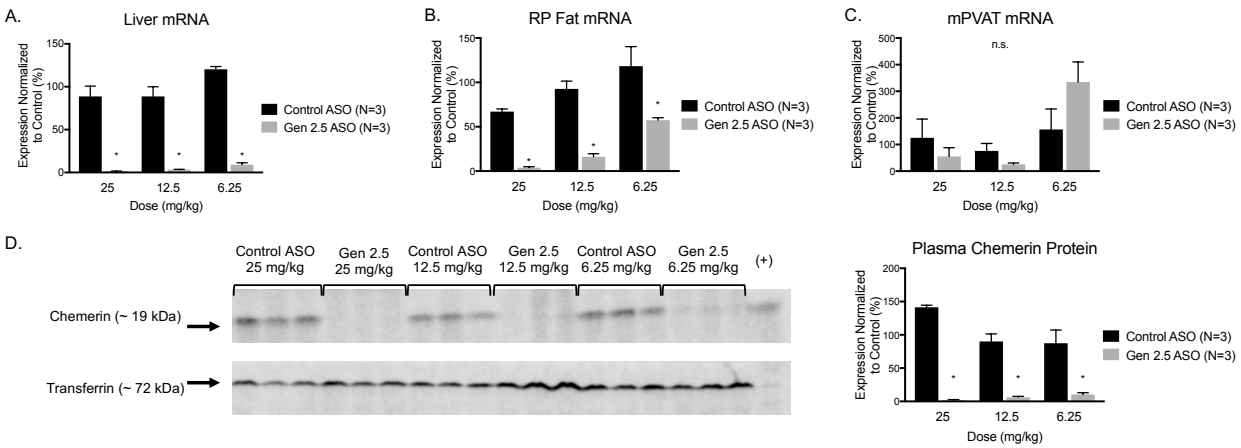

Figure 13: *Dosing of the chemerin ASO*

Chemerin mRNA measures of liver (A), retroperitoneal (RP) fat (B) and mesenteric perivascular adipose tissue (mPVAT; C) along with plasma chemerin (D) to determine the optimum dosing scheme for Gen 2.5 chemerin ASO (gray bars) against a scrambled control ASO (black bars). Amount of RNA was first normalized to total RNA then normalized to an average of all controls, making a percent. Densitometry data were normalized to transferrin. * = $p < 0.05$ and n.s. = no statistical significance by One-Way ANOVA with a Sidak Correction. Western blots are representative samples of the included bar graph. (+) represents the liver positive control separate from all treatments. Arrows indicate the levels of the indicated molecular weights.

3.2 Minimal off-target effects with a 4 week chemerin ASO regimen

Using established doses of Gen 2.5 chemerin ASO and GalNAc chemerin ASO, the effects of chemerin on physiologic parameters outside of MAP were minimal. There was no change in final body weight (Fig 14A) among any of the treatment groups. In addition, there was no difference in the total weight of the RP fat (Fig 14B) or heart (Fig 14E). The kidney showed a slight increase when compared to GalNAc chemerin ASO treatment (Fig 14F), but because there was no increase compared to control ASO or Gen 2.5 chemerin ASO, it is not considered physiologically significant with regards to chemerin. The only differences in organ weight as associated with ASO that modified chemerin were observed with liver (Fig 14C) and spleen (Fig 14D). Both exhibited differences between the control groups (PBS and control ASO) and groups where chemerin was removed (Gen 2.5 and GalNAc). Spleen weight increased 2.0-fold when treated against chemerin compared to controls.

3.3 Whole-body removal of chemerin lowers blood pressure

Gen 2.5 Chemerin ASO at 25 mg/kg significantly reduced chemerin mRNA expression in the liver (Fig 15A), RP fat (Fig 15C), and mPVAT (Fig 15E) down to 0.5 ± 0.1%, 3.9 ± 0.4%, and 30.7 ± 9.7% of control levels, respectively. More importantly, this reduction in chemerin mRNA led to a proportional reduction in chemerin protein expression to 2.7 ± 0.5% in liver (Fig 15B), 0.8 ± 0.7% in RP fat (Fig 15D), and 6.0 ± 1.1% in mPVAT (Fig 15F). Representative blots are shown on the left of the sub-figure while densitometry and normalization are shown on the right. Using the Gen 2.5 Chemerin ASO, circulating levels of chemerin were also undetectable (95% CI -0.02 – 0.24; Fig 16).

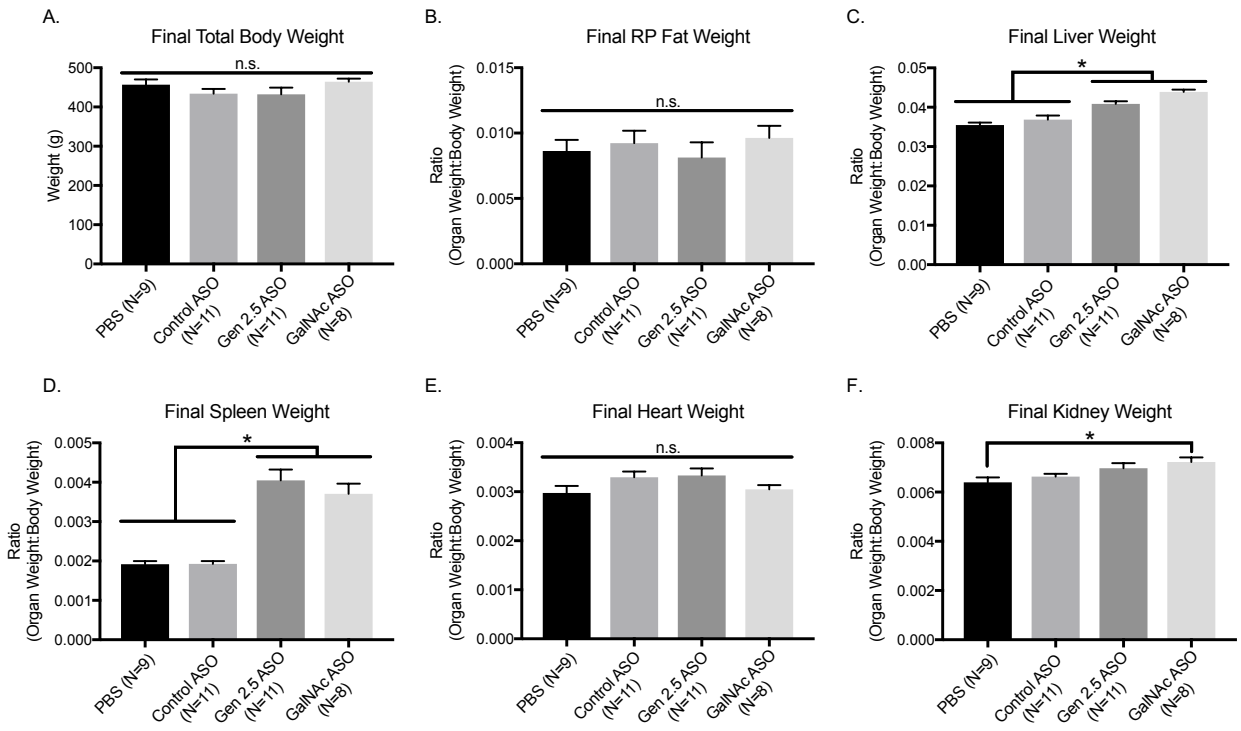

Figure 14: *Body and organ weights after given ASO*

Final weights of total mass (A), retroperitoneal (RP) fat (B), liver (C), spleen (D), heart (E), and kidney (F) after four injections of PBS, scrambled control ASO, Gen 2.5 chemerin ASO, or GalNAc chemerin ASO. All individual organs were normalized to their total body weight to give a ratio. * = $p < 0.05$ and n.s. = no statistical significance by One-Way ANOVA with a Sidak Correction.

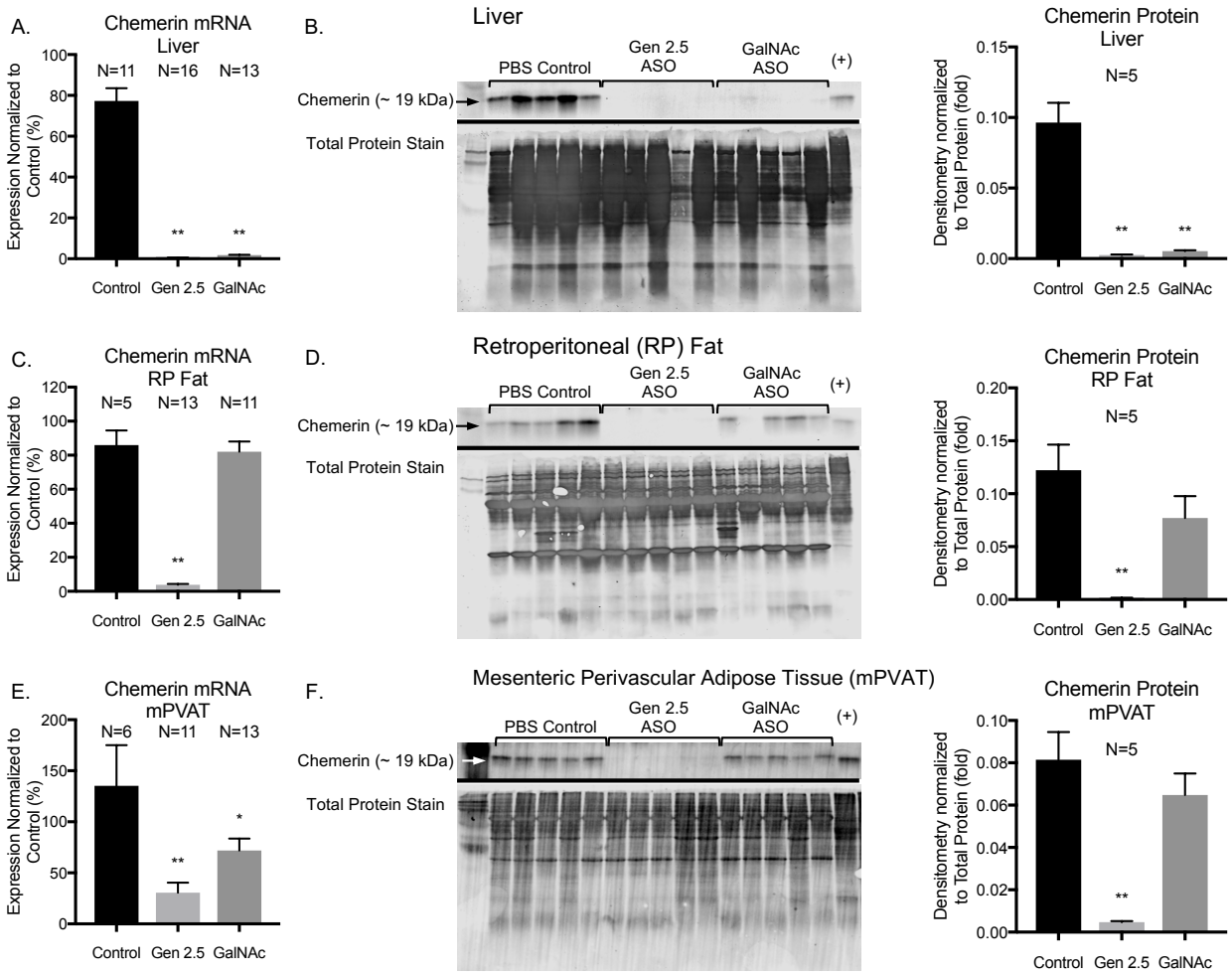

Figure 15: *Chemerin ASO knockdown of mRNA and protein*

Final measurements of chemerin mRNA and protein from liver (A-B), retroperitoneal (RP) fat (C-D), and mesenteric perivascular adipose tissue (mPVAT; E-F) after four treatments of PBS, Gen 2.5 Chemerin ASO, or GalNAc chemerin ASO. Amount of RNA was first normalized to total RNA then normalized to an average of all controls, making a percent. Densitometry was normalized to total protein. * = $p < 0.05$ and ** = $p < 0.01$ by One-Way ANOVA with a Sidak Correction. Western blots are representative samples of the included bar graph. (+) represents the liver positive control separate from all treatments. Arrows indicate the levels of the indicated molecular weights.

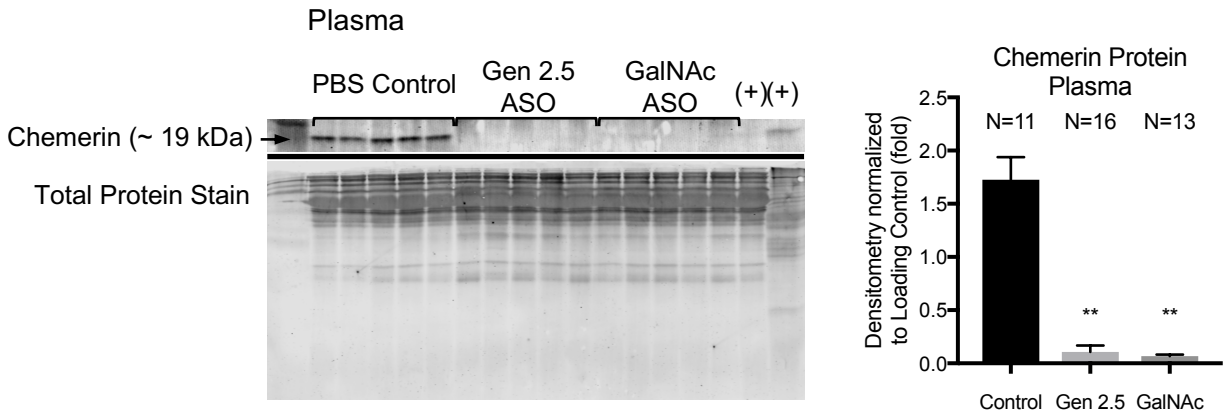

Figure 16: *Chemerin ASO reduces circulating chemerin protein*

Plasma chemerin is reduced after treatment with both Gen 2.5 Chemerin ASO and GalNAc chemerin ASO. Densitometry was normalized to the loading control (either transferrin or total protein) then normalized to their respective PBS control for comparison between blots. * = $p < 0.05$ and ** = $p < 0.01$ by One-Way ANOVA with a Sidak Correction. Western blots are representative samples of the included bar graph. (+) represents the liver positive control separate from all treatments. Arrows indicate the levels of the indicated molecular weights.

With this systemic loss of chemerin, MAP was reduced to a nadir of 7 ± 2.1 mmHg within 48-72 hours after each injection (Fig 17A). Among the Gen 2.5 ASO animals, there was no significant change in heart rate (Fig 17B) but there was a reflexive temperature rise with any chemerin ASO treatment (Gen 2.5 and GalNAc; Fig 17C).

3.4 Removal of liver chemerin alone does not show the same blood-lowering effects

When treated with an ASO modified to specifically deliver its cargo to the liver (GalNAc), the 10 mg/kg dose maintained its complete knockdown of liver chemerin mRNA (Fig 15A) and protein (Fig 15B). RP fat was not significantly affected by GalNAc chemerin ASO either in mRNA (Fig 15C) or protein expression (Fig 15D). While chemerin mRNA was modestly reduced in the mPVAT with GalNAc chemerin ASO (Fig 15E), its levels were significantly increased from Gen 2.5 Chemerin ASO levels ($p = 0.01$). Likewise, the chemerin protein expression in mPVAT was not significantly reduced from control (Fig 15F). Even with the fat depots expressing higher levels of chemerin, plasma chemerin levels were still reduced by 90% ± 5% by the GalNAc chemerin ASO (Fig 16). However, when MAP of the GalNAc chemerin ASO-treated animals was measured, there was no significant reduction in MAP (Fig 17A). Similar to Gen 2.5 ASO, rats treated with GalNAc chemerin ASO did not show a change in heart rate (Fig 17B) but did cause spikes in temperature with injections (Fig 17C). A liver-effective dose of GalNAc chemerin ASO at 10 mg/kg was confirmed by the knockdown of chemerin from liver and maintenance of chemerin expression and protein in the RP fat and mPVAT (Fig 15).

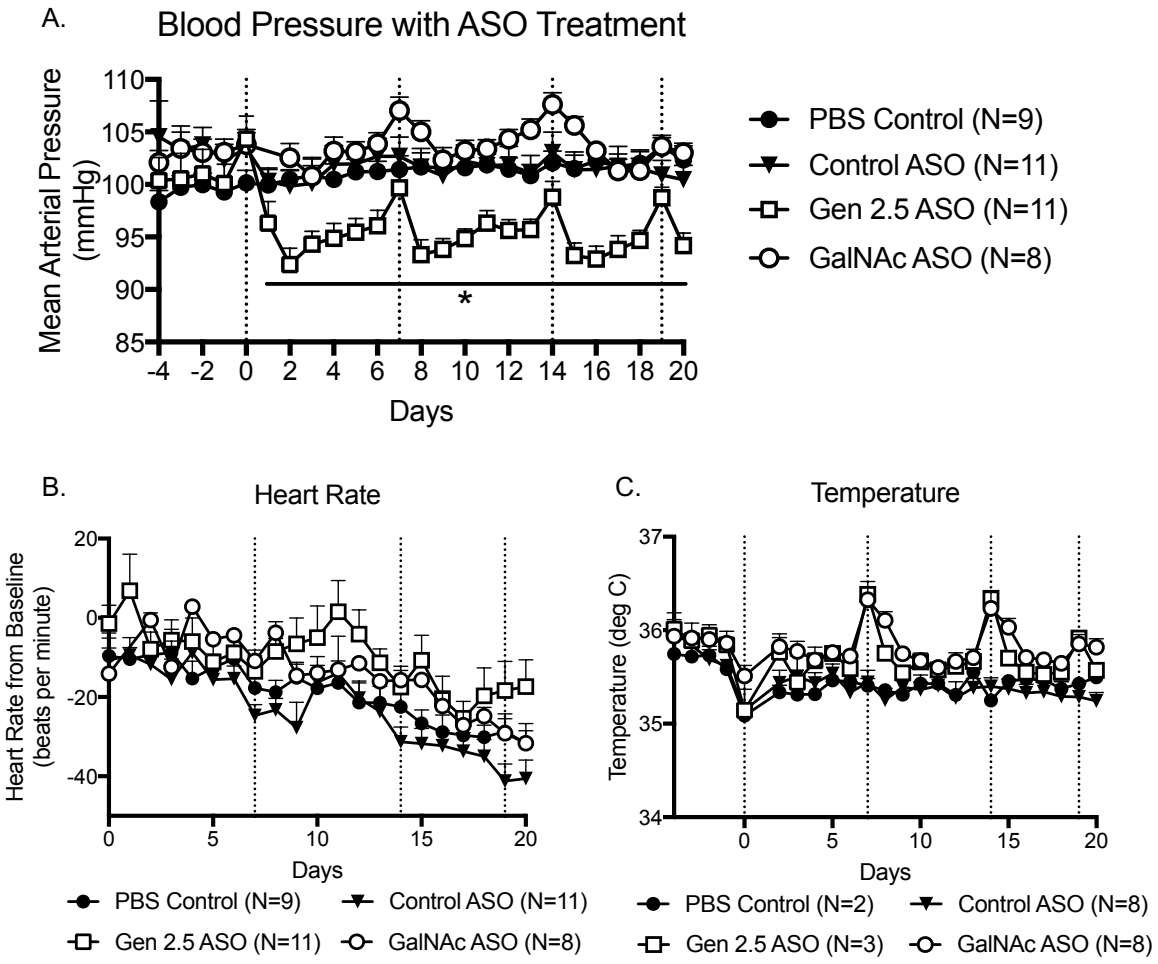

Figure 17: *Chemerin ASO reduces blood pressure in SD rats*

Mean arterial blood pressure (A), heart rate (B), and temperature (C) collected by radiotelemetry during a 5-day baseline and 20-day treatment with four injections on days 0, 7, 14, and 19 (dotted lines). * = $p < 0.05$ by Two-Way ANOVA with Sidak Correction comparing the entire datasets. Baseline measures for heart rates: PBS control, 383 ± 7 beats/min; control ASO, 389 ± 7 beats/min; Gen 2.5 Chemerin ASO, 379 ± 8 beats/min; and GalNAc chemerin ASO, 362 ± 9 beats/min. The baseline period (days -4 to -1) is not shown because it was used to calculate the subsequent values.

4. Discussion

The literature of chemerin promotes two major roles for this molecule. First, chemerin is a chemokine with the ability to promote chemotaxis of dendritic cells [46], natural killer cells [160], macrophages [42], and T lymphocytes [54]. Second, chemerin is an adipokine [38] with the ability to promote blood vessel formation [50]. This dichotomy seems to be supported by the two classes of major producers of chemerin: liver and fat. Our goal was to take the first step towards understanding the role of chemerin, ultimately in the adiposity-associated hypertensive models, by performing these critical studies in the normal rat.

4.1 The liver provides the majority of circulating chemerin

When the chemerin mRNA expression by the liver is virtually abolished (Fig 15A-B) and adipose tissue expression remains high (Fig 15C-F), the plasma chemerin levels are drastically reduced (Fig 16). This not only supports previous literature that the liver is the primary producer of chemerin mRNA [35], but is also the first to show that the majority of chemerin protein in the plasma of the rat is derived from the liver.

The role of the liver in promoting circulating chemerin levels supports the role of chemerin as a chemokine. Our understanding of the liver as an organ that regulates immune responses and inflammation is expanding. The liver is a highly perfused organ exposed to a variety of toxins and insults (especially from the gastrointestinal system) and must manage the balance of healthy inflammation with hazardous stimuli [161]. The prominent association of the liver with circulating chemerin uncovered by this study

indicates that chemerin may have a role to play in this evolving story of the liver as an immunomodulatory organ.

Both the liver and spleen had increased final weights when treated with both the Gen 2.5 Chemerin ASO and GalNAc chemerin ASO (Fig 14C-D). While ASOs can cause tissue hypertrophy, the treatments that caused a difference were those that targeted chemerin mRNA. Because the control ASO did not cause a spleen enlargement, the hypertrophy most likely is a result of the loss of chemerin and not an off-target effect of the ASO. While future studies will have to assess the microscopic and histological changes of these two organs, we can reasonably assume that because this hypertrophy also happened modestly in the liver of the GalNAc chemerin ASO-treated animal, the hypertrophy is related to liver function or plasma chemerin levels. The hypertrophy of the spleen was prominent in these studies and highlights a possible new role of chemerin in the body.

4.2 Blood pressure is locally regulated by chemerin

While the liver may support chemerin as a chemokine and provide circulating stores of the protein, it is not significantly involved in blood pressure regulation. Based on our initial hypothesis that the liver and circulating chemerin levels contribute to blood pressure regulation, we would have expected a proportional change between plasma chemerin levels and a lowering of MAP. With the GalNAc chemerin ASO, MAP remained at control levels (Fig 17A) while plasma chemerin levels still dropped by 90% (Fig 16). By contrast, MAP reduction in the whole-body knockdown of chemerin (Fig 17A) demonstrates that chemerin still has a role to play in blood pressure regulation. This is in

accordance with previous *in vitro* studies on blood vessel contractility [39, 142]. A 7 mmHg fall in MAP with the whole-body chemerin ASO may seem modest, but this reproducible indication of blood pressure control by chemerin in a normal SD rat gives continued studies promise for an interaction between chemerin and blood pressure. Future studies will focus on the effects of chemerin in hypertensive and obesity rat models.

The most reasonable explanation for the reduction in MAP outside of circulating chemerin levels lies with the adipose tissue. First, chemerin is an adipokine. Second, amongst all organs in the body, the liver and white adipose are the primary producers of chemerin. Lastly, fat pads where chemerin production is regulated (RP and mPVAT) are also implicated in being important for the hypertensive pathology. The MAP with ASO treatment does not seem to be affected by other cardiovascular factors like reductions in heart rate (Fig 17B) or cardiac hypertrophy (Fig 14E).

The maintenance of body weight across the treatments (Fig 14A) along with the specific maintenance of RP fat pad weights (Fig 14B) supports that Gen 2.5 chemerin ASO given over a 4-week period did not have effects on the adipogenesis of this adipokine but still effected the secretion of the cells. While chemerin secreted by the fat can certainly make its way into the circulation, the proportional loss in plasma chemerin protein and MAP between Gen 2.5 chemerin ASO and GalNAc chemerin ASO (Fig 16-17) does not match. As such, the output of these adipocytes may also have a paracrine-like effect on the vascular beds they surround and protect.

4.3 Limitations

The ASO technology was necessary and invaluable for its ability to help us manipulate chemerin protein expression *in vivo*. However, there are no currently known ways to specifically target an ASO to the adipocytes. As a result, we can draw direct conclusions about the function of the liver and chemerin but only inferences about the role of fat. This study can only conclude that the loss in MAP is due to chemerin production in sites outside the liver. However, this study provides (indirect) support for the role of chemerin and fat in regulation of blood pressure. Future *in vivo* studies will have to approach directly this association but the technology to do so does not currently exist.

While chemerin mRNA expression in the RP fat (Fig 13B) was reduced to 67 ± 3% with 25 mg/kg control ASO and chemerin protein seemed to increase to 141 ± 3% in the plasma (Fig 13D) with 25 mg/kg control ASO, the complete reduction in chemerin expression that comes with the Gen 2.5 Chemerin ASO at 25 mg/kg is necessary to draw conclusions about chemerin and other physiological measures. While these effects of the control ASO may be of a therapeutic concern, we do not make any claims about the ideal therapeutic dosing in this study – only the effective dose for chemerin knockdown. This increase of chemerin mRNA expression with the 25 mg/kg dose of control ASO did not change any other physiological parameters such as MAP, temperature, or heart rate (Fig 17). As such, the apparent increase in chemerin mRNA with control ASO is an acceptable event to accomplish the complete knockdown of chemerin with the whole-body ASO.

These studies were performed on normotensive, healthy rats. Future studies will apply this technology and method to models of hypertension and obesity to observe if these changes in blood pressure are conserved or exacerbated in these pathological

states. While we cannot use the present study to make any direct conclusions about chemerin in hypertension or obesity, linking chemerin to blood pressure and suggesting that blood pressure control is dependent on adipose tissue is an important stepping stone towards connecting chemerin to pathology.

4.4 Conclusions

Understanding the responsibilities of liver and fat in the biological mechanisms of chemerin is important for reasons that are expanding and evolving, but the specific association of chemerin and blood pressure should focus on the fat. Thanks to the improving technology of ASOs, we were able to assess the role of chemerin *in vivo* in a way that efficiently targeted specific organs. We demonstrate that chemerin continues to be important in the world of blood pressure regulation but the mechanism by which it accomplishes this regulation may be unconventional. All signs point toward chemerin as having a local effect through the fat on the vasculature.

AIM 2.2: In vivo effects of chemerin on obesity-associated hypertension

This chapter was adapted from:

Ferland DJ, Flood ED, Garver H, Yeh ST, Riney S, Mullick AE, Fink GD, Watts SW. Different blood pressure responses in hypertensive rats following chemerin mRNA inhibition in dietary high fat compared to dietary high-salt conditions. Physiol Genomics. 2019 Nov 1;51(11):553-561. doi: 10.1152/physiolgenomics.00050.2019.

1. Introduction

While the diagnosis of hypertension is important because it identifies an individual as having a higher risk of a potentially fatal secondary event like a stroke or heart attack, different circumstances can lead to the same elevation in blood pressure. One sub-population with an important connection to hypertension are people with obesity [4]. Up to 75% of primary hypertension can be attributed to visceral adiposity [152]. Hypertension and obesity are essential elements to the diagnosis of metabolic syndrome, which includes alterations in waist circumference, fasting glucose, blood pressure, plasma HDL and triglycerides [7].

Chemerin is a protein that has recently emerged in the epidemiological literature because of positive associations of circulating chemerin with blood pressure [24, 26, 27, 29, 30, 86, 92], glucose levels [162], and obesity [24, 26, 29, 33, 34]. These associations led to chemerin being proposed as a marker for metabolic syndrome [36, 163]. Studies are beginning to provide mechanistic support for these epidemiological associations. First, chemerin is an adipokine, with primary production in the liver and adipose tissue [35], that enhances the development of adipocytes as well as maintenance of mature adipocytes [38]. Second, chemerin is contractile in vasculature of both humans and rats with the literature attributing this mechanism to its actions on the endothelium [100, 153], smooth muscle cells [64, 142], and local nerves [154]. Despite the *in vitro* vasoactivity of chemerin, few studies have evaluated the role of chemerin on blood pressure regulation. Recently, we demonstrated that antisense oligonucleotide (ASO)-mediated reductions of whole-body chemerin resulted in small, yet statistically significant blood pressure reductions in normal chow-fed Sprague Dawley (SD) male rats [164].

Through Watson and Crick pairing, ASOs bind to target pre-mRNA in the nucleus of cells, facilitating its destruction thereby preventing its protein translation [155]. ASOs can be delivered subcutaneously and have a half-life on the order of weeks to months. Following systemic administration, ASOs distribute to various tissues except for the CNS [80]; the primary sites of systemic tissue uptake and ASO potency include liver and kidney, followed by adipose tissue. Ligands can be covalently attached to the ASO to enhance delivery into specific cell types. Notable to this project is the use of N-acetylgalactosamine (GalNAc) ligand that enhances uptake into hepatocytes via the asialoglycoprotein receptor (ASGPR), thereby markedly reducing uptake into non-ASGPR expressing cells such as adipose tissue [156, 157]. In our previous study, administration of the liver-specific chemerin ASO abolished circulating plasma levels of chemerin, but did not decrease chemerin production from fat or blood pressure as did the whole-body chemerin ASO in lean SD male rats [164]. This makes it doubtful that the liver or plasma contribute chemerin that regulates blood pressure. Chemerin's classification as an adipokine suggested that the fat may be an important contributor to chemerin's blood pressure effects. Fat-specific ASOs are not available, so to make inferences about the relation of fat-derived chemerin and blood pressure, we can target the other major source of chemerin (liver) and compare different etiologies of hypertension (high-fat vs. high-salt diet).

For the current study, we hypothesized that rats made hypertensive by high-fat (HF) diet would demonstrate a reduction of blood pressure with the whole-body ASO against chemerin but not with the liver-specific ASO against chemerin. To determine whether this effect might be specific for fat-associated hypertension rather than a general

response of hypertensive animals, we also tested the effect of the same ASO treatment on blood pressure in lean animals made hypertensive from ingestion of a high-salt (HS) diet (another recognized risk factor for hypertension).

The Dahl S rat was chosen as a model of both normal-weight hypertension and fat-associated hypertension. The Dahl S HF-diet rat is unique as one of the few diet-induced models of obesity-associated hypertension among both mice and rats. Dahl S animals fed a HS [165] or HF [163, 166] diet will develop high blood pressure on their respective diet versus an animal fed a control diet. Dahl S HF animals also have increased visceral adiposity compared to control diet controls [166]. Even though the mechanism of elevated blood pressure in a Dahl S animal fed HF diet is still under investigation, this model is advantageous because animals of the same genetic background and age develop similar levels of hypertension with different stimuli. If chemerin secreted from fat is unique to the etiology of hypertension in the HF Dahl S rat, the chemerin ASO will reduce blood pressure to a greater degree in the HF animal than the HS animal. These data suggest a major role of chemerin in HF, but not HS-induced hypertension.

2. Methods

2.1 Animal handling

All procedures that involved animals were performed in accordance with the institutional guidelines and animal use committee of Michigan State University. Animals were maintained on a 12/12 hour light/dark cycle at a temperature of 22-25°C.

2.2 Rat models of disease

For the high-fat (HF) model, Dahl salt-sensitive (Dahl S) rats were purchased from Charles River Laboratories (Portage, MI, USA) and placed on a HF diet (60% kcal from fat, 0.3% NaCl; D12492, Research Diets, New Brunswick, NJ, USA), *ad libitum*, from weaning at three weeks of age for 21 weeks before ASOs were administered. Rats were single-housed and remained on their respective diets for the duration of the experiment.

For the high-salt (HS) model, Dahl S rats were purchased from Charles River Laboratories (Portage, MI, USA) and placed on a HS diet (12% kcal from fat, 4% NaCl; D17013, Research Diets), *ad libitum*, starting at 20 weeks of age for four weeks until ASO treatment began. High-salt diet was continued through the duration of the experiment.

2.3 Radiotelemetry and ASO administration

Catheters for radiotelemetry were placed in the femoral artery and the radiotelemeter body was placed subcutaneously (HD-S10, DSI, MN, USA). Catheters for both diet groups were implanted between 16 and 18 weeks of age. Rats were allowed to recover for at least one week and baseline measurements were collected over four days before ASO administration. Physiologic measures were sampled for ten seconds every ten minutes for the duration of the experiment. Data are represented as 24-hour averages of the aforementioned sampling.

ASO synthesis and sequences are exactly as previously described [164]. The following are lists of the scrambled control, liver-specific and whole-body ASOs used in this study:

Scrambled control (5’-3’): GGCCAATACGCCGTCA

Liver-specific (5’-3’): GalNAc-ACAGTTTTATTAGCCTGGAG

Whole-body (5’-3’): GTTTTATTAGCCTGGA

ASOs were designed to avoid any perfect match rat mRNA and where chosen from >300 ASOs as being well-tolerated and potent. In silico off-target analysis of the liver-specific 20mer ASO shows no off-targets with zero- or one-base mismatches, and only 1 off-target (Zfp804b) with 2 base mismatches. The 16mer whole body chemerin ASO does have 22 one-base mismatch targets, this is common given its shorter size. None of these targets are regulators of blood pressure or adipocyte development.

Experiments were carried out in three cohorts, separated in time, and pooled for a final result: 1) HF Dahl S with control and whole-body ASO, 2) HS Dahl S with control and whole-body ASO, and 3) HF Dahl S with whole-body and liver-specific ASO. To administer ASOs, animals were anesthetized with 1-2% isoflurane, weighed, and subcutaneously injected with 25 mg/kg control ASO, 25 mg/kg whole-body ASO, or 10 mg/kg liver-specific ASO on days 0, 7, 14, and 19. Samples were collected on day 21 and euthanasia was performed under 1-2% isoflurane with pneumothorax. Kidney, liver, epididymal fat, retroperitoneal fat (dissected from the posterior abdominal wall), and heart were dissected and weighed. Samples of blood (collected in EDTA), liver, epididymal fat, retroperitoneal fat, mesenteric fat (taken from the distal superior mesenteric artery avoiding mesenteric resistance vessels), and aortic fat were collected for protein and mRNA analysis. Blood was stored at 4°C and tissue was placed in liquid nitrogen.

2.4 Western blots

Protein analysis for plasma and tissue was performed as described [164]. Blood was centrifuged for 20 minutes at 4ºC and 500 xg. Plasma was collected and diluted 1:25 before performing a bicinchoninic acid assay for total protein (#BCA1, Sigma Chemical Co, St. Louis, MO, USA, RRID:SCR_008988). Fat pads were homogenized in an Omni Bead Ruptor 24 (5.65 m/s, 2 cycles, 30 second cycles, 30 seconds between cycles, 6ºC; Omni International, Kennesaw, GA, USA). One-hundred µg of protein was added to a 15% polyacrylamide gel and run at 120 V. Protein was transferred to a PVDF-FL membrane (#IPFL00010, EMD Millipore, Billerica, MA, USA) for 1 hour at 100 V. Blots were dried, Total Protein Stain (#926-11011, Li-Cor) was added and reverted, then blocked with chick egg ovalbumin for 3 hours. Chemerin antibody (1:1000; Abcam Cat# ab112520, RRID:AB_10864055, Cambridge, MA, USA) was incubated with blots for 48 hours at 4ºC, and the secondary antibody (1:1000; IRDye 800 anti-Mouse, LI-COR Biosciences Cat# 926-32210, RRID:AB_621842, Lincoln, NE, USA) was incubated with blots for one hour at 4ºC. Total Protein Stain was the loading control for tissues. Total protein quantification is becoming a preferred method of performing a loading control because it does not rely on the expression of one protein and can more ubiquitously control for leading over a large range of tissue types [159]. Blots were visualized using the Odyssey CLx Infrared Imaging (Odyssey CLx, RRID:SCR_014579) and quantified using Image Studio (5.2.5, LI-COR Image Studio Software, RRID:SCR_015795). When quantifying signal within Image Studio, adjustment of LUTs does not affect the signal result.

2.5 PCR

Analysis for mRNA was performed as described in our previous study [164]. Quantitative qRT-PCR (qPCR) mRNA analysis was performed with TaqMan primer probes (Thermo Fisher-Applied Biosystems, Foster City, CA, USA). Total RNA was extracted from whole tissue with the RNeasy RNA isolation kit (Qiagen, Valencia, CA, USA, RRID:SCR_008539). Samples (50 ng total RNA) were subjected to qPCR analysis with commercial reagents (Thermo Fisher-Invitrogen, Carlsbad, CA, USA) and analyzed with the ABI StepOne Plus Sequence Detector (Thermo Fisher-Applied Biosystems). TaqMan primers and probe for chemerin are as follows: Forward Sequence, CAGGAGATCGGTGTGGACAGT; Reverse Sequence, GAGCTTAAATTCC-AGCCTCACAA; Probe Sequence, TGATGACCTGTTCTTCTCAGCTGGCACCX. The PCR probes were labeled with 5′-FAM (a 6- carboxyfluorescein reporter) and 3′-TAMRA [a 5(6)-carboxytetramethyl rhodamine quencher]. After 40 amplification cycles, absolute values were obtained with SDS analysis software (Thermo Fisher-Applied Biosystems). Values were normalized to total RNA via Ribogreen measurement (Thermo Fisher-Invitrogen). The use of total RNA as a calibration control is validated [158].

2.6 Analyses and statistics

After sample collection, researchers performing the western and PCR analysis were blinded as to the treatment of the animal. In PCR, averages of normalized (total RNA) control ASO were used to establish the percentage of mRNA expression with whole-body and liver-specific treatments. Westerns were normalized to total protein. Contrast and brightness have been adjusted on Western images (whole, not in part) but

these adjustments do not affect the measurements in the Image Studio software. Statistical analysis was performed on GraphPad Prism (7.0c, Graph Pad, La Jolla, CA, USA, RRID:SCR_002798). Data are reported as mean ± SEM. Comparisons of one variable were made using one-way ANOVA and Tukey's correction for multiple comparisons (if more than two groups were being compared) or students t-test (if only two groups were being compared). Comparisons involving two variables (treatment and time) were performed using a 2-way ANOVA with a Tukey correction for multiple comparisons. Statistics used for each analysis are shown in each figure legend.

3. Results

3.1 Chemerin ASOs knockdown mRNA expression and translated protein

Absolute mRNA levels of chemerin from animals given control ASO (figure 18A; measurements made against a standard curve relative to total RNA in each sample) indicate that chemerin expression was higher in the mesenteric and retroperitoneal fat of the HF-fed animals versus the HS-fed animals. In both models of hypertension (HF and HS), chemerin mRNA (figure 18B) was present and detectable in rats that received scrambled control ASOs. We have previously validated that chemerin mRNA expression in tissue is representative of protein expression in that tissue [164]. We have also validated that while mesenteric chemerin mRNA expression is more variable than the others, chemerin protein is highly expressed with administration of control ASOs [164]. In both HF and HS animals, whole-body chemerin ASOs completely abolished chemerin mRNA expression in the liver, mesenteric (mes) fat, and retroperitoneal (retro) fat relative to levels in diet-matched control ASO animals. Circulating chemerin levels as measured

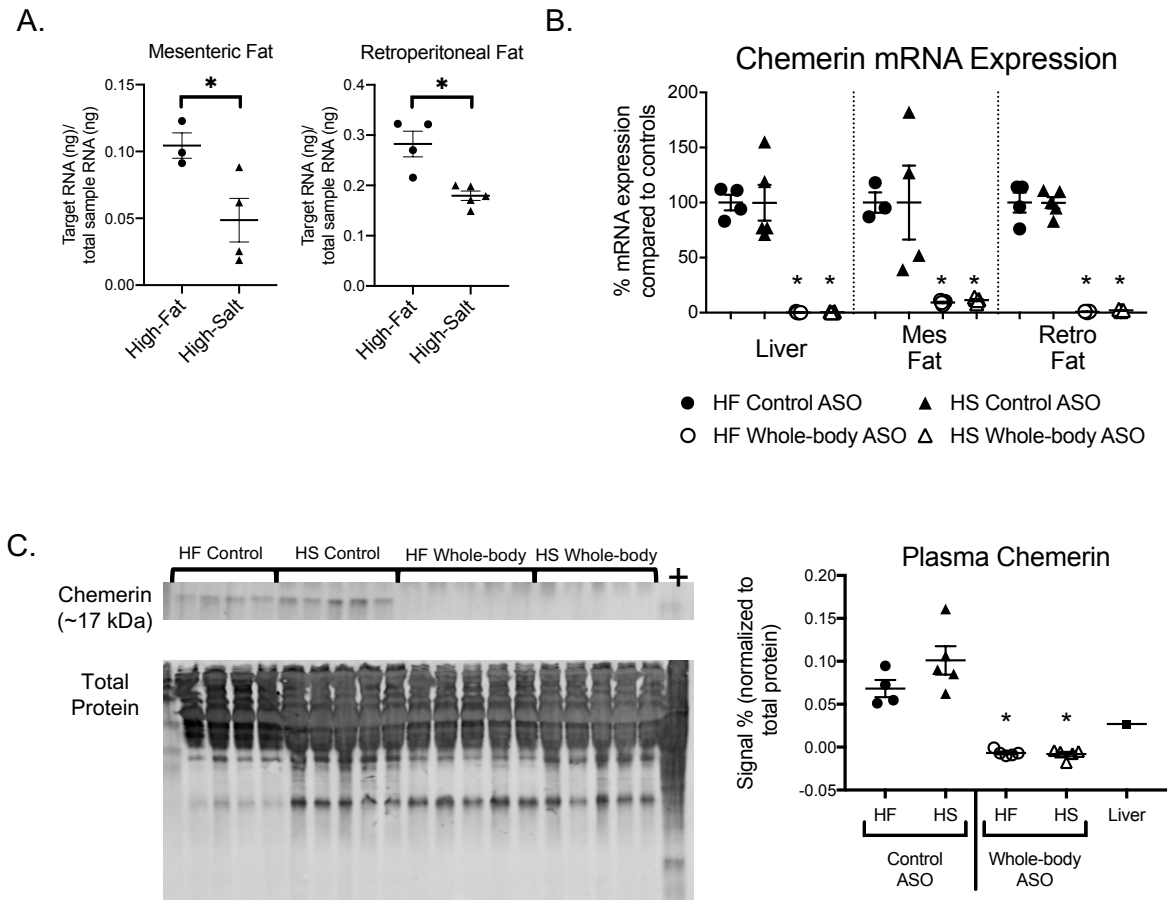

Figure 18: *ASOs knocked down chemerin expression in HF and HS animals*

Absolute quantifications of animals receiving control ASO measure chemerin mRNA expression using standard curves normalized to total RNA in the sample. In both mesenteric and retroperitoneal fat, chemerin expression is higher in the HF fed animals versus the HS fed animals (A). When HF animals, along with HS animals, are given scrambled control or whole-body ASOs against chemerin, mRNA expression (as measured by PCR) was abolished in liver, mesenteric (mes) fat, and retroperitoneal (retro) fat (B). Plasma chemerin protein levels (measured by Western blot) are also completely knocked down with whole-body ASO (C). In all Western blots, the chemerin band (~17 kDa) is shown on top and total protein stain (used as loading control) on bottom. Positive control (+) for westerns was liver homogenate isolated from normal SD animals. Negative numbers in Westerns represent instances where the band at the specified molecular weight was lighter than the average background signal for that lane. For HF Control ASO, N = 4; HF Whole-body ASO N = 5; HS Control ASO, N = 5; HS Whole-body ASO, N = 5 where N represents biological replicates. Scatter plots display data distribution as well as mean ± SEM. * represents $p < 0.05$ statistically significant change in the indicated group compared to its control as measured by a One-way ANOVA and Tukey multiple comparisons test (if more than two groups are compared) or by students t-test (if only two groups are being compared).

by Western blot (figure 18C) were undetectable in animals treated with the whole-body chemerin ASO in both diets and maintained in rats that received control ASO.

3.2 Organ analysis of HF vs. HS Dahl S animals

Age-matched Dahl S animals fed a HF diet were the same final weight as HS animals at the end of ASO administration (figure 19A). Total body weight as a difference from baseline did not change over the course of the drug treatment (data not shown). When controlled for overall body weight, HF animals had more epididymal and retroperitoneal fat mass than their HS counterparts (figure 19B-C). The epididymal and retroperitoneal fat masses are prime examples of white fat depots in the rat and are relatively easy to dissect upon euthanasia. While not as easily measured, we expect that other white adipose depots, like the mesenteric adipose tissue, are also increased relative to body weight with HF feeding. We have previously validated, in our hands, that HF Dahl S rats have an expanded visceral fat depot compared with control diet Dahl S rats [166]. Neither heart nor kidney weight (indexed to total body weight) were changed with administration of chemerin ASO (figure 19D-E).

3.3 Chemerin ASOs in HF Dahl S animals cause a fall in blood pressure

A one-way ANOVA of the average blood pressure at baseline in the four treatment groups (HS Control, HS Whole-body, HF Control, HF Whole-body; Table 2; https://figshare.com/s/ccd53be88eaefd81f466) revealed no significant differences with a 0.83 power. After the first administration of the whole-body ASO, mean arterial pressure (MAP) reached its lowest point in 48 hours (figure 20A). Previous studies with ASOs of

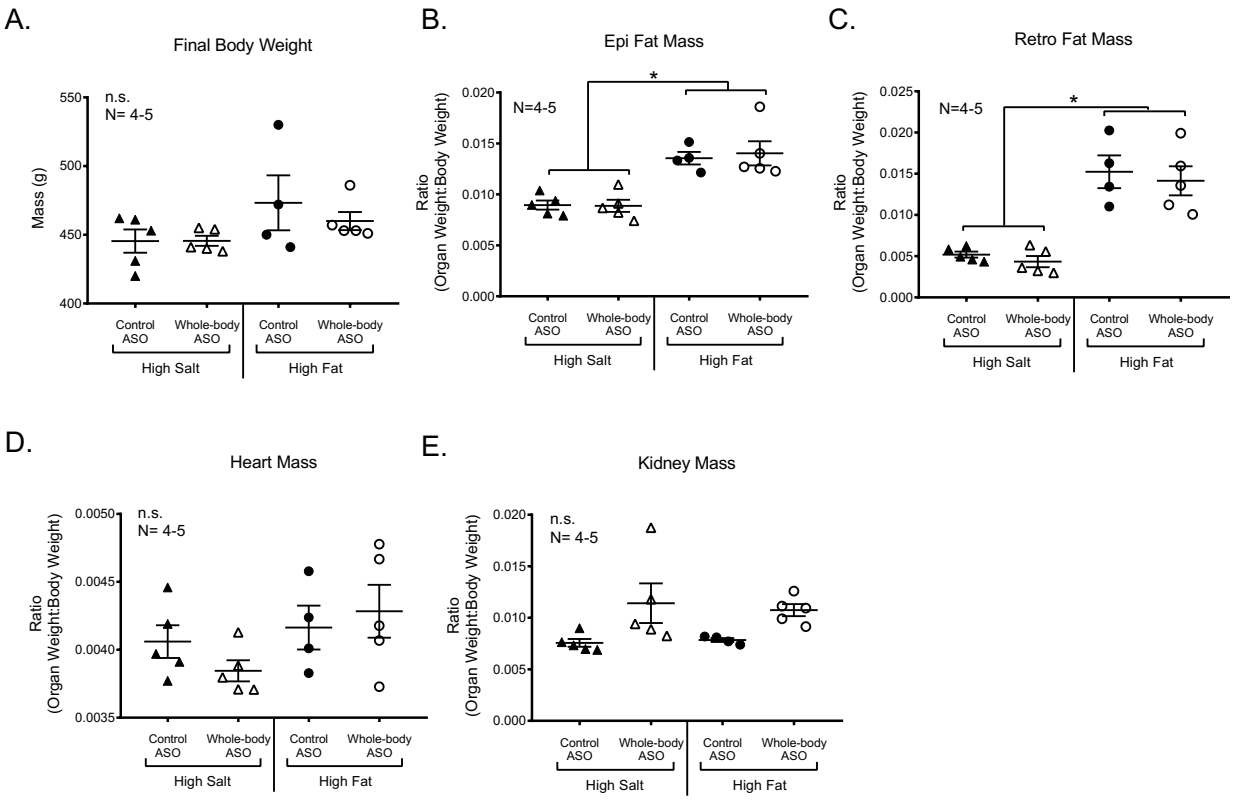

Figure 19: *High-fat animals have increased proportional fat mass*

On day 21, rats were euthanized and body weight was recorded (A). Epididymal (epi; B) and retroperitoneal (retro; C) fat pads were increased in mass when controlled for total body weight. Heart (D) and kidney (E) mass were not increased. Scatter plots are representative of the biological replicate (N) listed in the figure and show mean ± SEM. * represents $p < 0.05$ and n.s. represents “no significance” by One-way ANOVA with Tukey’s multiple comparison test.

Baseline measures of treatment groups

Baseline Values	MAP (mmHg)	HR (bpm)	PP (mmHg)
HS Control (N=5)	163 ± 5	373 ± 14	55 ± 2
HS Whole-body (N=5)	167 ± 7	361 ± 10	59 ± 1
HF Control (N=4)	174 ± 6	366 ± 7	61 ± 1
HF Whole-body (N=9)	170 ± 7	363 ± 5	58 ± 2
HF Liver-specific (N=3)	153 ± 9	346 ± 5	55 ± 1

Table 2: *Baseline values of treatment groups are similar*

Baseline values for mean arterial pressure (MAP), heart rate (HR), and pulse pressure (PP) for data used in figures 20 and 22 are listed here. Data represent mean ± SEM for the N value (biological replicate) listed for each group. Each N represents a four-day average before the first injection.

the same backbone confirm that knockdown of the RNA persists through acute changes of blood pressure [157]. Additionally, the homeostatic response we observed is typical of virtually all antihypertensive drugs. In the HF animal, this lowest point after first injection was about 21 ± 2 mmHg below baseline while in the HS animal, it was only 6 ± 2 mmHg below baseline. Over the course of the entire experiment, the nadir of MAP captured in the HF animals was 29 ± 2 mmHg below baseline and was 12 ± 4 mmHg below baseline in the HS animals. MAP in the HS control ASO animals continued to rise throughout the experiment given the continuing HS diet. The largest difference in MAP between HS rats receiving control ASO and HS rats receiving chemerin ASO was 19 ± 4 mmHg, statistically lower than the difference seen in the HF animals, 30 ± 3 mmHg (by $p < 0.05$; figure 20A).

HF whole-body ASO rats experienced a temporary spike in heart rate (HR) the day after ASO administration. Overall, none of the treatment groups experienced a significant change in heart rate over the course of the experiment (figure 20B). Pulse pressure (PP; difference between systolic and diastolic blood pressure) was significantly reduced in the HF animals treated with chemerin ASO versus all other treatment groups (figure 20C).

3.4 Liver-specific ASOs have a minor effect on fat-associated hypertension

HF animals were given the liver-specific ASO (GalNAc), paired with rats given whole-body ASO. These data were combined with other individual data points from previous cohorts given the same treatment scheme to make comparisons between whole-body ASO and liver-specific ASO. However, Western blots were re-run with samples from multiple cohorts to make comparisons of plasma chemerin levels. With the liver-specific

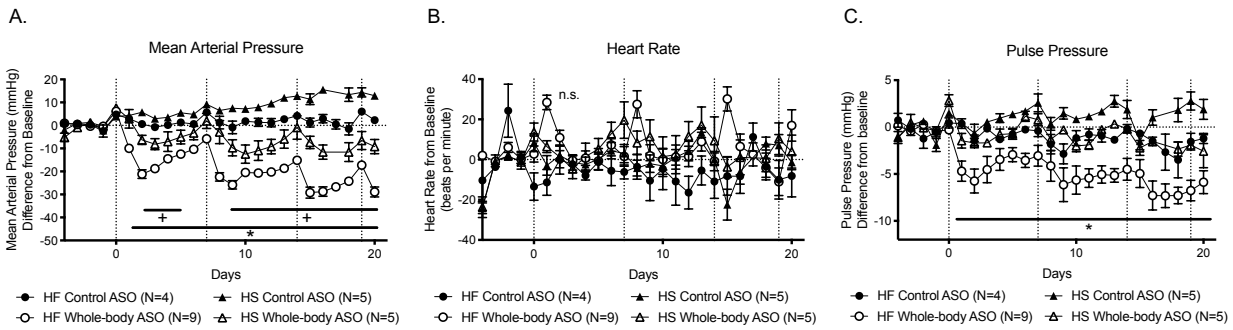

Figure 20: *HF animals experience a profound drop in blood pressure with whole-body chemerin ASO*

Dahl S animals receiving HF diet experienced a larger fall in mean arterial pressure (MAP) with whole-body ASO compared to Dahl S HS animals, even when the difference is calculated from the control ASO of the same diet (A). Heart rate (HR) did not change with ASO or diet (B). Pulse pressure (PP) was decreased in HF animals receiving whole-body ASO compared to all other groups (C). Dotted vertical lines represent dates of ASO injection and dotted horizontal lines represent baseline. Baseline values are listed in the table 1. * represents $p < 0.05$ of the HF whole-body group compared to all other groups. + represents $p < 0.05$ of the HS whole-body ASO group compared to all other groups. Points and error bars represent mean ± SEM. Statistics were measured using 2-way ANOVA and Tukey's multiple comparison test. N values represent biological replicates and are listed in the figures. Cardiovascular measures of HF animals administered whole-body ASO in the cohort also receiving the liver-specific ASO were pooled and included in this figure. Because analysis of Westerns and PCR should not be pooled outside of their respective blots or plates, they were not included in the previous figure 19 but were still analyzed and shown in figure 21.

ASO, chemerin mRNA expression in the mesenteric fat and retroperitoneal fat remained at control levels but was abolished in the liver (figure 21A). Plasma chemerin protein levels of the Dahl S HF animals given liver-specific ASO were decreased by 96% ± 1% compared to those in control ASO treated rats, but remained at levels above those observed in whole-body ASO treated rats (figure 21B).

After the first injection, the lowest point of blood pressure occurred in 48 hours. Rats given liver-specific ASO exhibited a MAP only 3 ± 1 mmHg below baseline (figure 22A). The MAP nadir was 6 ± 2 mmHg below baseline for the liver-specific ASO versus 29 ± 2 mmHg in the HF whole-body ASO. Neither HR nor PP were significantly affected in rats given the liver-specific ASO compared to the HF whole-body ASO or HF control ASO (figure 22B-C).

4. Discussion

4.1 Chemerin's influence on high-fat diet hypertension

The magnitude of blood pressure fall in the HF Dahl S rat treated with a whole-body ASO supports a significant role for chemerin in the regulation of blood pressure. Comparing responses in the HS Dahl S rat and the HF Dahl S controls for a number of important variables that could influence the magnitude of blood pressure response to chemerin ASOs. The similarity obtained here between groups in genetic background, age, species, strain, supplier, and pre-treatment blood pressure is not usually available when comparing blood pressure responses to treatment in models with different pathophysiology. Our results with two different Dahl S models allow us to conclude that 1) fat-associated hypertension is caused, at least in part, by a mechanism distinct from

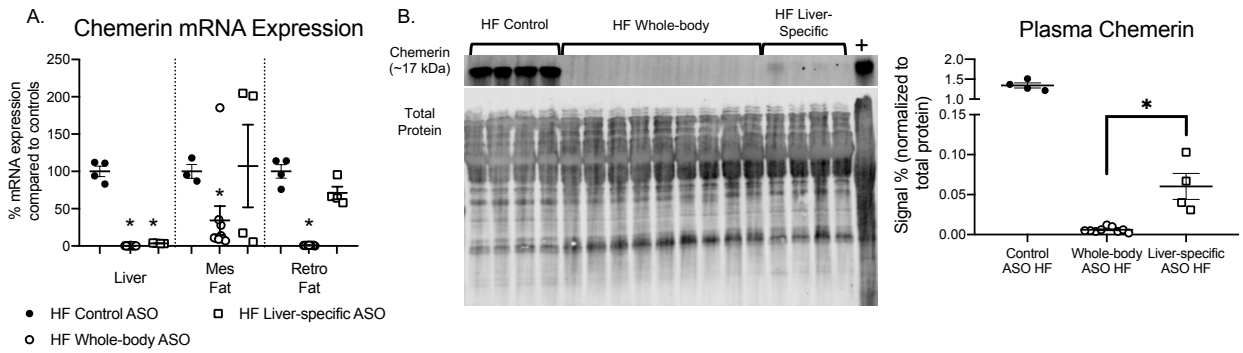

Figure 21: *Liver-specific ASOs knock down chemerin in liver but not completely in plasma*

Liver-specific ASOs given to HF Dahl S animals reduced chemerin expression (measured by PCR) in liver but not mesenteric (mes) fat or retroperitoneal (retro) fat (A). Plasma chemerin protein (measured by Western blot) was eliminated in animals given whole-body ASO (some samples used in figure 19D were run again in this blot), levels of circulating chemerin were markedly reduced after liver-specific ASO treatment, however, residual levels were still present (B). The chemerin band (~17 kDa) is shown on top and total protein stain (used as loading control) on bottom. Positive control (+) for westerns was liver homogenate isolated from normal SD animals. For Control ASO HF, N = 4; Whole-body ASO HF, N = 9; Liver-specific ASO HF, N = 4 where N represents biological replicates. Matching HF whole-body ASO plasma samples from figure 19 were pooled and run again in this figure. Scatter plots display data distribution as well as mean ± SEM. * represents $p < 0.05$ statistically significant change in the indicated groups as calculated by an unpaired students t-test.

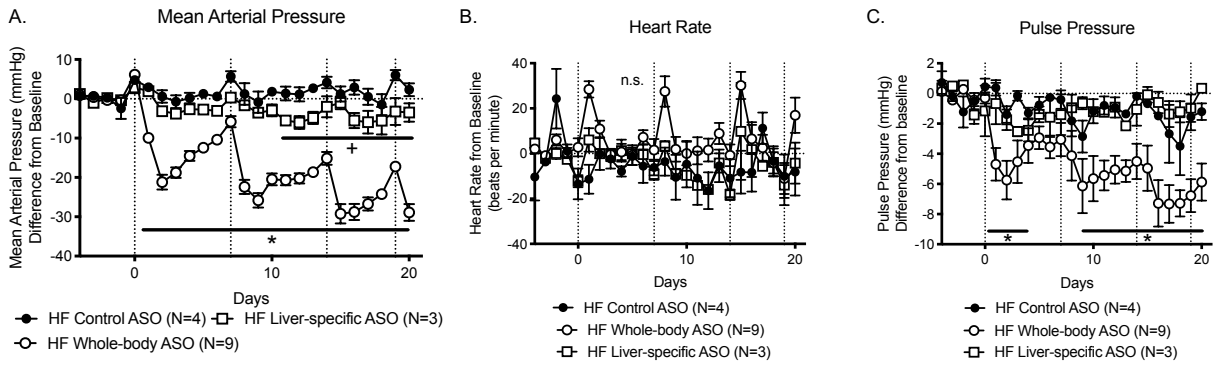

Figure 22: *Liver-specific ASOs in HF animals result in a modest fall in blood pressure*

Dahl S animals receiving HF diet and the liver-specific ASO displayed a modest fall in mean arterial pressure (MAP) that did not approach the large fall in blood pressure observed with the whole-body ASO (A). Heart rate (HR) did not change with any of the treatments (B). Pulse pressure (PP) was significantly decreased with the whole-body ASO but not the liver-specific ASO (C). Dotted vertical lines represent dates of ASO injection and dotted horizontal lines represent baseline. Baseline values are listed in table 1. Points and error bars represent mean ± SEM. * represents $p < 0.05$ of the HF whole-body group compared to all other groups. + represents $p < 0.05$ of the HF liver-specific ASO group compared to all other groups. HF whole-body ASO and control ASO data were pooled with matching HF data from figure 20. Statistics were measured using 2-way ANOVA and Tukey's multiple comparison test. N values represent biological replicates and are listed in the figures.

mechanisms responsible for salt-associated hypertension; and 2) chemerin plays a significant role in the pathology of HF but not HS hypertension.

Despite substantial changes in blood pressure, the gross appearance and weight of the heart and kidney did not change with any ASO treatment (in rats on either diet). Our failure to observe a lower heart or kidney weight in animals with markedly lower blood pressures probably reflects an inadequate time for structural cardiac adaptations in response to a lower blood pressure to occur, but we cannot rule out a direct effect of chemerin on cardiac or renal structure.

Whole-body ASO did reduce blood pressure in the HS Dahl S rat when compared to the control ASO. The magnitude from baseline (6 ± 2 mmHg) was similar to what we previously observed in normotensive SD rats [164]. However, there are two ways to interpret blood pressure data: 1) a difference from the baseline of that treatment group and 2) a difference from a control treatment group (scrambled control ASO). Even with the increasing baseline of the HS control ASO group, the control ASO versus whole-body ASO in Dahl S HS animals (19 ± 4 mmHg) and the whole-body versus control ASO in the Dahl S HF (30 ± 3 mmHg) were significantly different. The fall in blood pressure in the HF animal versus control ASO (a difference of 30 ± 3 mmHg) is likely due to a mechanism specific to the high fat diet and not the hypertension alone.

4.2 Source of the chemerin matters

In the experiments described here, we used the same liver-specific ASO as in our previous study [164], but now in the Dahl S HF model of fat-associated hypertension. While giving the HS Dahl S rat a liver-specific ASO would satisfy all the permutations of

the variables we are manipulating (diet and ASO type), it would not answer the goals of this study which were to assess whether blood pressure changes due to chemerin in a HF model are due to general blood pressure status (comparison to HS model) or contributions of the other major producer of chemerin (liver in the HF rat). In the Dahl S HF rat, treatment with a liver-specific ASO reduced MAP by about 6 ± 2 mmHg versus control ASO. This was a fraction of the 30 ± 3 mmHg fall in blood pressure observed with the whole-body ASO versus control ASO. This relatively small decrease in blood pressure with the liver-specific ASO emphasizes that circulating chemerin from the liver (96% of total circulating chemerin) has only modest effects on blood pressure, since plasma chemerin was nearly eliminated by the liver-specific ASO. This observation is in agreement with our previous study using the liver-specific ASOs in male SD rats [164] where we showed that the liver is the main source of chemerin in the circulation, but does not contribute to the chemerin responsible for maintaining blood pressure.

Both the endothelium and smooth muscle cells contain the chemerin receptor [39] and primary smooth muscle cells are able to respond with a calcium flux directly in response to both the chemerin analog (chemerin-9) and recombinant chemerin [142]. Given that chemerin is produced in such high amounts by the fat [35, 38], it is probable that the chemerin secreted from perivascular adipose tissue can act on smooth muscle cells without entering the circulation. Especially if the chemerin in the circulation is quickly degraded [44] or of a different isoform [46] than that produced by the fat, this is a mechanism by which blood pressure can be regulated by chemerin independent of the circulation.

A recent study testing male Wistar rats fed high-fat diet found that circulating chemerin protein levels did not increase compared to normal diet rats. However, in these same animals, expression of chemerin protein and the chemerin receptor in the vasculature and perivascular adipose tissue were increased [167]. Our study supports the idea that chemerin mRNA expression is increased in fat with HF feeding and that plasma chemerin protein does not influence blood pressure. This study provides the first mechanistic proof that while chemerin *does* directly influence blood pressure, blood pressure is not directly associated with plasma levels of the chemerin protein, at least in the rat. Together, our study and the previous study with Wistar rats suggests that the actions of chemerin may be local.

Dahl S rats fed HF diet do exhibit increased renal injury compared to control diet rats in the form of hyaline casts, interstitial fibrosis, glomerular sclerosis, and tubular atrophy [166]. However, specific local role of chemerin on the kidney is unlikely given that Chemerin1 receptor is not expressed in the kidney [35, 38]. Another possibility is that chemerin from the fat is influencing the mesenteric resistance vessels that influence blood pressure [19, 168]. The perivascular adipose tissue (PVAT) around these resistance vessels is one of the components of visceral adipose tissue implicated in the positive correlation between high blood pressure and fat [4, 152]. We know that chemerin is produced in this mesenteric PVAT and that these mesenteric resistance vessels have the ability to contract to chemerin [39]. The present study is one approach to determine if adipose tissue is important to chemerin-dependent changes in blood pressure. Here, we increased fat burden to increase (local) chemerin burden. Another tactic would be to target fat directly. Future *in vivo* studies should focus on targeting the ASO to the fat.

Because of limitations in drug delivery, *in vitro* studies may be needed to differentiate chemerin derived from different locations of white adipose tissue.

Future studies also need to assess the target of the chemerin derived from the fat. In an isolated tissue bath, chemerin is contractile to the vasculature [39, 100, 142] but there are other influences chemerin could have in the whole body to support blood pressure. We have previously shown that the Chemerin1 receptor antagonist alone (CCX832) reduces electrical field stimulated contracted blood vessels in a PVAT-dependent manner [154]. This points toward a possible role of the sympathetic nervous system in the actions of chemerin as well as affirming the importance of local chemerin production. In support of that idea, chemerin and the Chemerin1 receptor are also present in the adrenal gland [169]. Sympathetic mechanisms of blood pressure modification by chemerin need to be considered as a possible means through which chemerin could affect blood pressure.

4.3 Limitations

HF Dahl S treatment was replicated in different sets to confirm the large magnitude of effect produced by the whole-body ASO. The HF Dahl S animals used here were first employed in a one-month oral estradiol treatment protocol. The current study was, in part, an experiment of opportunity where instrumented Dahl S rats fed high fat diet for 6 months, seemingly unaffected by previous intervention, were available for study with the chemerin ASO. Estradiol treatment of the HF animals did not affect their blood pressure and the animals were allowed to recover for three weeks before the initiation of the present study. Orally administered estradiol has a half-life of 13-20 hours so we believe

a three-week washout period was sufficient to clear any remaining drug. Studies with the Dahl S fed HS were designed to complement the data from the HF rats. Dahl S animals on normal diet were not used for this study but have been used previously to confirm the model of Dahl HF hypertension [166].

Additionally, because the animals receiving liver-specific ASO were in a separate cohort from most other animals (but still containing some animals receiving control and whole-body ASO), the mean of the liver-specific treatment group baseline blood pressures were slightly lower from the other treatment groups. When combined with all other treatment groups, baseline blood pressures of this group were not statistically different than the others but the reduced biological replicates in this group may have skewed the power analysis. The purpose of this smaller liver-specific group was to follow-up on a similar experiment done on normal Sprague Dawley rats [164] where we saw similar trends in both groups.

4.4 Conclusions

Adiposity is an established risk factor for hypertension. This study suggests that biological actions of the adipokine chemerin could be an explanation for this association. Although, it is likely that chemerin is only one part of a network of vasoactive factors found in enlarged and dysfunctional adipocytes, specifically, fat that is adjacent to blood vessels. In the large number of human subjects with obesity-associated hypertension, manipulation of chemerin production may be uniquely effective in the treatment of hypertension.

AIM 2.3: In vivo targeted destruction of chemerin mRNA in fat

The following data are currently unpublished but reported here with generous contributions from Kunli Liu, Seyedmehdi Hossaini Nasr, Alexis Orr, Emma Flood, Dieter Kubli, Adam Mullick, Xuefei Huang and Stephanie Watts.

1. Introduction

Obesity is characterized as a disease with an expansion of adipocyte mass causing an increased body-mass index. There are still few drugs that directly target the adipocyte. Part of the reason for this lies in our developing knowledge about the role of the adipocyte in obesity. Research has recently expanded the role of the adipocyte from being a passive storage module for carbohydrate and energy to being an active member in homeostatic metabolism [18] and immune function [17]. Adipocytes directly secrete hormones and interact with cells throughout the body. Furthermore, the profile of these interactions change in obesity [18].

Obesity has been positively associated with blood pressure [6]. With the developing obesity epidemic around the world [170], obesity-associated hypertension has become a recent concern. One of the novel adipokines linking these two diseases is chemerin. Plasma levels of this protein are positively associated with both BMI [24, 26, 31-34] and blood pressure [24-30]. Mechanistically, chemerin supports the adipogenesis/lipogenesis of adipocytes [35, 38] but can also directly stimulated the contraction of blood vessels and smooth muscle cells [39, 142].

In recent studies, we have been able to use antisense oligonucleotides (ASO) which tag chemerin pre-mRNA for destruction to lower the blood pressure of high-fat-fed Dahl salt-sensitive rats (a model of obesity-associated hypertension) [171]. These ASOs are free to distribute throughout the entire body but are particularly adept at inhibiting chemerin production in the liver and the fat (the two major depots of chemerin in the body [35, 38]). Additionally, an N-acetylgalactosamine (GalNAc) tag can be added to the ASO to selectively target it towards the liver [156, 157]. However, unlike the blood pressure

effects seen with a whole-body ASO, the liver-specific ASO does not affect blood pressure while still abolishing plasma circulating levels of chemerin.

The liver and the fat are the two largest producers of chemerin mRNA in the body [35, 38]. If the liver does not contribute chemerin that influences blood pressure, it is likely that the local production of chemerin by the fat is conferring the chemerin related to blood pressure control. However, this direct correlation requires a tool that allows us to selectively deliver the ASO to the fat, a tool that does not yet exist.

Initial research in this arena points to the use of a peptide titled the “adipocyte targeting sequence” (ATS) with a 9-arginine (9R) tail. This ATS-9R has been proposed to target the prohibitin receptor to gain entry into either adipocytes or passage through the vasculature of adipose tissue. Prohibitin is a constitutively expressed protein in the mitochondria of most cells but is unique to the adipocyte in that it is expressed on the surface of the cells [172]. Using the ATS-9R as a targeting molecule, two labs have attempted to use this peptide to facilitate entry of specific nucleic acid drugs into the fat [84, 172, 173], albeit with limited success.

We hypothesize that the ATS-9R surrounding the chemerin ASO will be able to increase the selectivity of the ASO for the fat over the liver. Our goals with the study are to optimize the ATS-9R for delivery of an ASO in a rat but also to simply validate the limited research on ATS-9R that has come before us.

2. Methods

2.1 Animal handling

All procedures that involved animals were performed in accordance with the institutional guidelines and Animal Use Committee of Michigan State University. Animals were maintained on a 12/12 hour light/dark cycle at a temperature of 22-25°C. Normal Sprague Dawley rats (Charles River Laboratories, Inc., Portage, MI, USA) were used.

2.2 Drug and nanoparticle development

"NP" refers to the iron-oxide nanoworm used to concentrate and facilitate electrostatic binding of the ATS peptide to the ASO (Figure 23A). A second formulation of the nanoparticle referred to as ATS9R-FITC-ASO uses the ATS pre-bound by the manufacturer to a 9-arginine (9R) sequence and FITC. The ATS9R-FITC is electrostatically bound to the ASO through mixing and sonication (Figure 23B). Binding of the NP to the ATS requires a chemical linker. Linker conjugation to NP is as follows (Figure 23C): 2 mL 5 mg/mL NP solution, 2 mL 1M MES buffer and 2 mL DMSO was added into a 20 mL vial. 0.5 mmol 5-hexynoic acid (60 uL) into the solution and 10 mmol EDC (3830 mg) into the solution. The reaction was allowed to proceed overnight. Purification was carried out by dialysis with PBS for 2 hours and with water overnight.

Peptide conjugation to the NP (with linker) occurred as follows (Figure 23D): 2 mL 1 mg/mL NP-alkyne was added into 20 mL vial. Premixed 300 uL 50 mM THPTA and 60 uL 50 mM $CuSO_4$ and added into the vial. 300 uL 100 mM aminoguanidine solution, 300 uL 100 mM sodium ascorbate solution 200 uL 1 mg/100 uL peptide solution was added

into the vial. The reaction was allowed to proceed for 24 hours and was purified by dialysis. The loading of peptide was quantified by BCA assay.

ASO was attached to NP-ATS through electrostatic interaction. Excess ASO was wash off via 30 kDa centrifuge filter.

2.3 ICP analysis of iron-oxide nanoparticle

Media and washes were kept and combined for each sample to determine the iron-oxide nanoparticle that did not enter the cells. Concentrated nitric acid was added to each sample and heated at 60ºC for two hours. Three mL of water was added to each sample and pushed through a 0.22 um filter. Added water up to 5 mL and processed with inductively coupled plasma (ICP) chromatography for iron content.

2.4 Primary adipocyte isolation

The entire ilium and jejunum of the rat was dissected out with each end tied with suture to prevent leaking of fecal matter into the dissection tray. Perivascular adipose tissue was stripped from second order mesenteric resistance vessels and placed in Krebs Ringer bicarbonate buffer (KRBB) with HEPES (10 mM, pH = 7.4; Thermo Fisher, Waltham, MA, USA). Adipose tissue was digested with 1 mg/mL collagenase I (Worthington Biochemical, Lakewood, NJ, USA) for 1 hour and centrifuged at 800 xg for 5 minutes. Liquid was removed from the bottom and cells were washed two more times with KRBB and centrifugation. Viable cells were counted with a Cellometer Vision (Nexcelom Bioscience, Lawrence, MA) and AOPI (CS2-0106, Nexcelom Bioscience; with at least 50% viable) and 100,000 cells (in a total 100 uL in primary adipocyte media:

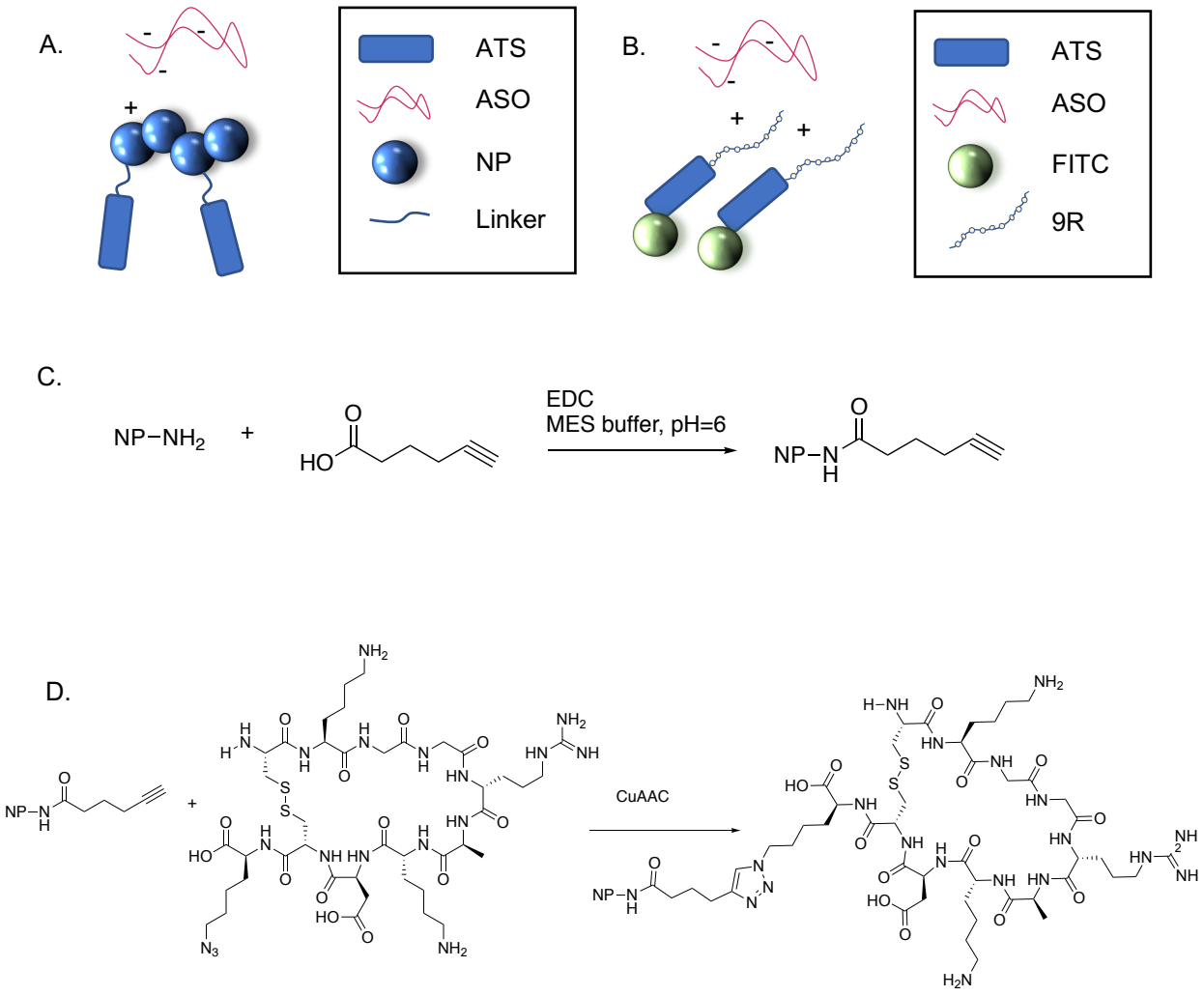

Figure 23: *Chemical reactions for drug development*

Cartoons of the two drug formulations used in these experiments: NP-ATS-ASO (A) and ATS9R-FITC-ASO (B). Reactions that depict the nanoworm (NP) to the linker (C) and the linker to the peptide (D) in the creation of NP-ATS-ASO.

DMEM/F12 Corning 90-090PB at 11.69 g/L, 44.05 mM bicarbonate, 100 uM ascorbic acid, 33 uM biotin, 17 uM Pantothenate, 10% FBS, 5 nM troglitazone, ITS 10 mL/L, 0.2 nM T3, 144 uL/L octanoate, 2 mM L-Glutamine, 10 mL Antimycotic/Antibiotic) were dispensed into a 0.5 mL microcentrifuge tube. An additional 100 uL of media containing the indicated treatment was added to the tube and incubated at 37ºC for 24 hours. Liquid was removed with a 30G needle and washed three times with PBS.

2.5 Primary hepatocyte isolation

The liver was removed and placed into hepatocyte media: Williams Medium E (W4125, Sigma Chemical, St. Louis, MO), 26 mM sodium bicarbonate, 10 mL antibiotic/antimycotic, pH to 7.4. The entire liver was diced into small pieces with a sharp blade or scalpel and placed divided into two tubes with 20 mL of media each. Five (5) mg collagenase (C9891, Sigma) was added to each tube and rotated or 10 minutes at 37ºC. The digested hepatocytes were filtered through gauze to remove large pieces of liver then centrifuged for 2 minutes at 50 xg. Cells were gently washed with 10 mL of media (each), centrifuged, washed with 5 mL of media (each), counted with the Cellometer/AOPI (with a minimum of 50% viable), centrifuged, and reconstituted at 250,000 cells/mL. In a 24-well plate, 500 uL of hepatocyte cells were added along with the drug. Cells were incubated for 24 hours and washed once with PBS before further processing.

2.6 Ex vivo effects of peptide and IVIS analysis

For ex vivo assays, animals were euthanized with pentobarbital and pneumothorax. Tissue was dissected out of the animal, trimmed to similar weights within

tissue type, and placed in a 48-well plate. Drug was made up in PBS at 1.5 mg/mL and placed in the 48-well plate at a working volume of 500 uL. Samples were incubated for 30 minutes on a rocker at room temperature then washed eight times with PBS. In Vitro Imaging Systems (IVIS) samples were placed on black paper and placed in the IVIS with a 13.4 cm field of view for an analysis of total radiance. Tissue from each animal were imaged and analyzed (with regions of interest) individually but total radiance measures are comparable between images.

2.7 In vivo injection

Animals were anesthetized with 1-2% isofluorane, weighed, and injected with drug intraperitoneally (volumes between 0.6 and 1 mL depending on weight). Samples were collected after 48 hours. Tissue for IVIS analysis of fluorescence were placed in PBS and shielded from light. Tissue for PCR were flash frozen in liquid nitrogen. Blood was collected and centrifuged at 500 xg for 20 minutes at 4ºC. IVIS, PCR, and Western blots were performed as previously described.

2.8 PCR

Analysis for mRNA was performed as previously described [174]. Tissue was processed by the Zymo Research QuickRNA kit (Irvine, CA), High Capacity cDNA Reverse Transcription kit (Applied Biosystems, Foster City, CA), and SimpliAmp Thermal Cycler (10 minutes 25°C, 2 hours at 37°C, 5 minutes at 85°C, then hold at 4°C). Analysis of cDNA for chemerin was performed with TaqMan primer probes (Thermo Fisher Biosystems, Foster Cit, CA): Forward Sequence, CAGGAGATCGGTGTGGACAGT;

Reverse Sequence, GAGCTTAAATTCCAGCCTCACAA; Probe Sequence, TGATGACCTGTTCTTCTCAGCTGGCACCX. The PCR probes were labeled with 5′-FAM (a 6- carboxyfluorescein reporter) and 3′-TAMRA [a 5(6)-carboxytetramethyl rhodamine quencher]. Beta actin was used as a housekeeper gene. PCR was performed with Quant Studio 7 Flex and PerfeCTa FastMix II (Quanta Bio, Beverly, MA).

2.9 Western blots

Tissues were frozen and protein was isolated using a bead rupture (5.65 m/s, 2 cycles, 30-second cycles, 30 seconds between cycles, 6°C; Omni International, Kennesaw, GA), while plasma was centrifuged for 20 minutes at 4°C and 2000 rpm. Protein concentration was established using a bicinchoninic acid assay for total protein (cat. no. BCA1; MilliporeSigma, St. Louis, MO). Gel electrophoresis was run on a 15% polyacrylamide gel and run at 120 V, loading 50 ug of plasma protein and 100 mg for all other tissue samples. Protein was transferred to an Immobilon FL PVDF Membrane (cat. no. IPFL00010; MilliporeSigma, Billerica, MA) for 1 hour at 100 V. Total Protein was measured on dried blots (Total protein stain, cat. no. 926-11011; Li-Cor, Lincoln, NE), stain was removed (Revert, cat. no. 926-11012; Li-Cor, Lincoln, NE), then blots were blocked with Chick Egg Ovalbumin for 3 hours. Chemerin antibody (1:1000; cat. no. 112520; Abcam, Cambridge, MA) was incubated for 3-4 days at 4°C and the secondary antibody (1:1000; IRDye 800 anti-Mouse, cat. no. 926-32210; Li-Cor) was incubated for 1 hour at 4°C. Blots were imaged using the CLx Infrared Imaging and quantified with Image Studio (5.2.5, LI-COR Image Studio Software). The main benefit to quantifying with this software is that analysis of signal strength is user bias independent/resistant, as it

measures the image data regardless of the manual brightness corruption. Chemerin bands were normalized to full lane of total protein stain, creating smaller numbers but a broader, more accurate, and more consistent normalization across the board.

2.10 Analysis and statistics

Where possible, researchers were blinded to the treatment group of the samples analyzed. Many experiments contained in this section are preliminary, meaning the biological replicates are less than three. For those groups with three or greater biological replicates, a student's t-test was used when comparing two groups and a One-way ANOVA with a Holm-Sidak correction when comparing more than two groups. A $p < 0.05$ was considered statistically significant. For instances with multiple points along a curve, a Two-way ANOVA was used to compare the entirety of the curves.

3. Results

3.1 Iron-oxide nanoparticle delivers ASO but does not confer specificity

The initial nanoparticle was created using an iron-oxide nanostring core as previously published [175] and combined with ASO (electrostatically). All references to ASO refer to whole-body chemerin ASO unless otherwise indicated. When incubated with cells, using chemerin mRNA expression as an endpoint, the nanoparticle reduced chemerin expression in a concentration-dependent manner (Figure 24A-B). This same iron-oxide nanostring conjugated to adipocyte targeting sequence (ATS, CKGGRAKDC) was administered to cells (without ASO). By separating the cell and wash fraction of the

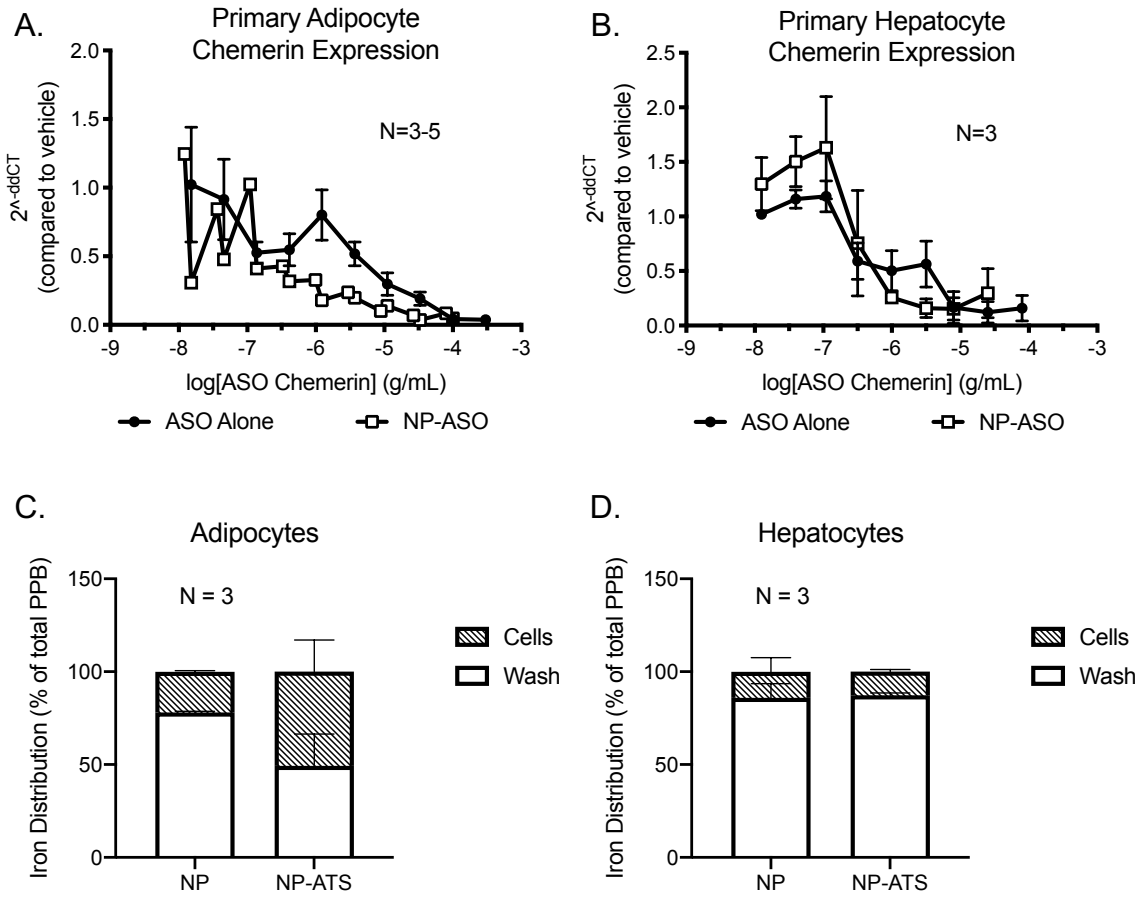

Figure 24: *NP-ASO is efficacious and NP-ATS appears selective*

Chemerin expression, as measured by PCR, is knocked down by both chemerin ASO alone and chemerin ASO electrostatically bonded to an iron-oxide nanoworm (NP-ASO) in primary adipocytes (A) and hepatocytes (B). The targeting ATS sequence increases the iron content (from the NP) of the cellular fraction of adipocytes (C) but not hepatocytes (D). For PCR, ddCT represents a comparison to the housekeeper gene (beta actin) and a vehicle control for that cell type. Points and error bars represent mean ± SEM. N values represent biological replicates and are listed in the figures.

cultured cells and analyzing for iron content, we determined the relative fraction of drug that was able to enter the cells during the 24-hour period. The relative fraction of iron in the hepatocytes did not change with addition of ATS but the relative fraction of iron in adipocytes increased by ~30% with the addition of ATS (Figure 24C-D).

However, the addition of ASO to the iron-oxide nanoworm (with ATS) did not create a leftward shift in the chemerin expression curve as expected (Figure 25). While the nanoworm-ATS-ASO did not confer specificity, it still demonstrated an ability for the ASO to be efficacious (knock down chemerin mRNA) when in the nanoparticle complex. Preliminary studies where ASO with and without NP was washed and centrifuged (30 kDa filter) showed that ASO (measured by 280 nM spectrophotometry) was maintained in the NP fraction (Table 3).

3.2 Transition to ATS9R-FITC supports specificity for fat

Previous studies with success using the ATS also used a 9-arginine (9R) sequence. When adding the 9R, the iron-oxide nanoworm was not needed to facilitate electrostatic interactions. FITC was also added to ATS9R for analysis of nanoparticle location using the IVIS. Two different companies were sourced for the ATS9R-FITC due to production complications with the first company. Mass spectrometry confirmed identical composition between the products of the two vendors (Figure 26).

When mesenteric fat, retroperitoneal fat, and liver were dissected and subjected to a 1.5 mg/mL ex vivo administration of ATS9R-FITC or scrambled-9R-FITC (Scr9R-FITC), there were no differences between the ATS or Scr in any tissue group (Figure 27).

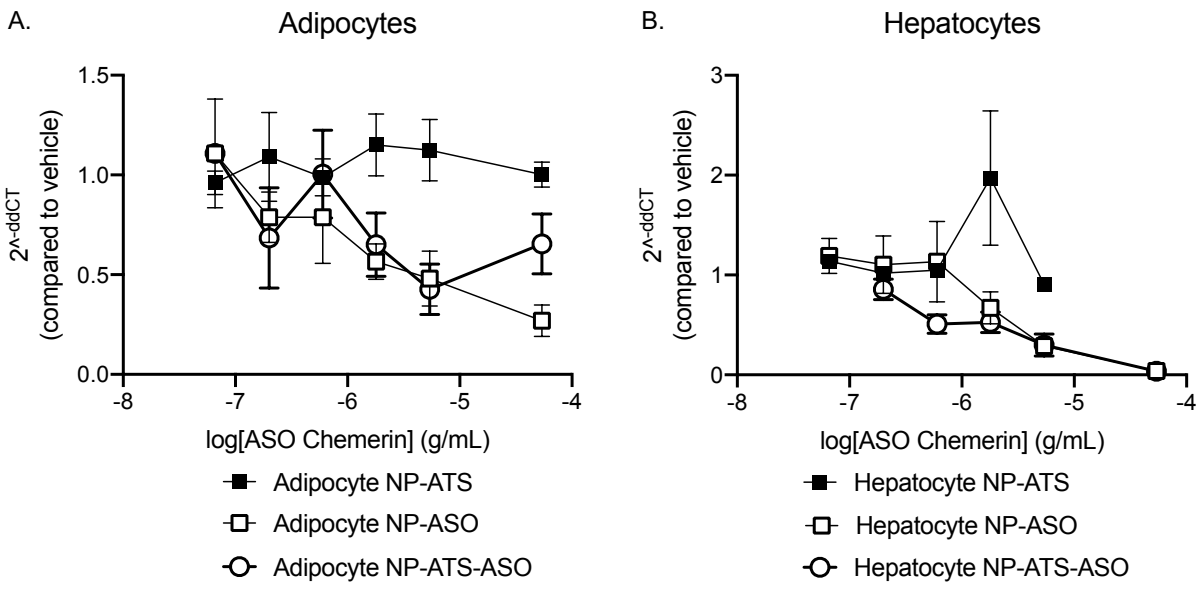

Figure 25: *NP-ATS-ASO knocks down chemerin but not better than ASO alone*

Cells were treated with NP-ATS (negative control), NP-ASO (positive control), and NP-ATS-ASO. The NP-ATS-ASO did not produce a leftward shift in chemerin expression compared to the NP-ASO in either the adipocytes (A) or hepatocytes (B). For PCR, ddCT represents a comparison to the housekeeper gene (beta actin) and a vehicle control for that cell type. Points and error bars represent mean ± SEM. N=3 for each point.

	Retained, mg	Washoff, mg
0.12mg ASO without NP	0.02	0.06
0.6mg ASO without NP	0.13	0.44
0.12mg ASO on NP-ASO	0.13	-0.02
0.6mg ASO on NP-ASO	0.12	-0.01

Table 3: *ASO does not wash off the NP*

A preliminary test (N=1) where NP-ASO was washed with PBS, centrifuged with a 30 kDa filter, and analyzed for presence of ASO in the NP or wash fraction. Even though the NP and ASO were connected by electrostatic interactions, the ASO did not appear to separate from the NP during washes.

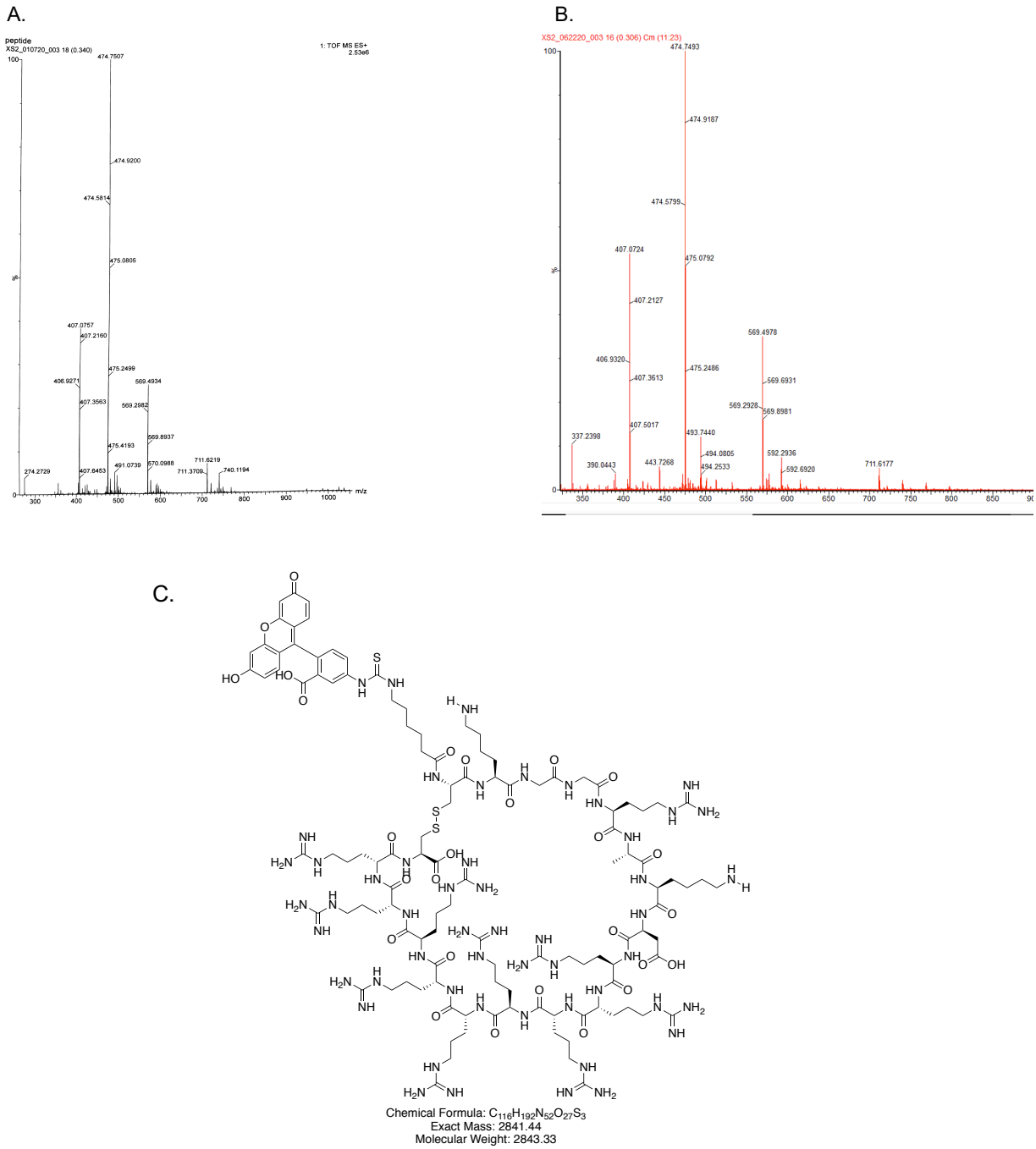

Figure 26: *Validation of the ATS9R-FITC*

ATS9R-FITC from two different vendors, Synpeptide (A) and GLBiochem (B) were analyzed by mass spectrometry to ensure a similar makeup. Both peptides support the structure of the protein (C).

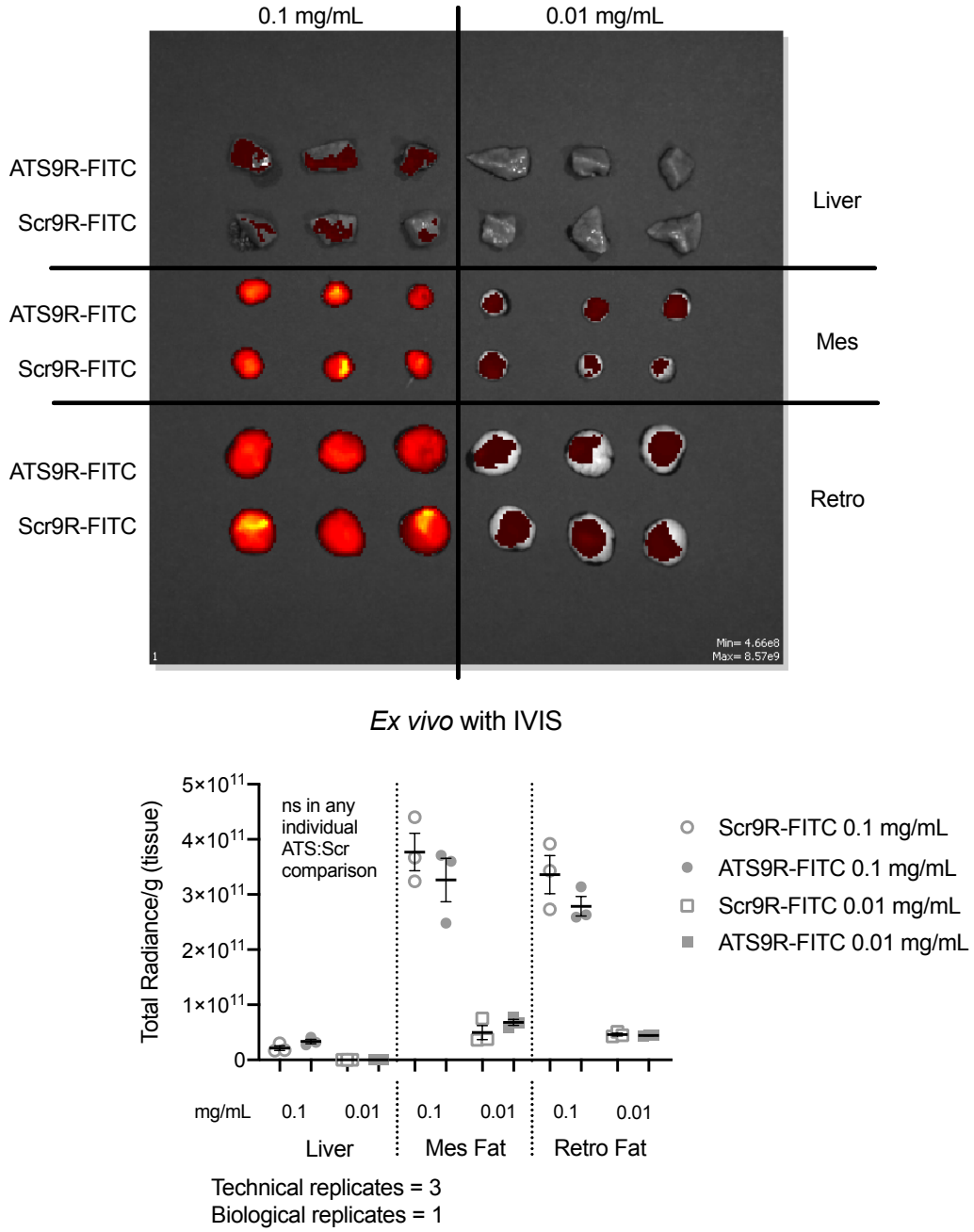

Figure 27: *Ex vivo testing of the ATS9R-FITC*

ATS9R-FITC or Scr9R-FITC (scrambled sequence) were incubated with pieces of liver, mesenteric fat (mes) or retroperitoneal fat (retro), washed, and analyzed with the IVIS for fluorescence. There were no differences in fluorescence between ATS9R-FITC and Scr9R-FITC but the fat exhibited strong fluorescent signal. Statistical significance was based on individual t-test comparisons of ATS9R with the adjacent Scr9R with a $p < 0.05$ considered significant.

However, the nanoparticle itself (without ASO) demonstrated an ability to bind to fat which led to in vivo injections.

3.3 Validation of single-injection ASO administration

In previous in vivo assays with chemerin ASO, administration occurred approximately once per week for four weeks with samples collected two days after the last ASO administration [164]. Given the large amount of ATS peptide needed for ASO-ATS9R administration in the rat at effective concentrations of ASO, we studied the ability of one ASO injection to effectively knockdown chemerin expression.

Animals were given standard doses of ASO (25 mg/kg for whole-body ASO and control ASO; 10 mg/kg for liver-specific ASO) subcutaneously and sacrificed two days after administration. In liver, chemerin expression was reduced with both whole-body and liver-specific ASO compared with control ASO and tissue protein followed the same trend (Figure 28A-B). Retroperitoneal fat chemerin expression was reduced with whole-body ASO but not liver-specific ASO when compared with control ASO and protein quantification also followed the same trend (Figure 28C-D). Mesenteric fat had reduced chemerin expression with the whole-body ASO but not the liver-specific ASO when compared with control ASO but the protein quantification was variable (Figure 28E-F). Given the results of chemerin mRNA expression in mesenteric fat alongside both the mRNA and protein expression in the retroperitoneal fat, the actions of chemerin ASO in the fat after one injection follow the expected trends.

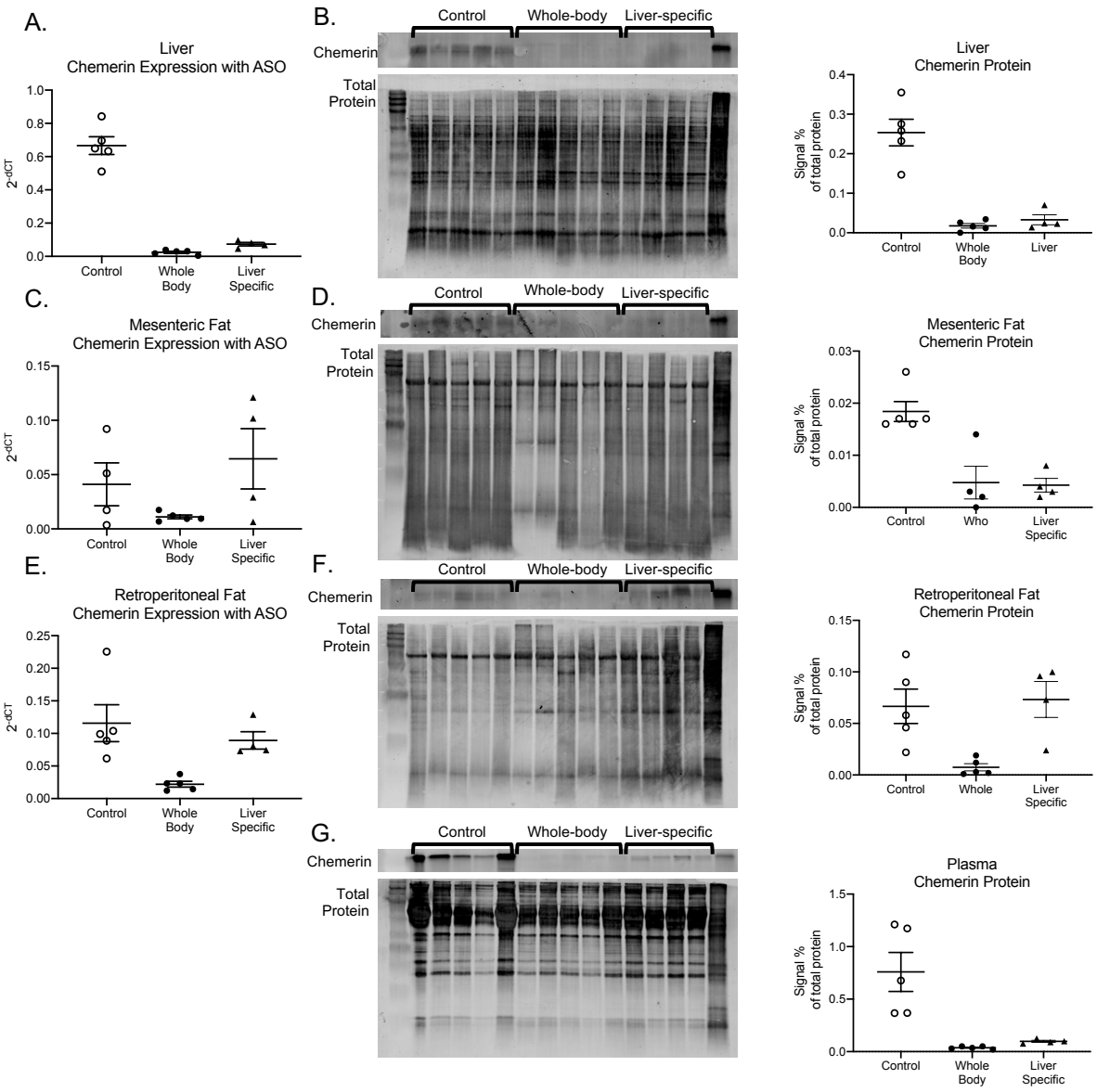

Figure 28: *One injection of chemerin ASO is sufficient to induce chemerin knockdown*
After one injection, chemerin mRNA and protein was knocked down in the liver with whole-body and liver-specific ASO compared with control ASOs (A-B). Mesenteric fat mRNA expression was not significantly changed by ASO and protein expression was similarly variable (C-D). Retroperitoneal fat mRNA and protein exhibited knockdown with whole-body ASO compared to control ASO but not with liver-specific ASO (E-F). Plasma chemerin protein was significantly reduced with both whole-body and liver-specific ASOs compared with control ASO (G). In PCR, dCT represents a comparison to the housekeeper gene (beta actin). Points and bars represent mean ± SEM and statistical significance was determined by One-way ANOVA with a Holm-Sidak correction for multiple comparisons. N = 4 (biological replicates) for every point.

Plasma chemerin protein was also reduced with whole-body and liver-specific ASO administration (compared with control ASO) but we did not see the completely abolished signal that we saw in the past (Figure 28G).

3.4 ASO-ATS9R-FITC lacks efficacy for chemerin knockdown

An initial intraperitoneal injection of 3.3 mg/kg ATS9R-FITC or Scr9R-FITC (peptide alone, no ASO) after 2 hours demonstrated that the ATS9R-FITC was able to successfully get into the cells of the retroperitoneal and mesenteric fat whereas the Scr9R-FITC was not (Figure 29A-B). The dose of peptide replicates the amount of peptide given to mice in Won et al. 2014 [84]. This in vivo data provided support for the fat specificity provided by the ATS peptide in vivo.

Animals were injected with 25 mg/kg ASO alone, 10 mg/kg ASO alone, and 10 mg/kg ASO-ATS9R-FITC with peptide at a 20:1 molar ratio (replicating the ratio of peptide to shRNA in Won et al. 2014). Fluorescence captured from ASO alone (no fluorescence) and ATS9R-FITC-ASO shows that the complex is able to distribute to the liver and fat (Figure 29C). As expected, based on previous ASO dosing data [164], chemerin expression generally increased when the ASO dose was lowered from 25 mg/kg to 10 mg/kg. When comparing 10 mg/kg ASO alone with 10 mg/kg ASO-ATS9R-FITC, chemerin expression increases further and to a point comparable with chemerin expression from animals without any treatment (Figure 29D). While the drug was able to distribute to the target organs, the chemerin expression was not affected. If ASO dissociated from the nanoparticle before reaching the target organ, we would have

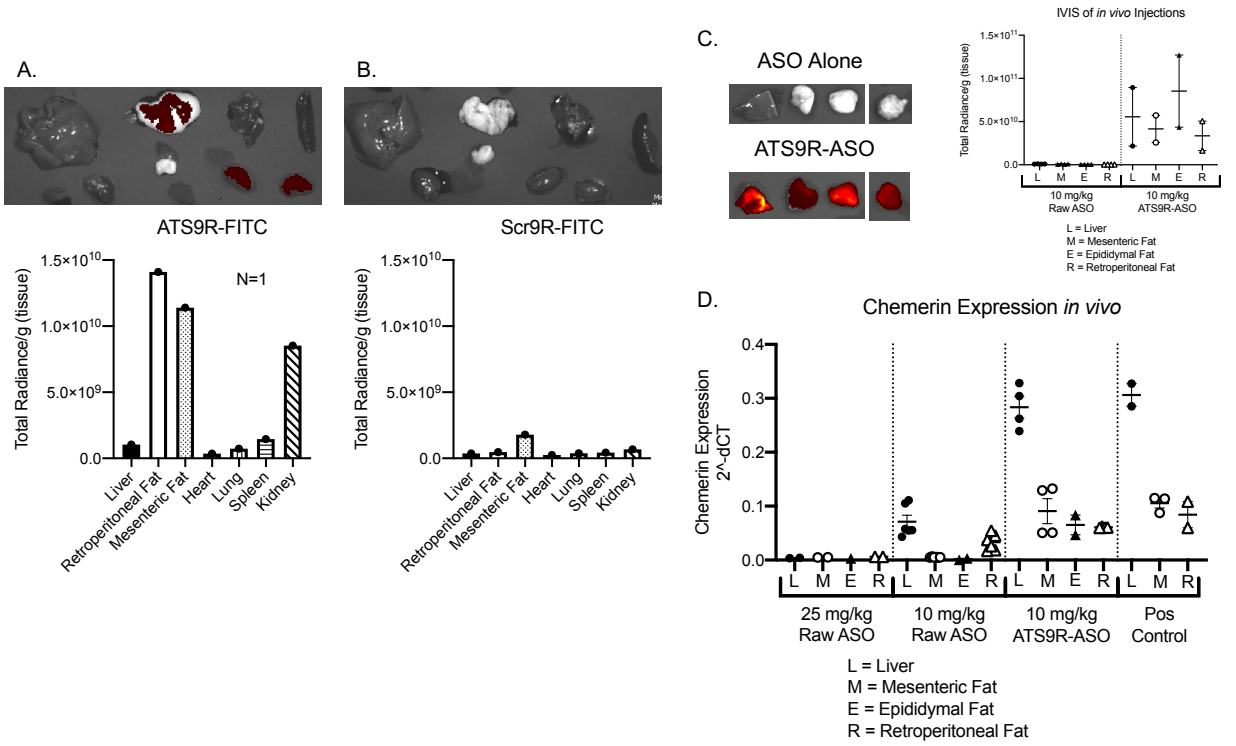

Figure 29: *ATS9R appears to have in vivo specificity but not efficacy*

Animals were injected with ATS9R-FITC or Scr9R-FITC at concentrations of 3.3 mg/kg (mg of peptide). After incubation, tissue was dissected and analyzed with IVIS for fluorescence. ATS9R-FITC exhibited high fluorescence in adipose tissues compared with liver also given ATS9R-FITC or adipose tissue given Scr9R-FITC (A-B). The ATS9R-FITC-ASO is able to distribute to the organs of interest as visualized by fluorescence captured by the IVIS (C). But when ASO is added to ATS9R-FITC and dosed at an efficacious ASO dose (10 mg/kg ASO with ATS:ASO at 20:1), chemerin expression was not reduced compared to chemerin expression from untreated animals (pos control; D). Panels A and B represent an N=1 and panels C and D represent an N=2-4. In PCR, dCT represents a comparison to the housekeeper gene (beta actin). Points and bars represent mean ± SEM and statistical significance was determined by One-way ANOVA with a Holm-Sidak correction for multiple comparisons with statistical significance considered $p < 0.05$.

expected to see chemerin expression with the ASO-ATS9R-FITC to be similar to the results of the ASO alone.

3.5 ATS9R peptide may stimulate chemerin production

In vitro administration of the ATS9R-FITC and ASO-ATS9R-FITC (20:1 ATS:ASO ratio) complexes both increase chemerin expression in adipocytes and hepatocytes (Figure 30). The ASO alone is still able to decrease chemerin expression as expected.

4. Discussion

4.1 Uncovering the efficacy of ASO after the first injection

Previous studies using chemerin ASO injected the ASO four times over the course of about four weeks [164, 171]. Given the feasibility limitations of testing an experimental drug in vivo, we decided to first test if chemerin knockdown could be detected after the first injection. In previous studies, the nadir of blood pressure occurred about 48 hours after each injection and in this current test, samples were collected 48 hours after injection. In that time, we accomplished complete knockdown of chemerin mRNA where we hypothesized it should be knocked down. Protein analysis gave slightly more variable results, especially in the mesenteric fat. The chemerin protein was reduced with liver-specific ASO in the mesenteric fat but this is not the first time we have seen mesenteric fat give variable results [164]. Given the promising data provided by mRNA analysis and protein measurements in the retroperitoneal fat, we still believe the ASO is performing properly at this time point. This allows a more rapid turn around and iterative testing of the nanoparticle.

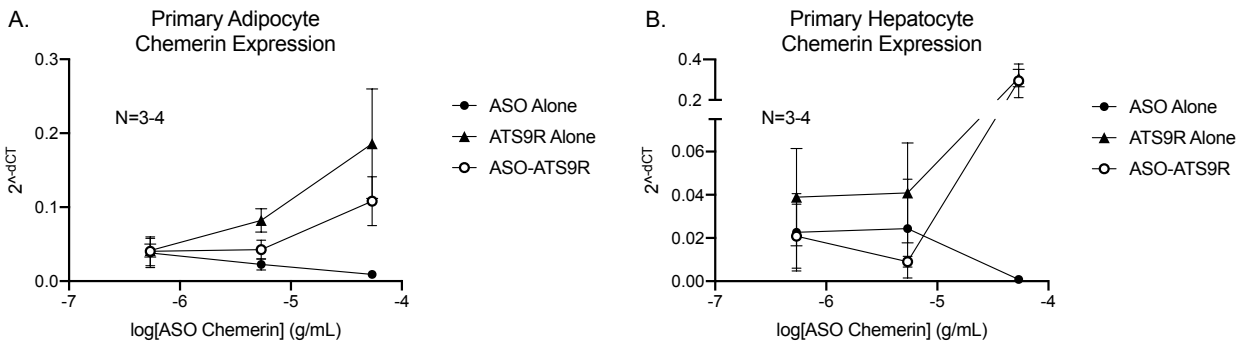

Figure 30: *ATS9R increases chemerin expression*

When incubated with primary adipocytes (A) and hepatocytes (B), ASO alone is able to reduce chemerin mRNA expression but both ATS9R alone and ATS9R-ASO increase chemerin expression at the highest dose. In PCR, dCT represents a comparison to the housekeeper gene (beta actin). Points and bars represent mean ± SEM and statistical significance was determined by One-way ANOVA with a Holm-Sidak correction for multiple comparisons with statistical significance considered $p < 0.05$. N values (biological replicates) are listed in the figure panel.

One additional unexpected result from this study was that plasma chemerin did not decrease as much with liver-specific ASO treatment as whole-body ASO treatment. We had previously hypothesized that the liver was the primary contributor of plasma chemerin. At this early time point, the liver is still responsible for the majority of circulating chemerin but there are likely more sources contributing chemerin to the plasma whose secretion might be inhibited by additional administrations of liver-specific ASO (cumulative effects of non-selective ASO efficacy).

4.2 Using iron nanoworms for ASO delivery

While the initial basic science research into prohibitin and the use of the ATS9R provided promising first indications for the creation of a fat-specific drug [84], we were aware of the inherent limitations when the majority of data on a subject comes from a single lab. For this reason, in our own initial exploration of creating a fat-specific drug, we relied on techniques we had extensive experience with, namely, the iron-oxide nanoworm [85, 175].

We started with a simple iron-oxide nanoworm electrostatically bonded with an ASO directed towards chemerin and tested whether the nanoworm (NP) would be able to deliver an effective ASO. The actual mechanisms of ASO delivery to the nucleus of a cell are a matter of debate [80] so this was an important first step. Fortunately, the chemerin knockdown observed with ASO alone in primary hepatocytes and adipocytes matched what we saw with the ASO-NP. The iron core of the NP also allowed us to use iron-based assays to follow the movement of the nanoparticle. While the overall iron content of the hepatocytes was higher than adipocytes, incubation with a NP-ATS

complex resulted in a higher cellular fraction of iron (compared with the NP alone) in the adipocyte but not the hepatocyte. To now, our NP-ASO was efficacious at its target and our NP-ATS was selective at its target.

However, the NP-ATS-ASO (covalent bonding of NP-ATS and electrostatic bonding of ASO) at a 5:1 (ATS:ASO) molar ratio did not produce the leftward shift in chemerin mRNA expression of primary adipocytes and hepatocytes that we hypothesized. It was still able to decrease chemerin expression but did not confer specificity. In retrospect, the paradoxical increase in chemerin expression at higher concentrations with NP-ATS-ASO in the adipocyte would predict future issues with the nanoparticle.

We did not believe the NP-ATS-ASO was simply dissociating because after three washes with PBS, the ASO did not wash off the NP. We also knew that one group had suggested the ATS mechanism might work through targeting of blood vessels in adipose tissue [172]. Thus, we decided to make two major changes: 1) move to ex vivo and in vivo assays rather in vitro, and 2) change our nanoparticle formulation to more closely match what had previously been published (drop the iron-oxide nanoworm, add 9R to the ATS, and increase the ATS:ASO ratio to 20:1).

4.3 Moving in vivo with ATS9R

Initial ex vivo experiments using sections of liver, mesenteric fat, and retroperitoneal fat did not display a difference in binding between ATS9R-FITC and Scr9R-FITC sequences but did highlight that both peptides persisted on fat longer than on liver. We recognize there were limitations to this experiment. Namely, we did not take

into consideration that the hydrophobicity alone of the fat could be contributing to the binding (especially with the FITC molecule) and no actual binding values were able to be calculated from the data collected. But again, previously published studies suggested in vivo pharmacokinetics might also play a role in conferring specificity.

Indeed, when injected with either ATS9R-FITC or Scr9R-FITC, ATS9R-FITC was discovered in fat at higher levels of fluorescence than the scrambled peptide. However, when we analyzed the efficacy of the drug, there was no knockdown of chemerin when compared to normal tissue.

Seeing as how we had dramatically changed the formulation of our drug, we decided to return to some basic in vitro experiments to see if the new drug formulation still had the ability to knockdown chemerin mRNA at the hepatocyte and adipocyte. Not only did the ATS9R-ASO fail to reduce chemerin expression in these two cell cultures, but both treatments with ATS9R appeared to stimulate chemerin expression. In retrospect this is consistent with data in the adipocytes from our first in vitro experiments with the NP-ATS-ASO. Additionally, we observed that several animals receiving the ATS9R (at peptide concentrations replicating the 20:1 ratio of ATS:ASO ASO dosed at 10 mg/kg) were dying within 24 hours. All animals had matched drug vehicles and volume of water injected (intraperitoneally). Taken together, the ATS9R appears to be stimulating an intense inflammatory response both in our in vivo and in vitro models. New in vivo studies are currently underway with a 5:1 ATS:ASO ratio that will assess if the increased chemerin expression with ATS9R is dose-dependent and if a lower amount of ATS9R will allow the ASO to once again be efficacious at reducing chemerin expression.

4.4 Conclusions

The ATS9R has promise as a targeting molecule but requires mechanistic understanding. Our data support a clear fat-specificity when given in vivo but have mix results when given in vitro. The sequence may rely on both pharmacokinetics (specificity for blood vessels within adipose tissue limiting the distribution to fat) and pharmacodynamics (entering adipocytes via prohibitin expressed on the surface of the cell). Having a molecule like the ATS9R that could directly target the ASO to fat both serves as a tool to analyze the role of fat-secreted chemerin on blood pressure but is also flexible enough to be applied to many other diseases in need of a fat-specific delivery system.

CONCLUSIONS

1. Reframing the epidemiology

1.1 Giving context to new chemerin mechanisms in the cardiovascular system

Going into our initial experiments, we knew there was positive correlation to chemerin and blood pressure [24-30]. There were even early indications that chemerin was acting through the blood vessel [39]. Two important findings of this research are the confirmation of chemerin's role in the vasculature, specifically the smooth muscle cell, and the elucidation of somewhat unconventional messengers in its calcium flux signaling.

The smooth muscle of the vasculature is an important component to blood pressure regulation and solidifies the relevance of chemerin to hypertension. In the same animal model, the Sprague Dawley rat, we were able to, 1) determine a signaling mechanism of chemerin in primary vascular smooth muscle cells; 2) use a whole vessel to demonstrate direct contraction to chemerin in a chemerin$_1$-dependent fashion; and 3) silence that gene to reduce conscious blood pressure. Similar experiments with primary human tissue would be difficult to achieve but given the homology in both chemerin and chemerin$_1$ between rat and human [41] as well as the positive correlation between our experiments and the epidemiological literature, we are confident chemerin plays a significant role in blood pressure regulation.

While the mechanism of chemerin in the smooth muscle we interrogated supports the effect of chemerin ASO in vivo, there are other body systems that are likely involved in chemerin's control of blood pressure. The sympathetic nervous system holds the most promise for future study. While the investigations within this thesis were being conducted, several other important studies looking at the interaction between chemerin and the

sympathetic nervous system were underway. Contraction by an electrical field of an artery with perivascular adipose tissue (PVAT) can be inhibited by CCX832 alone. This effect is also lost when the PVAT is removed and chemerin receptors were discovered on the nerve itself [154]. What is unclear is the location of the chemerin receptor that is directly mediating the blood pressure effects of chemerin (Figure 31). It is possible that sympathetic nerves stimulate PVAT to release chemerin that modulates the smooth muscle, but this implies that chemerin is held in vesicles in the adipocyte for quick release. One group has suggested that chemerin is not only held in intracellular vesicles, but it is also pre-activated (cleaved to chemerin S^{157}) by enzymes within the vesicle [176]. Adipocytes are also known to store and secrete a number of other factors influencing vascular contractility, including adiponectin [18] and norepinephrine [177, 178]. Sympathetic nerves could be influencing the chemerin receptors on the fat to alter contractile secretions which may or may not involve chemerin itself. There are a dozen of chemerin isoforms with different potencies for the chemerin receptor, may induce biased agonism at the chemerin receptor, and there are ligands completely separate from chemerin, like lipid resolving E1, that can have their own agonist effects on the chemerin receptor [96].

The kidney and heart also have connections to chemerin, though it is unlikely they are activated directly by chemerin to stimulate a rise in blood pressure. Because there is a role for chemerin in the adrenal [169] and sympathetic nerves [154], it is possible the heart is affected by those products but one study suggests that cardiomyocytes have the ability to secrete chemerin. The major inflammation regulator, TNF-alpha, can even stimulate the release of chemerin [179, 180]. In our in vivo studies using chemerin

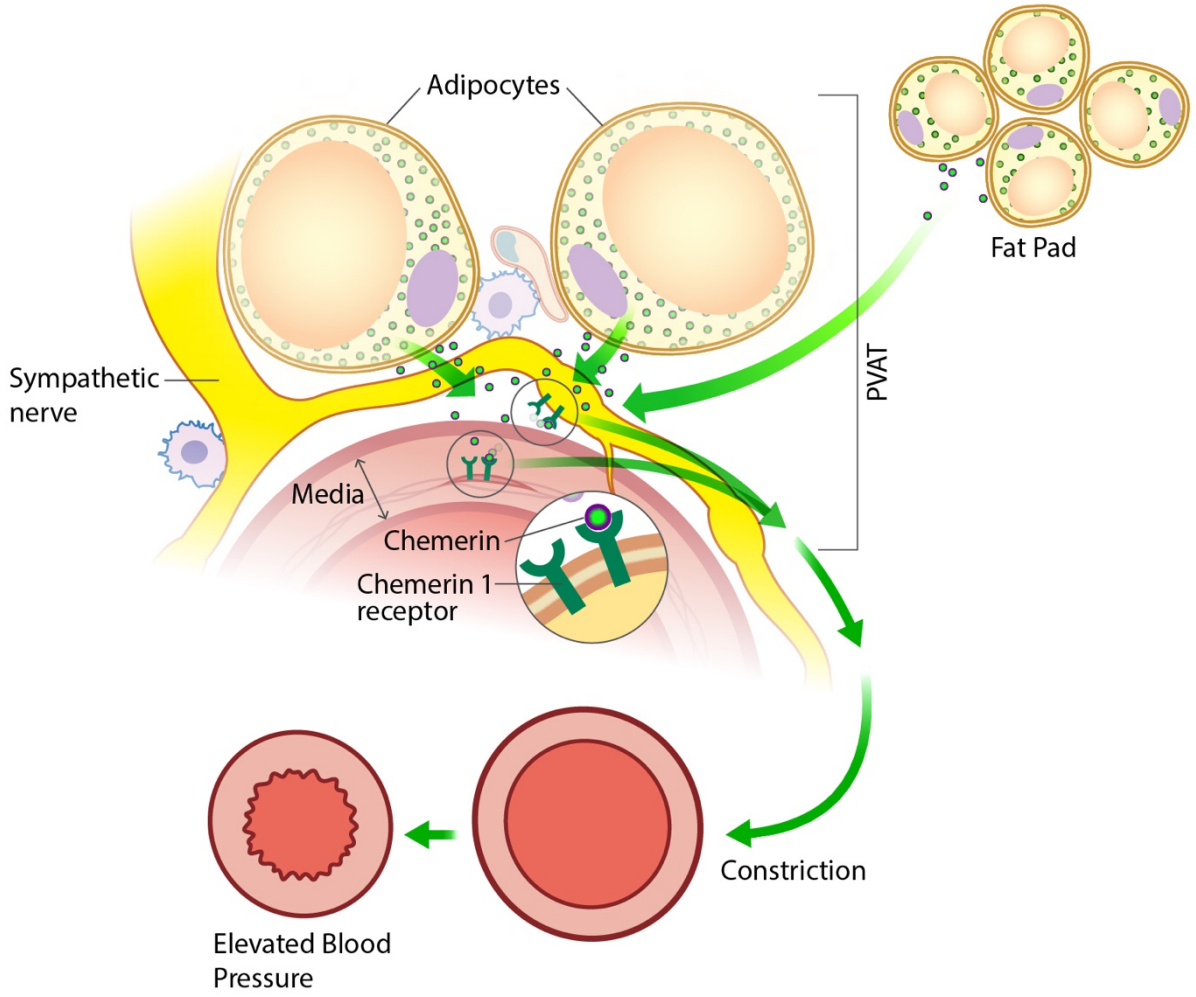

Figure 31: *Chemerin in the vasculature*

antisense oligonucleotides (ASO), blood pressure is drastically reduced with little to no change in heart rate. This is extremely unusual given the baroreceptor reflex that would be expected to follow a drop in blood pressure that occurs over the course of 48 hours. A temporary knockdown of chemerin in either the sympathetic nervous system or the cardiomyocyte could work against these reflexes to keep heart rate low.

The kidney does not appear to contain any functional chemerin receptors [35, 38]. The only current link between chemerin and the kidney is through angiotensin converting enzyme (ACE). ACE converts angiotensin I to angiotensin II (ANGII). In addition to being directly vasoconstrictive, ANGII also stimulates the secretion of vasopressin and aldosterone which work at the kidney tubules to increase water reabsorption and increase blood pressure. One group has proposed that chemerin is cleaved from an inactive to active isoform by ACE [71]. Thus, it is possible that in a physiological (or pathophysiological) effort to increase blood pressure, the upregulation of ACE could also increase the levels of active chemerin that act on the vasculature.

Even with these mechanisms, it is difficult to determine the role chemerin plays in blood pressure regulation on a long-term scale. A germline knockout (KO) of chemerin does not alter blood pressure compared with their wild-type (WT) counterparts. Even when faced with a hypertensive challenge, the KO rats do not respond differently from their WT littermates [78]. These data are in contrast to the ASO studies where a temporary (albeit, complete) knockdown of chemerin in the normal Sprague Dawley rat (the same rat used in the germline KO) caused a reproducible fall of 7 mmHg in blood pressure. In every instance of blood pressure fall with the chemerin ASO, blood pressure rebounds

after the 48-hour post-injection nadir. This short-term compensation does not appear to be occurring through a simple hemodynamic baroreceptor reflex because we do not see blood pressure-related changes in heart rate, even on the hourly level. It is possible that the kidney or some other unique mechanism is involved with the ASOs, but an investigation of this short-term ASO compensatory mechanism may provide insight into why the KO animals don't initially exhibit a different blood pressure from the WT animals. The question then becomes: *can the results of this chemerin ASO and its 30 mmHg fall in blood pressure translate to the clinic?*

In every ASO study, the blood pressure continued to fall with each injection, plateaued below baseline, and qualitatively, the reflexive response appeared to diminish with future injections. The blood pressure effects of the chemerin ASO were also dramatically enhanced in a model of obesity-associated hypertension (DahlS fed a high fat diet). The chemerin ASO KO was created in the Sprague Dawley model where blood pressure responses were relatively modest (at most, a 7 mmHg fall compared to control ASO). This further reinforces the hypothesis that hypertension can have several different etiologies that can be treated with specific medications. In published tests of the human mesenteric artery, chemerin appears to stimulate vascular contractility in a similar manner to the rat system [39, 64]. Taken together, it is possible that in the correct application and with repeated dosing, chemerin is a promising drug target with translatable potential.

1.2 Does circulating chemerin even matter?

Although these mechanisms and in vivo experiments lend to its translatable potential, these studies also create many questions concerning the clinic's interpretation

and application of chemerin. For years, the clinic has been relying on measures of circulating chemerin to draw conclusions about chemerin's relation to certain diseases. Our investigations in both the in vitro and in vivo aspects of chemerin have challenged previously held theories on the mechanisms and associations related to chemerin.

For example, the actions of L-type calcium channels and ROCK in smooth muscle cells fit with previous models of vascular smooth muscle contraction [112]. However, the involvement of Src, absence of ERK1/2, and lack of CCX832-dependent antagonism of recombinant chemerin were unexpected. While the involvement of L-type calcium channels and ROCK give us confidence that this calcium flux is leading to the contractile response we see in ex vivo isometric contractility, the later results are indicative of the way chemerin would continue to challenge some preconceived notions in chemerin physiology.

Administration of a liver-specific ASO that did not reduce blood pressure still completely abolished our ability to detect circulating plasma chemerin. Plasma chemerin was reduced to a similar extent with our whole-body chemerin ASO in both the Sprague Dawley and Dahl high-salt rat models where there was only a modest effect on blood pressure. The only instance where plasma chemerin was slightly detectible, was in our Dahl high-fat rat given whole-body ASO but this animal had the largest reduction in blood pressure. This finding has been one of the most reproducible effects observed over the five years of individual animal studies (Figure 32).

One assumption that is easy to make if only looking at the epidemiological data (showing a positive correlation between blood pressure and plasma chemerin) is that the increased chemerin in the plasma is causing the increased contractility of the blood vessel

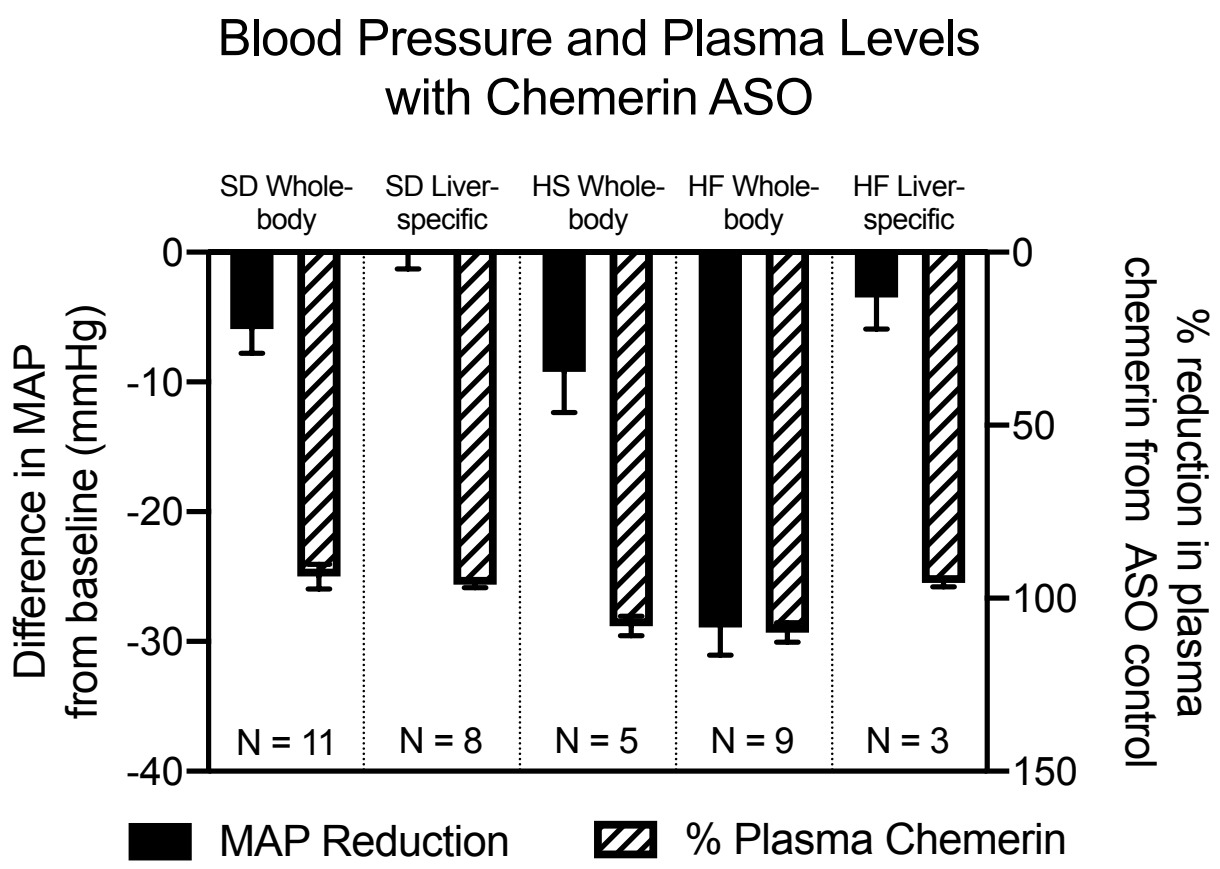

Figure 32: *Relationship between blood pressure and plasma chemerin*

Effect of ASOs on mean arterial blood pressure (MAP) and plasma chemerin protein expression in the male Sprague-Dawley (left) and high salt (HS) or high fat (HF) Dahl S male rat. Whole body ASO knocked down chemerin in all tissues, while the Liver-specific ASO knocked down chemerin largely in the liver. Dahl S rats were either on a control, high fat (60% fat) or high salt (4% salt) diet. Data are adapted from Aims 2.1 and 2.2. Bars represent means$\pm$SEM for number of animals indicated by N.

and leading to the hypertension. However, our data suggest that plasma chemerin is not the cause but the byproduct of the pathology leading to the hypertension. This does not mean that plasma chemerin is uninvolved, it just means that the source of vasoactive chemerin is somewhere other than the plasma.

1.3 Local vs. systemic roles of chemerin

A simple explanation for the increased Dahl high-fat plasma chemerin is that circulating chemerin has no effect on blood pressure but rather, the increased mRNA expression of chemerin in the Dahl fat [171] led to an increase in protein production that is passively secreted into the blood. The perivascular adipose tissue (PVAT), specifically the mesenteric PVAT, is opportunistically situated for its secretions to have a direct effect on the blood vessel from the outside-in (adventitia-lumen; Figure 31).

We have also established the physiologic necessity of chemerin in a homeostatic role. When chemerin is knocked-out from the animal, adipocytes of the mesenteric PVAT struggle to develop [174]. They have impaired expression of adipokines necessary for the appropriate accumulation of lipid.

This is where the physiologic and pathologic roles of chemerin come to a head. Small amounts of chemerin may be beneficial to maintain the growth and development of adipocytes but too much secretion can inappropriately activate smooth muscle cells to contract blood vessels and elevate blood pressure.

This is not meant to minimize the systemic measures or clinical relevance of chemerin in the blood. Chemerin that reaches the blood stream through this process is still a good marker for the status of this pathologic transition. This hypothesis is even in

strong agreement with the epidemiological data showing that plasma chemerin is more strongly associated with metabolic syndrome (a combination of elevated blood pressure and adipose tissue dysfunction) than either parameter of metabolic syndrome alone [28].

In addition to eliminating the chemerin protein in the plasma, the liver-specific ASO also effectively eliminated chemerin protein and mRNA from the liver, the largest producer of chemerin in the body. While this only allows us to directly conclude that chemerin from the liver and plasma do not contribute to blood pressure regulation, the development of the fat-specific nanoparticle for chemerin ASO delivery is an important step towards verifying the local importance of chemerin from the fat.

2. How chemerin isoforms could be impacting research

2.1 Re-examining chemerin pharmacology in the vasculature

The presence of chemerin isoforms and the absence of our understanding about them poses one of the largest remaining hurdles for the entire field of chemerin research. In this research, we did not have the proper tools to interrogate the isoform profile of rats but it is likely they were influencing our research in several ways.

In our investigation of the chemerin-dependent stimulation mechanisms in smooth muscle cells, we observed that chemerin-9-dependent calcium flux (a nonapeptide reflecting the last nine peptides of recombinant S^{157}) was antagonized by CCX832 and pertussis toxin (inhibiting the G-protein of $chemerin_1$). While recombinant chemerin S^{157} stimulated calcium flux to a similar degree as chemerin-9 and was also completely inhibited by pertussis toxin, calcium flux was not altered by CCX832 [142]. This highlights just how dynamic the interaction between chemerin and its receptor can be. In addition

to an investigation of how different amino acids at the C-terminus can affect the stimulation of chemerin$_1$, we need to consider how fragments of different isoforms influence the function of chemerin$_1$.

2.2 Antisense oligonucleotides and isoforms

One of the obvious limitations in our investigation of chemerin's effect on blood pressure was localization of chemerin and the ASO. We already had a tool to specifically target chemerin in the liver and developed a tool to specifically target chemerin of the fat. But when chemerin is knocked down by the ASO, the ASO is working at the pre-mRNA level, so every isoform is knocked down.

We assume that when chemerin is knocked down by ASO, it is inhibition of the S^{157} isoform that is conferring the beneficial fall in blood pressure. Researchers have tried to develop ELISAs that will detect specific isoforms and have linked plasma levels of recombinant S^{157} with blood pressure. But we are again faced with the data suggesting plasma chemerin is not directly linked to blood pressure.

Future studies should be directed to understand, 1) how the isoform profile of chemerin in the mesenteric PVAT changes in obesity-associated hypertension and, 2) how different chemerin isoforms can influence biased agonism of chemerin$_1$, especially if this biased agonism is different in different cells (immune cells, adipocytes, and smooth muscle cells).

3. Applications to other pathologies

3.1 Obesity alone

This study focused specifically on obesity-associated hypertension which limited our translatability to obesity alone in several ways: we did not use mouse models (poor applications to chemerin in blood pressure) and we focused specifically on mesenteric PVAT. But there are still several ways this research can inform the study of obesity alone.

First, in a broad sense, we offer confirmation that in the rat, chemerin is vital to the healthy development of adipocytes. Second, we highlight that chemerin's influence on adipocytes is location specific. The risk factors of obesity are often linked with specific depots of fats. Specifically, worse outcomes are often seen with visceral fat (which includes mesenteric PVAT) [4]. Our focus was on PVAT because of our interest in the interaction between blood vessel and adipocyte. Because the actions of chemerin on the adipocyte are believed to be paracrine and autocrine in nature [38, 176], this study highlights that both clinical and basic science researchers need to consider how different fat depots may have differences in chemerin secretion and agonism of chemerin$_1$.

Third, the development of a fat-specific nanoparticle has potential applications outside of obesity-associated hypertension. The initial developers of the ATS-9R targeting system were a direct treatment for obesity by targeting an element of fatty acid uptake [84]. Other ASOs or nucleic acid drugs can be conjugated to the nanoparticle for specific or enhanced delivery to adipocytes for the treatment of obesity.

3.2 Metabolic syndrome

While both obesity and hypertension are elements of metabolic syndrome, we did not address its elements, dyslipidemia and glucose handling. As emphasized several times in different parts of this thesis, there is an incredibly strong positive association with plasma chemerin levels and the diagnosis of metabolic syndrome [26, 28, 35, 37]. But given the discoveries in this research concerning the relationship between the source of chemerin and the levels of plasma chemerin, researchers need to consider why this positive association, more strongly associated with metabolic syndrome itself over any of the other individual elements of metabolic syndrome, exists.

It is certainly possible to point to the data provided in this thesis, draw a line between plasma chemerin and the liver, and conclude that the liver and its secretion of plasma chemerin are regulated by the general inflammatory status of the animal. As we argue in Section 1 of this discussion, the increase in plasma chemerin levels are likely secondary to the rise in blood pressure rather than being a primary cause of the rise in blood pressure. But once again, the mechanistic data we uncover about chemerin in the blood vessel and adipocyte (along with the data collected by other labs) highlights a gap in our understanding of the relationship between the local and systemic effects of chemerin. Metabolic syndrome must wrestle with the same local versus systemic chemerin dilemma.

3.3 Heart failure

Some of the most underrated data provided in this thesis establish the relationship between blood pressure and heart rate in animals given whole-body ASO. At times when

we see a sustained fall in blood pressure by 7 mmHg in SD rats and 20-30 mmHg in Dahl high-fat diet rats, we see no difference in heart rate when compared to their ASO controls.

Blood pressure control (more specifically, blood pressure reduction) is a major element in the treatment of heart failure with preserved ejection fraction (HFpEF; aka diastolic heart failure). However, direct-acting vasodilators often elicit a reflexive increase in heart rate which can be counterproductive to the treatment of the heart failure. Often, these direct-acting vasodilators must be paired with selective beta-blockers to control the heart rate [181].

We still believe that the direct effects of chemerin on blood pressure are mediated through vasoconstriction. However, this drug does not seem to carry along any of the adverse effects of an increased heart rate. This, paired with the long half-life of the ASO, provides a novel niche for a chemerin ASO in the clinic.

4. Next Steps

Immediately, the ATS9R-ASO nanoparticle needs to be validated and tested in vivo for efficacy against reducing blood pressure. Experiments should be performed similarly to the previous ASO experiments with the normal SD rat and HF DahlS rat. Given the recent (unpublished) success of using HF Dahl Resistant (DahlR) rats as a control for the HF DahlS obesity-associated hypertension model, these could also be used as a control to assess the role of the high fat diet itself on the effects of a chemerin ASO.

We would hypothesize that the ATS9R-ASO would reduce chemerin mRNA expression and protein levels in the fat to the same extent as whole-body ASO and the blood pressure fall with ATS9R-ASO would be the same as whole-body ASO alone. It is

hard to predict what would happen to plasma circulating chemerin but given the results with the liver-specific ASO, we would have to hypothesize that the ATS9R-ASO would not change plasma chemerin compared with whole-body ASO alone.

In this thesis we have brought together the ideas of chemerin in the blood vessel and chemerin in the fat to propose that chemerin mediates an interaction leading to increased blood pressure. Unfortunately, the exact mechanism of how chemerin mediates this effect is left unanswered. The mechanistic data surrounding the sympathetic nerves and the direct effect of CCX832 on EFS-induced contraction offer the most promising path for investigating exactly how chemerin facilitates this interaction leading to vasoconstriction.

Direct cellular assays measuring calcium flux could be performed on cultured sympathetic neurons with chemerin-9 to determine if chemerin has the ability to directly stimulate sympathetic nerve activity. In vivo, it would be interesting to see the effect of a chemerin ASO on an animal who has already undergone a sympathetic ganglionectomy. In both cases where we presume chemerin is mediating its blood pressure control through sympathetic nerves, we would hypothesize chemerin would directly stimulate calcium flux in the sympathetic neuron and lose its ability to lower blood pressure under when sympathetic ganglionectomy is present. However, given the wealth of knowledge already present on the ability of chemerin to directly stimulate contraction in the blood vessel and calcium flux in the smooth muscle cell, it is possible that both mechanisms are present and functioning at the same time.

5. Final perspectives

It is easy to forget that the entire field of chemerin is still in its infancy, especially when it comes to specific mechanisms of action. I have outlined a number of limitations and future directions for chemerin research that touch both the basic science and clinical worlds. The transition between beneficial actions and pathological actions of chemerin is still perplexing, as is the relationship between chemerin plasma levels and the various diseases. It is also important to consider that most of what we know about the secretion and intracellular processing of chemerin has not advanced in 17 years (the very first mechanistic publications) [42].

But this thesis ties together two important aspects of chemerin in a novel way. It takes the clinical and pathological data surrounding hypertension and juxtaposes it with the beneficial effects of chemerin in the adipose tissue. Obesity-associated hypertension alone is a critical and developing research area, but it also serves as an important crossroads in the advancement of our knowledge on chemerin.

REFERENCES

REFERENCES

1. Bluher, M., *Obesity: global epidemiology and pathogenesis.* Nature Reviews Endocrinology, 2019. **15**(5): p. 288-298.

2. Development., O.f.E.C.-o.a., *Obesity update 2017*. 2017, OECD.

3. Ezzati, M., et al., *Worldwide trends in body-mass index, underweight, overweight, and obesity from 1975 to 2016: a pooled analysis of 2416 population-based measurement studies in 128.9 million children, adolescents, and adults.* Lancet, 2017. **390**(10113): p. 2627-2642.

4. Kotchen, T.A., *Obesity-related hypertension: epidemiology, pathophysiology, and clinical management*, in *American Journal of Hypertension*. 2010, Oxford University Press. p. 1170-1178.

5. Whelton, P.K., et al., *2017 ACC/AHA/AAPA/ABC/ACPM/AGS/APhA/ASH/ASPC/NMA/PCNA Guideline for the Prevention, Detection, Evaluation, and Management of High Blood Pressure in Adults: Executive Summary*, in *Hypertension*. 2017. p. HYP.0000000000000066.

6. Abdelaal, M., C.W. le Roux, and N.G. Docherty, *Morbidity and mortality associated with obesity.* Annals of Translational Medicine, 2017. **5**(7): p. 12.

7. Alberti, K.G.M.M.G., et al., *Harmonizing the metabolic syndrome: a joint interim statement of the International Diabetes Federation Task Force on Epidemiology and Prevention; National Heart, Lung, and Blood Institute; American Heart Association; World Heart Federation; International*, in *Circulation*. 2009. p. 1640-1645.

8. Ahmad, A.F., et al., *The gut microbiome and cardiovascular disease: current knowledge and clinical potential.* American Journal of Physiology-Heart and Circulatory Physiology, 2019. **317**(5): p. H923-H938.

9. Knebel, B., et al., *Novel Insights into the Adipokinome of Obese and Obese/Diabetic Mouse Models.* International Journal of Molecular Sciences, 2017. **18**(9).

10. Azizi, M., P. Rossignol, and J.S. Hulot, *Emerging Drug Classes and Their Potential Use in Hypertension.* Hypertension, 2019. **74**(5): p. 1075-1083.

11. Carey, R.M., et al., *Prevalence of Apparent Treatment-Resistant Hypertension in the United States: Comparison of the 2008 and 2018 American Heart Association*

Scientific Statements on Resistant Hypertension. Hypertension, 2019. **73**(2): p. 424-431.

12. Ammori, B.J., et al., *Medical and surgical management of obesity and diabetes: what's new?* Diabet Med, 2020. **37**(2): p. 203-210.

13. Rebello, C.J. and F.L. Greenway, *Obesity medications in development.* Expert Opinion on Investigational Drugs, 2020. **29**(1): p. 63-71.

14. *Expert Panel on Integrated Guidelines for Cardiovascular Health and Risk Reduction in Children and Adolescents: Summary Report.* Pediatrics, 2011. **128**: p. S213–S256.

15. Fornari, E. and C. Maffeis, *Treatment of Metabolic Syndrome in Children.* Frontiers in Endocrinology, 2019. **10**: p. 9.

16. Correa, T.A.F., et al., *The Two-Way Polyphenols-Microbiota Interactions and Their Effects on Obesity and Related Metabolic Diseases.* Frontiers in Nutrition, 2019. **6**: p. 15.

17. McLaughlin, T., et al., *Role of innate and adaptive immunity in obesity-associated metabolic disease.* Journal of Clinical Investigation, 2017. **127**(1): p. 5-13.

18. Stern, J.H., J.M. Rutkowski, and P.E. Scherer, *Adiponectin, Leptin, and Fatty Acids in the Maintenance of Metabolic Homeostasis Through Adipose Tissue Crosstalk Graphical abstract HHS Public Access*, in *Cell Metab*. 2016. p. 770-784.

19. Christensen, K.L. and M.J. Mulvany, *Location of resistance arteries.* Journal of Vascular Research, 2001. **38**: p. 1-12.

20. Wilson, P.W.F., et al., *Overweight and obesity as determinants of cardiovascular risk: the Framingham experience.*, in *Archives of internal medicine*. 2002. p. 1867-1872.

21. Bartness, T.J., et al., *Neural innervation of white adipose tissue and the control of lipolysis.*, in *Frontiers in neuroendocrinology*. 2014, NIH Public Access. p. 473-93.

22. Brown, N.K., et al., *Perivascular Adipose Tissue in Vascular Function and Disease A Review of Current Research and Animal Models.* Arteriosclerosis Thrombosis and Vascular Biology, 2014. **34**(8): p. 1621-1630.

23. Kong, L.R., et al., *Decrease of Perivascular Adipose Tissue Browning Is Associated With Vascular Dysfunction in Spontaneous Hypertensive Rats During Aging.* Frontiers in Physiology, 2018. **9**: p. 8.

24. Shin, H.Y., et al., *Chemerin levels are positively correlated with abdominal visceral fat accumulation*, in *Clin Endocrinol (Oxf)*. 2012. p. 47-50.

25. Kunimoto, H., et al., *Chemerin promotes the proliferation and migration of vascular smooth muscle and increases mouse blood pressure.*, in *American journal of physiology. Heart and circulatory physiology*. 2015, American Physiological Society. p. H1017-28.

26. Dong, B., W. Ji, and Y. Zhang, *Elevated serum chemerin levels are associated with the presence of coronary artery disease in patients with metabolic syndrome.*, in *Internal medicine (Tokyo, Japan)*. 2011. p. 1093-1097.

27. Hu, W. and P. Feng, *Elevated serum chemerin concentrations are associated with renal dysfunction in type 2 diabetic patients*, in *Diabetes Res Clin Pract*. 2011. p. 159-163.

28. Stejskal, D., et al., *Chemerin is an independent marker of the metabolic syndrome in a Caucasian population--a pilot study.*, in *Biomedical papers of the Medical Faculty of the University Palacky, Olomouc, Czechoslovakia*. 2008. p. 217-21.

29. Feng, X., et al., *Elevated levels of serum chemerin in patients with obstructive sleep apnea syndrome*, in *Biomarkers*. 2012. p. 248-253.

30. Zylla, S., et al., *Serum chemerin is associated with inflammatory and metabolic parameters—results of a population-based study*, in *Obesity*. 2017. p. 468-475.

31. Schipper, H.S., et al., *Systemic inflammation in childhood obesity: circulating inflammatory mediators and activated CD14++ monocytes*, in *Diabetologia*. 2012. p. 2800-2810.

32. Landgraf, K., et al., *Chemerin as a mediator between obesity and vascular inflammation in children*, in *J Clin Endocrinol Metab*. 2012. p. E556-64.

33. Chakaroun, R., et al., *Effects of weight loss and exercise on chemerin serum concentrations and adipose tissue expression in human obesity*, in *Metabolism*. 2012. p. 706-714.

34. Cheon, D.Y., et al., *Serum chemerin levels are associated with visceral adiposity, independent of waist circumference, in newly diagnosed type 2 diabetic subjects*, in *Yonsei Medical Journal*. 2017, Yonsei University College of Medicine. p. 319-325.

35. Bozaoglu, K., et al., *Chemerin is a novel adipokine associated with obesity and metabolic syndrome*, in *Endocrinology*. 2007. p. 4687-4694.

36. Gu, P., et al., *Chemerin is associated with inflammatory markers and metabolic syndrome phenotypes in hypertension patients.*, in *Clinical and experimental hypertension (New York, N.Y. : 1993)*. 2014. p. 326-32.

37. Chu, S.H., et al., *Chemerin and adiponectin contribute reciprocally to metabolic syndrome*, in *PLoS One*, B. Ryffel, Editor. 2012. p. e34710.

38. Goralski, K.B., et al., *Chemerin, a novel adipokine that regulates adipogenesis and adipocyte metabolism*, in *J Biol Chem*. 2007. p. 28175-28188.

39. Watts, S.W., et al., *Chemerin connects fat to arterial contraction*, in *Arterioscler Thromb Vasc Biol*. 2013. p. 1320-1328.

40. Nagpal, S., et al., *Tazarotene-induced gene 2 (TIG2), a novel retinoid-responsive gene in skin*, in *Journal of Investigative Dermatology*. 1997. p. 91-95.

41. Schultz, S., et al., *Proteolytic activation of prochemerin by kallikrein 7 breaks an ionic linkage and results in C-terminal rearrangement*, in *Biochem J*. 2013. p. 271-280.

42. Wittamer, V., et al., *Specific recruitment of antigen-presenting cells by chemerin, a novel processed ligand from human inflammatory fluids*, in *J Exp Med*. 2003. p. 977-985.

43. Yamaguchi, Y., et al., *Proteolytic cleavage of chemerin protein is necessary for activation to the active form, Chem157S, which functions as a signaling molecule in glioblastoma*, in *J Biol Chem*. 2011. p. 39510-39519.

44. Wittamer, V., et al., *The C-terminal nonapeptide of mature chemerin activates the chemerin receptor with low nanomolar potency*, in *J Biol Chem*. 2004. p. 9956-9962.

45. Kulig, P., et al., *Staphylococcus aureus-derived staphopain B, a potent cysteine protease activator of plasma chemerin.*, in *Journal of immunology (Baltimore, Md. : 1950)*. 2007. p. 3713-3720.

46. Zabel, B.a., A.M. Silverio, and E.C. Butcher, *Chemokine-Like Receptor 1 Expression and Chemerin-Directed Chemotaxis Distinguish Plasmacytoid from Myeloid Dendritic Cells in Human Blood*, in *The Journal of Immunology*. 2005. p. 244-251.

47. Parolini, S., et al., *The role of chemerin in the colocalization of NK and dendritic cell subsets into inflamed tissues*, in *Blood*. 2007. p. 3625-3632.

48. Jialal, I., et al., *Increased chemerin and decreased omentin-1 in both adipose tissue and plasma in nascent metabolic syndrome*, in *Journal of Clinical Endocrinology and Metabolism*. 2013. p. 514-517.

49. Gu, P., et al., *Increased Circulating Chemerin in Relation to Chronic Microvascular Complications in Patients with Type 2 Diabetes*, in *International Journal of Endocrinology*. 2019.

50. Bozaoglu, K., et al., *Chemerin, a novel adipokine in the regulation of angiogenesis*, in *J Clin Endocrinol Metab*. 2010. p. 2476-2485.

51. Wang, N., et al., *Overexpression of chemerin was associated with tumor angiogenesis and poor clinical outcome in squamous cell carcinoma of the oral tongue*, in *Clin Oral Investig*. 2014. p. 997-1004.

52. Wen, J., et al. *Chemerin stimulates aortic smooth muscle cell proliferation and migration via activation of autophagy in VSMCs of metabolic hypertension rats*. in *Am J Transl Res*. 2019.

53. Gantz, I., et al., *Molecular cloning of a novel receptor (CMKLR1) with homology to the chemotactic factor receptors*, in *Cytogenet Cell Genet*. 1996. p. 286-290.

54. Samson, M., et al., *ChemR23, a putative chemoattractant receptor, is expressed in monocyte-derived dendritic cells and macrophages and is a coreceptor for SIV and some primary HIV-1 strains*, in *European Journal of Immunology*. 1998. p. 1689-1700.

55. Methner, A., et al., *A novel G protein-coupled receptor with homology to neuropeptide and chemoattractant receptors expressed during bone development*, in *Biochem Biophys Res Commun*. 1997. p. 336-342.

56. Owman, C., et al., *Molecular cloning and tissue distribution of cDNA encoding a novel chemoattractant-like receptor*, in *Biochem Biophys Res Commun*. 1997. p. 390-394.

57. Albanesi, C., et al., *Chemerin expression marks early psoriatic skin lesions and correlates with plasmacytoid dendritic cell recruitment*, in *J Exp Med*. 2009. p. 249-258.

58. Kaur, J., et al., *Identification of chemerin receptor (ChemR23) in human endothelial cells: chemerin-induced endothelial angiogenesis*, in *Biochem Biophys Res Commun*. 2010. p. 1762-1768.

59. Reverchon, M., et al., *CHEMERIN (RARRES2) decreases in vitro granulosa cell steroidogenesis and blocks oocyte meiotic progression in bovine species*, in *Biol Reprod*. 2014. p. 102.

60. Zhou, J.X., et al., *Chemerin C9 peptide induces receptor internalization through a clathrin-independent pathway*, in *Acta Pharmacol Sin*. 2014. p. 653-663.

61. Marchese, A., et al., *Cloning of human genes encoding novel G protein-coupled receptors*, in *Genomics*. 1994. p. 609-618.

62. Barnea, G., et al., *The genetic design of signaling cascades to record receptor activation*, in *Proc Natl Acad Sci U S A*. 2008. p. 64-69.

63. Parlee, S.D., et al., *Serum chemerin levels vary with time of day and are modified by obesity and tumor necrosis factor-{alpha}*, in *Endocrinology*. 2010. p. 2590-2602.

64. Kennedy, A.J., et al., *Chemerin Elicits Potent Constrictor Actions via Chemokine-Like Receptor 1 (CMKLR1), not G-Protein-Coupled Receptor 1 (GPR1), in Human and Rat Vasculature.*, in *Journal of the American Heart Association*. 2016, Wiley-Blackwell.

65. Rourke, J.L., et al., *Gpr1 is an active chemerin receptor influencing glucose homeostasis in obese mice*, in *J Endocrinol*. 2014. p. 201-215.

66. Rourke, J.L., H.J. Dranse, and C.J. Sinal, *CMKLR1 and GPR1 mediate chemerin signaling through the RhoA/ROCK pathway.*, in *Molecular and cellular endocrinology*. 2015. p. 36-51.

67. De Henau, O., et al., *Signaling Properties of Chemerin Receptors CMKLR1, GPR1 and CCRL2*, in *PLOS ONE*. 2016. p. e0164179.

68. Zabel, B.A., et al., *Mast cell-expressed orphan receptor CCRL2 binds chemerin and is required for optimal induction of IgE-mediated passive cutaneous anaphylaxis*, in *J Exp Med*. 2008. p. 2207-2220.

69. Ernst, M.C., et al., *Chemerin Exacerbates Glucose Intolerance in Mouse Models of Obesity and Diabetes.* Endocrinology, 2010. **151**(5): p. 1998-2007.

70. Guillabert, A., et al., *Role of neutrophil proteinase 3 and mast cell chymase in chemerin proteolytic regulation*, in *J Leukoc Biol*. 2008. p. 1530-1538.

71. John, H., et al., *Quantification of angiotensin-converting-enzyme-mediated degradation of human chemerin 145-154 in plasma by matrix-assisted laser desorption/ionization-time-of-flight mass spectrometry.*, in *Analytical biochemistry*. 2007. p. 117-25.

72. Wittamer, V., et al., *Neutrophil-Mediated Maturation of Chemerin: A Link between Innate and Adaptive Immunity*, in *The Journal of Immunology*. 2005. p. 487-493.

73. Zabel, B.A., et al., *Chemerin activation by serine proteases of the coagulation, fibrinolytic, and inflammatory cascades*, in *J Biol Chem*. 2005. p. 34661-34666.

74. Ramos-Junior, E.S., et al., *Adipokine Chemerin Bridges Metabolic Dyslipidemia and Alveolar Bone Loss in Mice*, in *Journal of Bone and Mineral Research*. 2016.

75. Neves, K.B., et al., *Upregulation of Nrf2 and Decreased Redox Signaling Contribute to Renoprotective Effects of Chemerin Receptor Blockade in Diabetic Mice.* International Journal of Molecular Sciences, 2018. **19**(8): p. 15.

76. Takahashi, M., et al., *Chemerin regulates beta-cell function in mice*, in *Sci Rep*. 2011. p. 123.

77. Ernst, M.C., et al., *Disruption of the chemokine-like receptor-1 (CMKLR1) gene is associated with reduced adiposity and glucose intolerance.*, in *Endocrinology*. 2012, Endocrine Society Chevy Chase, MD. p. 672-82.

78. Watts, S.W., et al., *The chemerin knockout rat reveals chemerin dependence in female, but not male, experimental hypertension*, in *FASEB Journal*. 2018. p. 6596-6614.

79. Bennett, C.F. and E.E. Swayze, *RNA Targeting Therapeutics: Molecular Mechanisms of Antisense Oligonucleotides as a Therapeutic Platform*, in *Annual Review of Pharmacology and Toxicology*. 2010, Annual Reviews: Palo Alto. p. 259-293.

80. Bennett, C.F., et al., *Pharmacology of Antisense Drugs*, in *Annu. Rev. Pharmacol. Toxicol*. 2017. p. 81-105.

81. Dias, S., S. Paredes, and L. Ribeiro, *Drugs Involved in Dyslipidemia and Obesity Treatment: Focus on Adipose Tissue.* International Journal of Endocrinology, 2018: p. 21.

82. Haas, B., et al., *Targeting adipose tissue.* Diabetology & Metabolic Syndrome, 2012. **4**: p. 11.

83. Huang, W., et al., *Targeting Visceral Fat by Intraperitoneal Delivery of Novel AAV Serotype Vector Restricting Off-Target Transduction in Liver*, in *Molecular Therapy: Methods & Clinical Development*. 2017. p. 68-78.

84. Won, Y.-W., et al., *Oligopeptide complex for targeted non-viral gene delivery to adipocytes.*, in *Nature materials*. 2014. p. 1157-64.

85. Nasr, S.H., et al., *Detection of beta-Amyloid by Sialic Acid Coated Bovine Serum Albumin Magnetic Nanoparticles in a Mouse Model of Alzheimer's Disease.* Small, 2018. **14**(3): p. 10.

86. Kukla, M., et al., *Serum chemerin and vaspin in non-alcoholic fatty liver disease*, in *Scand J Gastroenterol*. 2010. p. 235-242.

87. Klusek-Oksiuta, M., et al., *Chemerin as a novel non-invasive serum marker of intrahepatic lipid content in obese children*, in *Italian Journal of Pediatrics*. 2014.

88. Sell, H., et al., *Chemerin correlates with markers for fatty liver in morbidly obese patients and strongly decreases after weight loss induced by bariatric surgery*, in *J Clin Endocrinol Metab*. 2010. p. 2892-2896.

89. Dessein, P.H., et al., *Circulating concentrations of the novel adipokine chemerin are associated with cardiovascular disease risk in rheumatoid arthritis*, in *J Rheumatol*. 2014. p. 1746-1754.

90. Kostopoulos, C.G., et al., *Chemerin and CMKLR1 expression in human arteries and periadventitial fat: a possible role for local chemerin in atherosclerosis?*, in *BMC Cardiovasc Disord*. 2014. p. 56.

91. Lorincz, H., et al., *Strong correlations between circulating chemerin levels and lipoprotein subfractions in nondiabetic obese and nonobese subjects*, in *Clin Endocrinol (Oxf)*. 2014. p. 370-377.

92. Stepan, H., et al., *Serum levels of the adipokine chemerin are increased in preeclampsia during and 6 months after pregnancy*, in *Regul Pept*. 2011. p. 69-72.

93. Weigert, J., et al., *Systemic chemerin is related to inflammation rather than obesity in type 2 diabetes*, in *Clin Endocrinol (Oxf)*. 2010. p. 342-348.

94. Cash, J.L., et al., *Synthetic chemerin-derived peptides suppress inflammation through ChemR23*, in *J Exp Med*. 2008. p. 767-775.

95. Luangsay, S., et al., *Mouse ChemR23 is expressed in dendritic cell subsets and macrophages, and mediates an anti-inflammatory activity of chemerin in a lung disease model*, in *J Immunol*. 2009. p. 6489-6499.

96. Arita, M., et al., *Stereochemical assignment, antiinflammatory properties, and receptor for the omega-3 lipid mediator resolvin E1*, in *Journal of Experimental Medicine*. 2005. p. 713-722.

97. Yamawaki, H., et al., *A novel adipocytokine, chemerin exerts anti-inflammatory roles in human vascular endothelial cells*, in *Biochem Biophys Res Commun*. 2012. p. 152-157.

98. Barchetta, I., et al., *Sick fat: the good and the bad of old and new circulating markers of adipose tissue inflammation.* Journal of Endocrinological Investigation, 2019. **42**(11): p. 1257-1272.

99. Kelly, R.K., et al., *Development of hypertension in overweight adolescents: a review.*, in *Adolescent health, medicine and therapeutics*. 2015, Dove Press. p. 171-87.

100. Lobato, N.S., et al., *The adipokine chemerin augments vascular reactivity to contractile stimuli via activation of the MEK-ERK1/2 pathway.*, in *Life sciences*. 2012. p. 600-6.

101. Monaghan, A.E., *Chemerin receptor: chemerin receptor*, in *IUPHAR/BPS Guide to PHARMACOLOGY*. 2016.

102. Hill-Eubanks, D.C., et al., *Calcium signaling in smooth muscle.*, in *Cold Spring Harbor perspectives in biology*. 2011, Cold Spring Harbor Laboratory Press. p. a004549.

103. Jackson, W.F., *Ion Channels and Vascular Tone*, in *Hypertension*. 2000. p. 173-178.

104. Touyz, R.M., et al., *Role of c-Src in the regulation of vascular contraction and Ca2+ signaling by angiotensin II in human vascular smooth muscle cells.*, in *Journal of hypertension*. 2001. p. 441-9.

105. Uehata, M., et al., *Calcium sensitization of smooth muscle mediated by a Rho-associated protein kinase in hypertension.*, in *Nature*. 1997. p. 990-4.

106. Ureña, J., A. del Valle-Rodríguez, and J. López-Barneo, *Metabotropic Ca2+ channel-induced calcium release in vascular smooth muscle.*, in *Cell calcium*. 2007. p. 513-20.

107. Zabel, B.A., et al., *Chemokine-like receptor 1 expression by macrophages in vivo: Regulation by TGF-?? and TLR ligands*, in *Experimental Hematology*. 2006. p. 1106-1114.

108. Muruganandan, S., et al., *Chemerin neutralization blocks hematopoietic stem cell osteoclastogenesis.*, in *Stem cells (Dayton, Ohio)*. 2013. p. 2172-82.

109. Kumar, J.D., et al., *Mesenchymal stem cells exhibit regulated exocytosis in response to chemerin and IGF*, in *PLoS ONE*, X.-M. Shi, Editor. 2015. p. e0141331.

110. Zhang, Y., et al., *Urotensin-II receptor stimulation of cardiac L-type Ca2+ channels requires the βγ subunits of Gi/o-protein and phosphatidylinositol 3-*

kinase-dependent protein kinase C β1 isoform., in *The Journal of biological chemistry*. 2015. p. 8644-55.

111. Fujii, K., et al., *Sphingosine 1-phosphate increases an intracellular Ca(2+) concentration via S1P3 receptor in cultured vascular smooth muscle cells.*, in *The Journal of pharmacy and pharmacology*. 2014. p. 802-10.

112. Loirand, G. and P. Pacaud, *Involvement of Rho GTPases and their regulators in the pathogenesis of hypertension.*, in *Small GTPases*. 2014. p. 1-10.

113. Sakamoto, K., et al., *Inhibition of high K+-induced contraction by the ROCKs inhibitor Y-27632 in vascular smooth muscle: possible involvement of ROCKs in a signal transduction pathway.*, in *Journal of pharmacological sciences*. 2003. p. 56-69.

114. Urban, N.H., K.M. Berg, and P.H. Ratz, *K+ depolarization induces RhoA kinase translocation to caveolae and Ca2+ sensitization of arterial muscle.*, in *American journal of physiology. Cell physiology*. 2003. p. C1377-85.

115. Mita, M., et al., *Membrane depolarization-induced contraction of rat caudal arterial smooth muscle involves Rho-associated kinase.*, in *The Biochemical journal*. 2002. p. 431-40.

116. Kupittayanant, S., T. Burdyga, and S. Wray, *The effects of inhibiting Rho-associated kinase with Y-27632 on force and intracellular calcium in human myometrium.*, in *Pflügers Archiv : European journal of physiology*. 2001. p. 112-4.

117. Janssen, L.J., et al., *KCl evokes contraction of airway smooth muscle via activation of RhoA and Rho-kinase.*, in *American journal of physiology. Lung cellular and molecular physiology*. 2004, American Physiological Society. p. L852-8.

118. Davies, S.P., et al., *Specificity and mechanism of action of some commonly used protein kinase inhibitors.*, in *The Biochemical journal*. 2000, Portland Press Ltd. p. 95-105.

119. Ratz, P.H. and A.S. Miner, *Role of protein kinase Czeta and calcium entry in KCl-induced vascular smooth muscle calcium sensitization and feedback control of cellular calcium levels.*, in *The Journal of pharmacology and experimental therapeutics*. 2009. p. 399-408.

120. Shabir, S., et al., *Rho-kinase inhibition and electromechanical coupling in rat and guinea-pig ureter smooth muscle: Ca2+-dependent and -independent mechanisms.*, in *The Journal of physiology*. 2004, Wiley-Blackwell. p. 839-55.

121. Ghisdal, P., G. Vandenberg, and N. Morel, *Rho-dependent kinase is involved in agonist-activated calcium entry in rat arteries.*, in *The Journal of physiology*. 2003, Wiley-Blackwell. p. 855-67.

122. Abramowitz, J. and L. Birnbaumer, *Physiology and pathophysiology of canonical transient receptor potential channels.*, in *FASEB journal : official publication of the Federation of American Societies for Experimental Biology*. 2009. p. 297-328.

123. Kedziora, K.M., et al., *Rapid remodeling of Invadosomes by Gi-coupled receptors: Dissecting the role of Rho GTPases*, in *Journal of Biological Chemistry*. 2016. p. 4323-4333.

124. Rouach, N., et al., *S1P inhibits gap junctions in astrocytes: Involvement of Gi and Rho GTPase/ROCK*, in *European Journal of Neuroscience*. 2006. p. 1453-1464.

125. Kurt, A.H., et al., *G protein-coupled estrogen receptor1 (GPER1) may mediate Rho-kinase (ROCK-2) up-regulation in coronary endothelial cells*, in *Endocrine Regulations*. 2013. p. 75-84.

126. Shaifta, Y., et al., *Divergent modulation of Rho-kinase and Ca(2+) influx pathways by Src family kinases and focal adhesion kinase in airway smooth muscle.*, in *British journal of pharmacology*. 2015. p. 5265-80.

127. Katsumoto, T.R., et al., *The phosphatase CD148 promotes airway hyperresponsiveness through SRC family kinases.*, in *The Journal of clinical investigation*. 2013. p. 2037-48.

128. Brighton, P.J., et al., *Characterization of anandamide-stimulated cannabinoid receptor signaling in human ULTR myometrial smooth muscle cells.*, in *Molecular endocrinology (Baltimore, Md.)*. 2009. p. 1415-27.

129. Tanimoto, T., *Sphingosine 1-Phosphate Transactivates the Platelet-Derived Growth Factor Receptor and Epidermal Growth Factor Receptor in Vascular Smooth Muscle Cells*, in *Circulation Research*. 2004. p. 1050-1058.

130. Nakao, F., *Involvement of Src Family Protein Tyrosine Kinases in Ca2+ Sensitization of Coronary Artery Contraction Mediated by a Sphingosylphosphorylcholine-Rho-Kinase Pathway*, in *Circulation Research*. 2002. p. 953-960.

131. MacKay, C.E. and G.A. Knock, *Control of vascular smooth muscle function by Src-family kinases and reactive oxygen species in health and disease.*, in *The Journal of physiology*. 2015. p. 3815-28.

132. Vazquez, G., et al., *Obligatory role of Src kinase in the signaling mechanism for TRPC3 cation channels.*, in *The Journal of biological chemistry*. 2004. p. 40521-8.

133. Gui, P., et al., *Coordinated regulation of vascular Ca2+ and K+ channels by integrin signaling.*, in *Advances in experimental medicine and biology*. 2010. p. 69-79.

134. Boles, A., R. Kandimalla, and P.H. Reddy, *Dynamics of diabetes and obesity: Epidemiological perspective*, in *Biochimica et Biophysica Acta (BBA) - Molecular Basis of Disease*. 2017. p. 1026-1036.

135. Brunner, K.T., et al., *Nonalcoholic Fatty Liver Disease and Obesity Treatment*, in *Current Obesity Reports*. 2019. p. 220-228.

136. Henry, S.L., et al., *Developmental origins of obesity-related hypertension*, in *Clinical and Experimental Pharmacology and Physiology*. 2012, Blackwell Publishing Ltd. p. 799-806.

137. Engin, A., *The Definition and Prevalence of Obesity and Metabolic Syndrome*, in *Advances in experimental medicine and biology*. 2017. p. 1-17.

138. Gateva, A., et al., *Classical (adiponectin, leptin, resistin) and new (chemerin, vaspin, omentin) adipocytokines in patients with prediabetes*, in *Hormone Molecular Biology and Clinical Investigation*. 2018.

139. Spyrou, N., et al., *Classic and Novel Adipocytokines at the Intersection of Obesity and Cancer: Diagnostic and Therapeutic Strategies*, in *Current Obesity Reports*. 2018. p. 260-275.

140. Ernst, M.C. and C.J. Sinal, *Chemerin: at the crossroads of inflammation and obesity*, in *Trends in Endocrinology & Metabolism*. 2010. p. 660-667.

141. Ouwens, D.M., et al., *Chemerin as biomarker for insulin sensitivity in males without typical characteristics of metabolic syndrome*, in *Archives of Physiology and Biochemistry*. 2012. p. 135-138.

142. Ferland, D.J., et al., *Chemerin-induced arterial contraction is Gi- and calcium-dependent.*, in *Vascular pharmacology*. 2017, Elsevier Inc. p. 30-41.

143. Muruganandan, S., et al., *Chemerin, a novel Peroxisome Proliferator-activated Receptor γ (PPARγ) target gene that promotes mesenchymal stem cell adipogenesis*, in *Journal of Biological Chemistry*. 2011, American Society for Biochemistry and Molecular Biology. p. 23982-23995.

144. Shannon, P., et al., *Cytoscape: A Software Environment for Integrated Models of Biomolecular Interaction Networks*, in *Genome Research*. 2003. p. 2498-2504.

145. Hansen, L.B., *GLP-2 and mesenteric blood flow.*, in *Danish medical journal*. 2013. p. B4634.

146. Greenberg, A.S., et al., *Perilipin, a major hormonally regulated adipocyte-specific phosphoprotein associated with the periphery of lipid storage droplets.*, in *The Journal of biological chemistry*. 1991. p. 11341-6.

147. Berndt, J., et al., *Fatty acid synthase gene expression in human adipose tissue: association with obesity and type 2 diabetes*, in *Diabetologia*. 2007, Springer-Verlag. p. 1472-1480.

148. Suzuki, Y., et al., *The Regulation of Chemerin and CMKLR1 Genes Expression by TNF-α, Adiponectin, and Chemerin Analog in Bovine Differentiated Adipocytes.*, in *Asian-Australasian journal of animal sciences*. 2012, Asian-Australasian Association of Animal Production Societies (AAAP). p. 1316-21.

149. Roh, S.G., et al., *Chemerin--a new adipokine that modulates adipogenesis via its own receptor*, in *Biochem Biophys Res Commun*. 2007. p. 1013-1018.

150. Sell, H., et al., *Chemerin is a novel adipocyte-derived factor inducing insulin resistance in primary human skeletal muscle cells.*, in *Diabetes*. 2009, American Diabetes Association. p. 2731-40.

151. Garrison, R.J., et al., *Incidence and precursors of hypertension in young adults: the Framingham Offspring Study.*, in *Preventive medicine*. 1987. p. 235-51.

152. Hall, J.E., et al., *Obesity-Induced Hypertension: Interaction of Neurohumoral and Renal Mechanisms*, in *Circulation Research*. 2015. p. 991-1006.

153. Neves, K.B., et al., *Chemerin reduces vascular nitric oxide/cGMP signalling in rat aorta: a link to vascular dysfunction in obesity?*, in *Clin Sci (Lond)*. 2014. p. 111-122.

154. Darios, E.S., et al., *The adipokine chemerin amplifies electrical field-stimulated contraction in the isolated rat superior mesenteric artery*, in *American Journal of Physiology - Heart and Circulatory Physiology*. 2016. p. H498-H507.

155. Hung, G., et al., *Characterization of target mRNA reduction through in situ RNA hybridization in multiple organ systems following systemic antisense treatment in animals.*, in *Nucleic acid therapeutics*. 2013. p. 369-78.

156. Prakash, T.P., et al., *Comprehensive Structure-Activity Relationship of Triantennary N-Acetylgalactosamine Conjugated Antisense Oligonucleotides for*

Targeted Delivery to Hepatocytes., in *Journal of medicinal chemistry*. 2016. p. 2718-33.

157. Mullick, A.E., et al., *Blood Pressure Lowering and Safety Improvements with Liver Angiotensinogen Inhibition in Models of Hypertension and Kidney Injury*, in *Hypertension*. 2017. p. 566-576.

158. Hashimoto, J.G., A.S. Beadles-Bohling, and K.M. Wiren, *Comparison of RiboGreen® and 18S rRNA quantitation for normalizing real-time RT-PCR expression analysis*, in *BioTechniques*. 2004. p. 54-60.

159. Eaton, S.L., et al., *Total Protein Analysis as a Reliable Loading Control for Quantitative Fluorescent Western Blotting*, in *PLoS ONE*, P.J. Kahle, Editor. 2013. p. e72457.

160. Della Chiesa, M., et al., *Pathogen-induced private conversations between natural killer and dendritic cells*, in *Trends Microbiol*. 2005. p. 128-136.

161. Robinson, M.W., C. Harmon, and C. O'Farrelly, *Liver immunology and its role in inflammation and homeostasis*, in *Cellular & Molecular Immunology*. 2016. p. 267-276.

162. Takahashi, M., et al., *Chemerin enhances insulin signaling and potentiates insulin-stimulated glucose uptake in 3T3-L1 adipocytes*, in *FEBS Lett*. 2008. p. 573-578.

163. Beyer, A.M., et al., *Dahl salt-sensitive rats are protected against vascular defects related to diet-induced obesity.*, in *Hypertension (Dallas, Tex. : 1979)*. 2012. p. 404-10.

164. Ferland, D.J., et al., *Whole-Body but Not Hepatic Knockdown of Chemerin by Antisense Oligonucleotide Decreases Blood Pressure in Rats*, in *Journal of Pharmacology and Experimental Therapeutics*. 2018. p. 212-218.

165. Sullivan, J.M., *Salt sensitivity. Definition, conception, methodology, and long-term issues.*, in *Hypertension (Dallas, Tex. : 1979)*. 1991. p. I61-8.

166. Fernandes, R., et al., *Sex Differences in Renal Inflammation and Injury in High-Fat Diet-Fed Dahl Salt-Sensitive Rats*, in *Hypertension (Dallas, Tex. : 1979)*. 2018. p. e43-e52.

167. Weng, C., et al., *Effects of chemerin/CMKLR1 in obesity-induced hypertension and potential mechanism.*, in *American journal of translational research*. 2017. p. 3096-3104.

168. Szasz, T. and R.C. Webb, *Perivascular adipose tissue: more than just structural support.*, in *Clinical science (London, England : 1979)*. 2012, NIH Public Access. p. 1-12.

169. Moore, A., et al., *Short Communication Chemerin Peptide Releases Catecholamines from Rat Adrenal Medulla 1*, in *Pharmacologica*. 2016. p. 290-295.

170. Hruby, A. and F.B. Hu, *The Epidemiology of Obesity: A Big Picture.* Pharmacoeconomics, 2015. **33**(7): p. 673-689.

171. Ferland, D.J., et al., *Different blood pressure responses in hypertensive rats following chemerin mRNA inhibition in dietary high fat compared to dietary high-salt conditions*, in *Physiological genomics*. 2019. p. 553-561.

172. Kolonin, M.G., et al., *Reversal of obesity by targeted ablation of adipose tissue*, in *Nature Medicine*. 2004, Nature Publishing Group. p. 625-632.

173. Yong, S.B., Y. Song, and Y.H. Kim, *Visceral adipose tissue macrophage-targeted TACE silencing to treat obesity-induced type 2 diabetes.* Biomaterials, 2017. **148**: p. 81-89.

174. Ferland, D.J., et al., *Chemerin contributes to in vivo adipogenesis in a location-specific manner.* Plos One, 2020. **15**(2).

175. Nasr, S.H., et al., *Effects of Nanoprobe Morphology on Cellular Binding and Inflammatory Responses: Hyaluronan-Conjugated Magnetic Nanoworms for Magnetic Resonance Imaging of Atherosclerotic Plaques.* Acs Applied Materials & Interfaces, 2018. **10**(14): p. 11495-11507.

176. Dranse, H.J., et al., *Adipocyte-secreted chemerin is processed to a variety of isoforms and influences MMP3 and chemokine secretion through an NFkB-dependent mechanism.*, in *Molecular and cellular endocrinology*. 2016. p. 114-129.

177. Ahmad, M.F., et al., *Perivascular Adipocytes Store Norepinephrine by Vesicular Transport*, in *Arteriosclerosis, thrombosis, and vascular biology*. 2019. p. 188-199.

178. Ayala-Lopez, N., J.M. Thompson, and S.W. Watts, *Perivascular adipose tissue's impact on norepinephrine-induced contraction of mesenteric resistance arteries*, in *Frontiers in Physiology*. 2017, Frontiers Media SA. p. 37.

179. Rodríguez-Penas, D., et al., *The Adipokine Chemerin Induces Apoptosis in Cardiomyocytes.*, in *Cellular physiology and biochemistry : international journal of*

experimental cellular physiology, biochemistry, and pharmacology. 2015. p. 176-92.

180. Parlee, S.D., et al., *Elastase and tryptase govern TNFα-mediated production of active chemerin by adipocytes.*, in *PloS one*. 2012, Public Library of Science. p. e51072.

181. Feldman, D., et al., *Heart rate control with adrenergic blockade: Clinical outcomes in cardiovascular medicine.* Vascular Health and Risk Management, 2010. **6**: p. 387-397.